1.0

1.1

1.25   1.4   1.6

2.8   2.5
3.2   2.2
3.6
4.0   2.0

1.8

MICROCOPY RESOLUTION TEST CHART
NATIONAL BUREAU OF STANDARDS-1963-A

NUMERICAL DETERMINATION OF THE
EFFECTS OF BOUNDARY CONDITIONS ON
THE INSTABILITY OF COMPOSITE
PANELS WITH CUTOUTS

THESIS

Catherine E. Lee
Captain   USAF

AFIT/GA/AA/83D-4

DEPARTMENT OF THE AIR FORCE

AIR UNIVERSITY (ATC)

AIR FORCE INSTITUTE OF TECHNOLOGY

Wright-Patterson Air Force Base, Ohio

84 01 13 020

NUMERICAL DETERMINATION OF THE
EFFECTS OF BOUNDARY CONDITIONS ON
THE INSTABILITY OF COMPOSITE
PANELS WITH CUTOUTS

THESIS

Catherine E. Lee
Captain   USAF

AFIT/GA/AA/83D-4

NUMERICAL DETERMINATION OF THE
EFFECTS OF BOUNDARY CONDITIONS ON
THE INSTABILITY OF COMPOSITE
PANELS WITH CUTOUTS

THESIS

Presented to the Faculty of the School of Engineering

of the Air Force Institute of Technology

Air University

In Partial Fulfillment of the

Requirements for the Degree of

Master of Science in Astronautical Engineering

Catherine E. Lee, B.S.

Captain, USAF

December 1983

Accession For	
NTIS GRA&I	☒
DTIC TAB	☐
Unannounced	☐
Justification	
By	
Distribution/	
Availability Codes	
Dist	Avail and/or Special
A-1	

Approved for public release; distribution unlimited

Table of Contents

Acknowledgements

I wish to thank my advisor, Dr Anthony Palazotto, for his professional guidance and instruction in helping me complete this thesis. My thanks also go to Dr. Peter Torvik and Major Mike Wallace, my committee members, for their advice and valuable suggestions.

My classmates, whose sense of humor and professionalism helped make the past eighteen months bearable, also deserve my thanks.

I would also like to extend my appreciation to Captain Thomas Janisse who helped me immensely with learning the computer programs necessary to do my thesis. I also would like to thank Lt Mark Sobota for his assistance with the experimentation.

Finally and most importantly, I would like to extend my most sincere thanks to my husband, Doug, and my son, Jack, for their love and support. My husband deserves special thanks for his help with typing and preparing this thesis.

ii

List of Figures

List of Tables

List of Symbols

A_{ij}	Extensional stiffnesses
B_{ij}	Coupling stiffnesses
D_{ij}	Bending stiffnesses
E_i	Young's modulus in i direction
$\bar{F}$	Vector of applied forces
G_{ij}	Shear modulus in i-j plane
$K(x)$	Nonlinear stiffness matrix
$L(x)$	First derivative of Strain Energy Functional
M_x, M_y, M_{xy}	Moments
N_x, N_y, N_{xy}	Axial forces
Q_{ij}	Reduced stiffnesses
$\bar{Q}_{ij}$	Transformed reduced stiffnesses
R	Radius of Panel
Ru, Rv, Rw	Rotations
U	Strain energy
u, v, w	Displacements
V	Potential Energy
W	Work
x, y, z	Structural axes
$1, 2, 3$	Lamina principal axes
γ_{ij}	Shear strain components
ϵ_i	Normal strain components
θ	Fiber orientation angle
κ	Middle surface curvatures
ν	Poisson's ratio

σ_i	Normal stress components
τ_{ij}	Shear sress components
ϕ	Rotation

Superscript (o) refers to middle surface values

Abstract

An analytical study using the STAGSC-1 computer code
was conducted to determine the effects of notches and
unsymmetric boundary conditions on the load bearing
capability and radial displacements of axially loaded
cylindrical panels. The graphite-epoxy panel consisted of
an 8 ply laminate with symmetric ply orientations. A finite
element mesh refinement in the vicinity of the cutout was
conducted in order to study the non-linear collapse
analysis. In additon, the effect of different size cutouts
with aspect ratios (axial dimension of cutout divided by
circumferential dimension) of 2.0 or 0.5 was studied.
Finally, analytic results for a 2"x2" cutout with a varying
set of boundary conditions were compared to experimental
findings.

It was found that as the surface area of the cutout
increased, the buckling load decreased. Cutouts with aspect
ratios of 2.0 were found to be capable of carrying higher
loads than notches with an aspect ratio of 0.5. By
comparing analytic results with experimental data, it was
found that unsymmetric boundary conditions for the 2"x2"
cutout better approximated experimental data than when
symmetric boundary conditions were considered. It was also
determined that some of the discrepancy between experimental
and analytic results can be attributed to initial
eccentricities introduced into the panel by the test
apparatus.

xii

I. INTRODUCTION

Background

The strength and stability of aircraft and space vehicles are influenced by the presence of cutouts or notches in their skins. Many vehicles in the NASA space program are characterized by large, lightweight shell structures that can be either stringer stiffened or unstiffened, and can have either reinforced or non-reinforced cutouts. These shell structures can be analyzed by finite element techniques. Anderson [1] discusses how finite element techniques have been used in the Apollo launch vehicle analysis and Skylab stability analysis. Design studies have been conducted using finite element techniques on the Space Shuttle oxygen tanks and cargo doors [2]. Skogh [3] describes the use of finite element analysis in the Skylab structural design.

Of particular interest in space vehicle design is how structural stability is affected by cutouts in the shell structure. Very few references can be found, however, dealing with axially loaded composite cylindrical panels with cutouts. Considerable work has been done on isotropic plates and cylindrical panels [4-7]. Sobel [6] and Almroth [4] also studied how varying sets of boundary conditions affected the buckling behavior of unstiffened panels. Sobel [6] found that preventing circumferential edge displacement is the most important in-plane boundary condition from the

1

point of view of increasing buckling load.   Several authors
[8-13] have investigated the buckling behavior and stress
states of isotropic panels, with cutouts, under axially
compressive loads.   These studies were done numerically
generally using finite difference techniques.   Plates and
panels with reinforced cutouts have also been analyzed [13].
Most tests have been conducted using circular cutouts, but
some investigations have been done with elliptic and square
cutouts.

In recent years, there have been numerous technological
advances in the application of fiber-reinforced composites
to aircraft and space vehicles.   Research into composite
cylindrical panels without cutouts has been carried out in
the past [14-22], but relatively little work can be found
dealing with composite panels with cutouts.   Satyamurthy
[20] found that boundary conditions, load systems, location
of concentrated loads, and material properties influence the
nature of the buckling behavior in composite panels.   These
types of analyses must also be applied to composite
cylindrical panels with cutouts in order to more fully
understand the effect that a cutout has on buckling
behavior.

Janisse [23] is one of the few authors found to address
the problem of cutouts in composite cylindrical panels.
Singer [24] has consolidated much of the work done on
buckling of shells into a concise report.   This report
encompasses isotropic shells, stiffened shells, and
composite shells and addresses special problems and

2

techniques used in shell analysis.

Composite panels have been studied in greater detail from an analytic point of view than they have been experimentally. This is due to manufacturing difficulties and lack of experimental test fixtures needed to apply a purely compressive load. Analytic problems are more complex when working with composite materials because of their anisotropic material properties and the non-homogeneous complex fiber/matrix interactions. Numerous computer codes have been developed to analyze these types of structures. The Structural Analysis of General Shells (STAGSC-1) computer program was used for finite element analysis in this thesis.

Since composites are used almost exclusively in aerospace structures, more work needs to be done in the area of cylindrical panels with cutouts in order to more fully understand the effect of the cutout and how varying the boundary conditions affects the buckling behavior of a panel. This thesis, which is a continuation of the work done by Janisse [23], addresses the issue of small cutouts in composite cylindrical panels and the effect of unsymmetric boundary conditions on buckling behavior.

Objectives

The purpose of this thesis is threefold. First, the effect that cutouts or notches of various aspect ratios have on the buckling behavior of composite panels will be studied

3

analytically using the STAGSC-1 computer program. For the purposes of this thesis, a notch will be defined as a cutout of less than 5% of the total panel area. Second, the effects of unsymmetric boundary conditions on a panel with a square cutout will be analyzed. Finally, analytic results will be compared to experimental data. This thesis will enable a better overall understanding of the nature and stability of composite cylindrical panels under axial loads.

Approach

The STAGSC-1 finite element computer program [26] developed at Lockheed was used to study the collapse of cylindrical panels with cutouts. The analysis carried out is nonlinear due to the presence of a cutout. The nonlinear collapse analysis branch in STAGSC-1 uses large displacement theory and moderate rotations along with a modified Newton-Raphson iteration scheme.

Six different size cutouts located at the center of the panel were investigated. A panel with a 2"x2" notch (a cutout comprising less than 5% of panel area) was used as a basis for a mesh refinement study. These results were then applied to the finite element mesh design for the other five cutouts. Of these six cutouts, two were square, comprising 2.7% and 11% of the surface area of the panel, respectively. The other four cutouts were rectangular with aspect ratios of either 0.5 or 2.0. Aspect ratio is defined as the axial dimension of the cutout divided by the circumferential

4

dimension. The effect that notches and cutouts of different percentages of total panel area have on the stability and buckling behavior of panels was investigated.

Experimental data was obtained for a panel with a 2"x2" notch. The results appeared to lack consistency under the assumptions relative to a simply supported vertical edge. Thus, in order to rationalize the experimental results, unsymmetric boundary conditions were modeled analytically on the panel with the 2"x2" notch to study the effect of varied bounaries on the buckling behavior of curved panels.

II. THEORY AND MODELLING

Classical Lamination Theory

In order to understand composite laminae behavior,
basic constituitive relationships for an individual lamina
must be explained. The reader should refer to References
[14] and [26] for an in-depth development of these relations.

The stress-strain expressions for an individual lamina
are essentially the stress-strain relations for plane stress
in an orthotropic material. The following relations are the
basis for the stiffness and stress analysis of an individual
lamina subjected to forces in its own plane. For a laminae
of orthotropic material, the stress-strain equations in
principal material coordinates are

$$
\left\{
\begin{array}{c}
\sigma_1 \\
\sigma_2 \\
\tau_{12}
\end{array}
\right\}
=
\left[
\begin{array}{ccc}
Q_{11} & Q_{12} & 0 \\
Q_{12} & Q_{11} & 0 \\
0 & 0 & Q_{66}
\end{array}
\right]
\left\{
\begin{array}{c}
\epsilon_1 \\
\epsilon_{12} \\
\gamma_{12}
\end{array}
\right\}
\qquad (1)
$$

where ϵ_1 and ϵ_2 are normal strains and γ_{12} is the shear
strain for the lamina principal axes as in Figure 2.1, and

$$
Q_{11} = \frac{E_1}{1 - \nu_{12}\nu_{21}}
$$

$$
Q_{12} = \frac{\nu_{12}E_2}{1 - \nu_{12}\nu_{21}} = \frac{\nu_{21}E_1}{1 - \nu_{12}\nu_{21}} \qquad (2)
$$

$$
Q_{22} = \frac{E_2}{1 - \nu_{12}\nu_{21}}
$$

$$
Q_{66} = G_{12}
$$

z,3
(out)

x,y,z = Structural Axes

$1,2,3$ = Lamina Principal Axes

θ = Fiber Orientation Angle
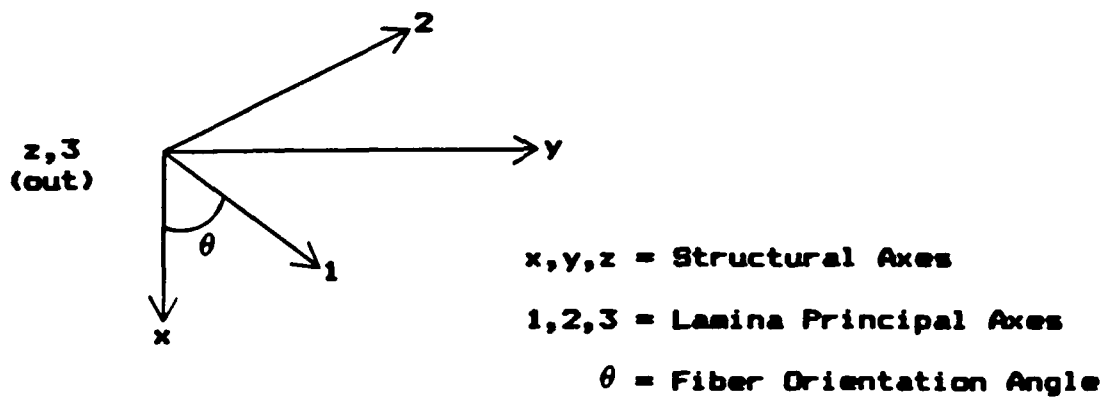
Figure 2.1. Definition of Coordinate Systems

where E_1 and E_2 are Young's moduli in the 1, and 2 directions, respectively. ν_{ij} is Poisson's ratio for transverse strain in the j direction when loaded in the i direction and G_{12} is the shear modulus in the 1-2 plane. Therefore,

$$\nu_{12} = \frac{-\epsilon_2}{\epsilon_1}$$

$$\nu_{21} = \frac{-\epsilon_1}{\epsilon_2} \qquad (3)$$

$$G_{12} = \frac{\tau_{12}}{\gamma_{12}}$$

The preceding stresses and strains were defined in the principal material directions for an orthotropic material. If the principal directions do not coincide with coordinate directions, stress and strain transformations are used to define the following stress-strain relations in xy coordinates.

7
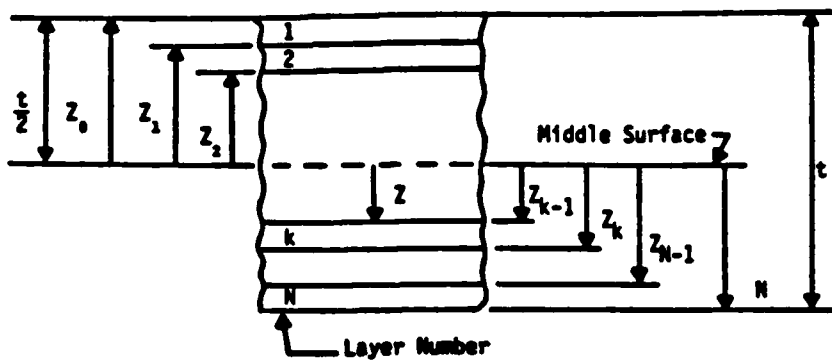
Figure 2.2. Geometry of an N Layered Laminate

Therefore,

$$
\begin{Bmatrix} \sigma_x \\ \sigma_y \\ \tau_{xy} \end{Bmatrix} = \begin{bmatrix} \bar{Q}_{11} & \bar{Q}_{12} & \bar{Q}_{16} \\ \bar{Q}_{12} & \bar{Q}_{22} & \bar{Q}_{26} \\ \bar{Q}_{16} & \bar{Q}_{26} & \bar{Q}_{66} \end{bmatrix} \begin{Bmatrix} \epsilon_x \\ \epsilon_y \\ \gamma_{xy} \end{Bmatrix}
\tag{4}
$$

where the material coefficients, Q_{ij}, are symmetric and defined as

$$
\bar{Q}_{11} = Q_{11}\cos^4\theta + 2(Q_{12}+2Q_{66})\sin^2\theta\cos^2\theta + Q_{22}\sin^4\theta
$$

$$
\bar{Q}12 = (Q11+Q22-4Q66)\sin^2\theta\cos^2\theta + Q12(\sin^4\theta+\cos^4\theta)
$$

$$
\bar{Q}_{22} = Q_{11}\sin^4\theta + 2(Q_{12}+2Q_{66})\sin^2\theta\cos^2\theta + Q_{22}\cos^4\theta
\tag{5}
$$

$$
\bar{Q}_{16} = (Q_{11}-Q_{12}-2Q_{66})\sin\theta\cos^3\theta + (Q_{12}-Q_{22}+2Q_{66})\sin^3\theta\cos\theta
$$

$$
\bar{Q}_{26} = (Q_{11}-Q_{12}-2Q_{66})\sin^3\theta\cos\theta + (Q_{12}-Q_{22}+2Q_{66})\sin\theta\cos^3\theta
$$

$$
\bar{Q}_{66} = (Q_{11}+Q_{22}-2Q_{12}-2Q_{66})\sin^2\theta\cos^2\theta + Q_{66}(\sin^4\theta+\cos^4\theta)
$$

For a detailed derivation of the transformed reduced stiffnesses, see Reference [26].

In order to define the stress and strain variations through the thickness of a laminate, stress-strain behavior of an individual lamina will be expanded. For the kth layer

8

of a multilayered laminate, Equation (4) can be written as

$$\{\sigma\}_k = [\bar{Q}]_k \{\epsilon\}_k \tag{6}$$

Refer to Figure 2.2 for the geometry of an N layered laminate of thickness t, middle surface location and location of the kth lamina.

It is assumed that each layer can be characterized as an orthotropic material whose properties are known with respect to its material axes. The laminate is assumed to consist of perfectly bonded laminae. The displacements are continuous across lamina boundaries so that no lamina can slip relative to one another. Also, for a thin laminate, normal sections remain normal to the middle surface after bending. These assumptions for a laminate constitute the Kirchoff-Love hypothesis for shells [26].

It is necessary to develop the nonlinear displacement cylindrical shell theory in order that the reader obtain an appreciation of the overall theoretical approach. The middle surface strain-displacement relations for a laminate with moderately large rotations of tangents to the panel reference surface are given by

$$\begin{aligned}
\epsilon_x^o &= u^o_{,x} = u_{,x} + 1/2\,\phi_x^2 + 1/2\,\phi^2 \\
\epsilon_y^o &= v^o_{,y} = v_{,y} + W/R + 1/2\,\phi_y^2 - 1/2\,\phi^2 \\
\gamma_{xy}^o &= v_{,x} + u_{,y} + \phi_x\phi_y
\end{aligned} \tag{7}$$

where u, v and w denote the axial, circumferential and radial components of the midsurface displacement and ϕ_x, ϕ_y and ϕ are the components of rotation about the coordinate
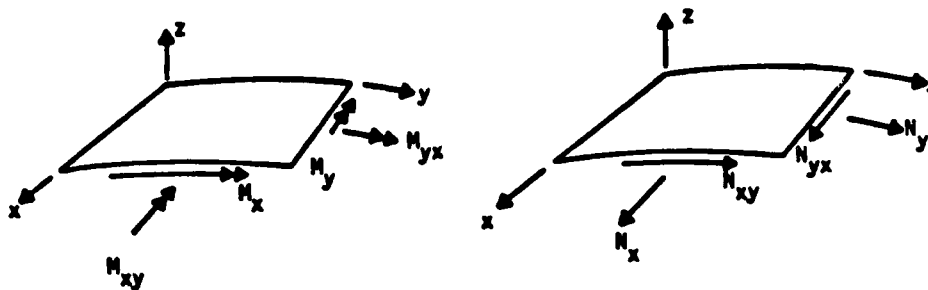
Figure 2.3. Positive Forces and Moments Acting on a Laminate

lines and about the normal to the surface. The middle surface curvatures are

$$\kappa_x = \phi_x,_x$$
$$\kappa_y = \phi_y,_y \qquad\qquad (8)$$
$$2\kappa_{xy} = 2\kappa_{yx} = \phi_y,_x + \phi_x,_y + \phi/R$$

In terms of displacements, the rotation components are

$$\phi_x = -W,_x$$
$$\phi_y = -W,_y + V/R \qquad\qquad (9)$$
$$\phi = 1/2 \ (v,_x - u,_y)$$

where R is the radius of curvature of the panel at the mid-thickness plane. These values for the strains and curvatures are given by Sanders' kinematic relations considering no initial shell imperfections [15].

By using the Kirchoff-Love hypothesis and knowing the

10

middle surface strains and curvatures, the strain-curvature relationship for a laminate becomes

$$
\left\{ \begin{array}{c} \epsilon_x \\ \epsilon_y \\ \gamma_{xy} \end{array} \right\} = \left\{ \begin{array}{c} \epsilon_x^{\,o} \\ \epsilon_y^{\,o} \\ \gamma_{xy}^{\,o} \end{array} \right\} + z \left\{ \begin{array}{c} \kappa_x \\ \kappa_y \\ 2\kappa_{xy} \end{array} \right\}
\tag{10}
$$

By substituting the strain variation through the thickness, Equation (10), into the stress-strain relations, Equation (6), the stress in the kth layer can be expressed in terms of the laminate middle surface strains and curvatures [29] as

$$
\left\{ \begin{array}{c} \sigma_x \\ \sigma_y \\ \tau_{xy} \end{array} \right\}_k = [\bar{Q}]_k \left\{ \left\{ \begin{array}{c} \epsilon_x^{\,o} \\ \epsilon_y^{\,o} \\ \gamma_{xy}^{\,o} \end{array} \right\} + z \left\{ \begin{array}{c} \kappa_x \\ \kappa_y \\ \kappa_{xy} \end{array} \right\} \right\}
\tag{11}
$$

where the $\bar{Q}_{ij}$ elements are as defined in Equation (5).

The resultant forces and moments acting on a laminate are obtained by integrating the stresses in each layer of the laminate. For N_x as a force per unit length and M_x as a moment per unit length, we have

$$
N_x = \int_{-t/2}^{t/2} \sigma_x \, dz
$$

$$
\tag{12}
$$

$$
M_x = \int_{-t/2}^{t/2} \sigma_x \, z \, dz
$$

The forces and moments acting on a flat laminate are shown on Figure 2.3.

11

For an N-layered laminate, the force and moment resultants are [26]

$$
\left\{ \begin{array}{c} N_x \\ N_y \\ N_{xy} \end{array} \right\} = \int_{-t/2}^{t/2} \left\{ \begin{array}{c} \sigma_x \\ \sigma_y \\ \tau_{xy} \end{array} \right\}_k dz = \sum_{k=1}^{N} \int_{z_{k-1}}^{z_k} \left\{ \begin{array}{c} \sigma_x \\ \sigma_y \\ \tau_{xy} \end{array} \right\}_k dz
$$

$$
\left\{ \begin{array}{c} M_x \\ M_y \\ M_{xy} \end{array} \right\} = \int_{-t/2}^{t/2} \left\{ \begin{array}{c} \sigma_x \\ \sigma_y \\ \tau_{xy} \end{array} \right\}_k z\, dz = \sum_{k=1}^{N} \int_{z_{k-1}}^{z_k} \left\{ \begin{array}{c} \sigma_x \\ \sigma_y \\ \tau_{xy} \end{array} \right\}_k z\, dz
$$

(13)

where the kth and k-1 layers are as defined in Figure 2.2.

If one substitutes Equation (11) into Equation (13) and takes into account the fact that the stiffness matrix is constant within the lamina, the stiffness matrix can be pulled outside the integration over each area and then summed with the resultants for each layer. The force and moment resultant equations become

$$
\left\{ \begin{array}{c} N_x \\ N_y \\ N_{xy} \end{array} \right\} = \sum_{k=1}^{N} [\bar{Q}]_k \left[\int_{z_{k-1}}^{z_k} \left\{ \begin{array}{c} \epsilon_x^o \\ \epsilon_y^o \\ \gamma_{xy}^o \end{array} \right\} dz + \int_{z_{k-1}}^{z_k} \left\{ \begin{array}{c} \kappa_x \\ \kappa_y \\ \kappa_{xy} \end{array} \right\} z\, dz \right]
$$

$$
\left\{ \begin{array}{c} M_x \\ M_y \\ M_{xy} \end{array} \right\} = \sum_{k=1}^{N} [\bar{Q}]_k \left[\int_{z_{k-1}}^{z_k} \left\{ \begin{array}{c} \epsilon_x^o \\ \epsilon_y^o \\ \gamma_{xy}^o \end{array} \right\} z\, dz + \int_{z_{k-1}}^{z_k} \left\{ \begin{array}{c} \kappa_x \\ \kappa_y \\ \kappa_{xy} \end{array} \right\} z^2\, dz \right]
$$

(14)

Since the strains and curvatures in Equation (14) are middle surface values and not functions of z, they can be removed from under the summation signs so that Equation (14) can be written as

$$
\begin{Bmatrix} N_x \\ N_y \\ N_{xy} \end{Bmatrix} = \begin{bmatrix} A_{11} & A_{12} & A_{16} \\ A_{12} & A_{22} & A_{26} \\ A_{16} & A_{26} & A_{66} \end{bmatrix} \begin{Bmatrix} \epsilon_x^{\,o} \\ \epsilon_y^{\,o} \\ \gamma_{xy}^{\,o} \end{Bmatrix} + \begin{bmatrix} B_{11} & B_{12} & B_{16} \\ B_{12} & B_{22} & B_{26} \\ B_{26} & B_{26} & B_{66} \end{bmatrix} \begin{Bmatrix} \kappa_x \\ \kappa_y \\ \kappa_{xy} \end{Bmatrix}
$$

$$
\begin{Bmatrix} M_x \\ M_y \\ M_{xy} \end{Bmatrix} = \begin{bmatrix} B_{11} & B_{12} & B_{16} \\ B_{12} & B_{22} & B_{26} \\ B_{16} & B_{26} & B_{66} \end{bmatrix} \begin{Bmatrix} \epsilon_x^{\,o} \\ \epsilon_y^{\,o} \\ \gamma_{xy}^{\,o} \end{Bmatrix} + \begin{bmatrix} D_{11} & D_{12} & D_{16} \\ D_{12} & D_{22} & D_{26} \\ D_{16} & D_{26} & D_{66} \end{bmatrix} \begin{Bmatrix} \kappa_x \\ \kappa_y \\ \kappa_{xy} \end{Bmatrix}
$$

$$(15)$$

where the A_{ij} are called the extensional stiffnesses, B_{ij} are the coupling stiffnesses and the D_{ij} are called the bending stiffnesses.

$$
A_{ij} = \sum_{k=1}^{N} (\bar{Q}_{ij})_k \; (z_k - z_{k-1})
$$

$$
B_{ij} = 1/2 \sum_{k=1}^{N} (\bar{Q}_{ij})_k \; (z^2_k - z^2_{k-1}) \qquad (16)
$$

$$
D_{ij} = 1/3 \sum_{k=1}^{N} (\bar{Q}_{ij})_k \; (z^3_k - z^3_{k-1})
$$

The basic solution technique followed is to use the finite element method in order to find the displacement vector, calculate the middle surface strains and curvature using Sanders' equations, calculate the transformed reduced stiffness matrix and then determine the resultant laminate forces and moments. All the applied forces are known so that the potential energy, as used in the finite element method, can be calculated and thus a check for static equilibrium using a nonlinear solution algorithm can be carried out.

13

STAGSC-1 Theory

The Structural Analysis for General Shells (STAGS) computer program is an energy based finite element program that has been under development by the Lockheed Palo Alto Research Lab since 1967. The latest version, STAGSC-1, is finite element based and uses a Newton-Raphson nonlinear equation solver. STAGSC-1 is a general purpose, thin-shell, structural analysis program that is designed principally for the nonlinear static and dynamic analysis of thin shells [27]. For studies of the collapse of shells with cutouts, the critical axial load is determined by the use of a nonlinear analysis [2].

Sobel [27] points out that the geometrically nonlinear analysis in STAGSC-1 is based on small engineering stress-strain relations ($\epsilon < .1$), moderate rotations (less than 0.3 radians) and incremental solution of force-displacement equations with the modified Newton-Raphson (MNR) method. In the MNR method the stiffness matrix is factored and its inverse is used instead of reforming the matrix for each load step. The matrix is inverted when the solution is slow to converge or diverges. The stiffness matrix is periodically updated (refactored) within the MNR method. Due to the nonlinearity of the problem, the geometric stiffnesses and displacwments are input into the stiffness matrix. At each load increment, a new set of displacement functions is developed. Periodically, the stiffness array is updated to include the new displacement functions.

14

The static, nonlinear problem is a solution of the equations of equilibrium with a Taylor expansion of the total force vector about the currently deformed state. The summation of forces includes all applied, restoring and residual force vectors present in the static equilibrium expressions and can be written as [27]

$$\{F(x_{n+1})\} = \{F(x_n)\} + \frac{d\{F\}}{d\{x\}}\Big|_{\{x\}=\{x^n\}} (\{x_{n+1}\} - \{x_n\}) + H.O.T.$$

$$= F(x_n) + \frac{d\{F\}}{d\{x\}}\Big|_{\{x\}=\{x^n\}} \{\Delta x\} + H.O.T. \qquad (17)$$

$$= \emptyset$$

where H.O.T. represents higher order terms. In this notation, $F(x)$ is the sum of the applied, restoring, and residual force vectors. The value $\{x\}$ defines the currently deformed state. Note that $\{G(x)\}\Big|_{\{x\}=\{x_n\}}$ means the evaluation of the vector $\{G(x)\}$ at the values of $\{x\}$. Therefore,

$$\frac{-d\{F(x_n)\}}{d\{x_n\}} \{\Delta x\} = \{F(x_n)\} + H.O.T. \qquad (18)$$

If one notes that the derivative of the force vector is the negative of the nonlinear stiffness matrix, $[K(x_n)]$, Equation (18) may be written as

$$[K(x_n)] \{ x\} = \{F(x_n)\} + H.O.T. = \emptyset \qquad (19)$$

The STAGSC-1 program treats the left hand side of Equation (19) as a nonlinear operator L acting on the

15

incremental displacements, and thus Equation (17) may be written as

$$\{F(x_{n+1})\} = \{L(x_n)\} - \{R\} + H.O.T. = 0 \qquad (20)$$

where $\{R\}$ is the vector of externally applied forces and the higher order terms are generated by the strain energy and residual forces. The operator L is the first derivative of the strain energy functional [27]. The MNR algorithm used in STAGSC-1 can be written as

$$\{x_{n+1}\} - \{x_n\} = [L'(x_n)]^{-1} \ (\{R\} - \{L(x_n)\}) \qquad (21)$$

where $[L'(x_n)]^{-1}$ is the factored stiffness matrix at some previous step. The nonlinearities included in the computation of $L(x_n)$ are purely geometric. Figure 2.4 represents the MNR algorithm used in STAGSC-1 as a conceptual flowchart. The STAGSC-1 calculation of the vector $\{L(x)\}$ is analogous to the method of calculating a pseudo-force vector to account for nonlinearities [27].

Since the sum of the forces is equal to zero (Equation (17)), the total potential energy must be stationary. The total potential energy of a body is equal to its internal strain energy minus the product of the external forces and deflections and can be written as

$$V = U - W \qquad (22)$$

where W is the work done and U (Equation (23)) is the strain energy of the body.

16
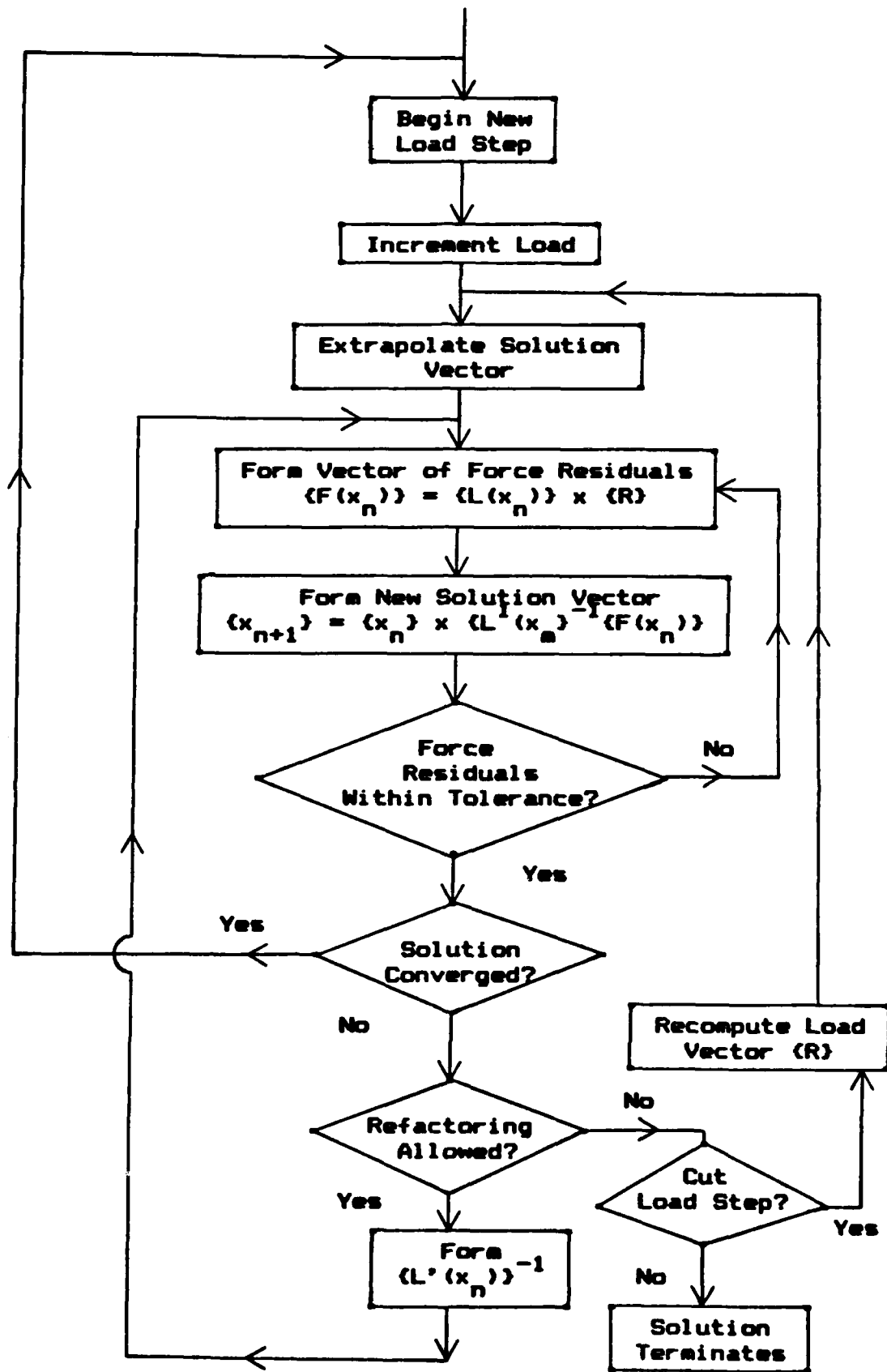
Figure 2.4. Nonlinear Solution Algorithm

17

Therefore,

$$U = 1/2 \int_{Vol} (\sigma_x \epsilon_x + \sigma_y \epsilon_y + \sigma_{xy} \gamma_{xy}) \, d \, Vol \qquad (23)$$

The values for the stresses and strains are calculated as in the Classical Lamination Theory section of this thesis.

STAGSC-1 uses a Cholesky triangular decomposition with forward and backward substitution to solve the equations. Finite element techniques are used to formulate the displacement vector in terms of the element shape functions and nodal degrees of freedom. The displacement vectors are finally calculated using a modified Newton-Raphson iteration scheme. Once this displacement vector is known, stresses, strains and resultant forces can be determined for the incremental loadstep.

Panel Properties

For the finite element analysis, a graphite epoxy composite panel was modeled. The panel was 12 inches long with a chord length of 12 inches, and a radius of curvature of 12 inches. The panel's dimensions and material properties are the same as those used by Hebert [22] and Janisse [23] in their work. Figure 2.5 shows the panel's material properties, dimensions and sign conventions. The cutout is shown on Figure 2.5 with dimensions a and b. The values for the corresponding dimensions of the notches and cutouts studied are listed in Table 2.1. The panel has a
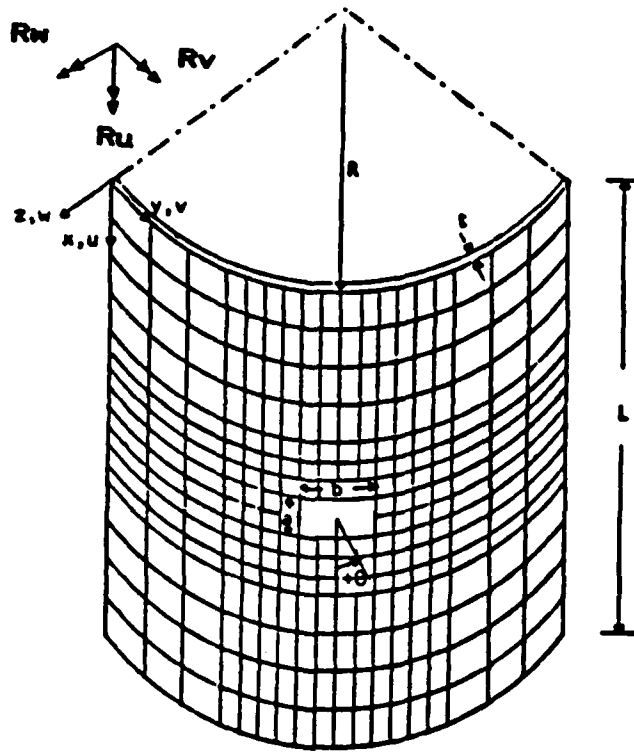
Dimensions and Material Properties

Material: Graphite-Epoxy

Radius: R = 12"

Length: L = 12"

Number of Plies: 8

Orientation of Plies, θ: $(0,45,-45,90)_S$

Thickness: 8 plies at .005" = .04"

Elastic Moduli: E_1 = 20500 ksi, E_2 = 1300 ksi

Shear modulus: G = 750 ksi

Poisson's Ratio: ν_{12} = .33

x, y, z: Structural Coordinates

u, v, w: Displacements

Ru, Rv, Rw: Rotations

Figure 2.5. Panel Notation and Material Properties

19

Table 2.1

Dimensions of Cutouts Analyzed

Size of Cutout
(inches)

a	b
2	2
1	2
2	2
2	4
4	2
4	4

symmetric ply layup $[0,45,-45,90]_S$ consisting of 8 plies of 0.005 inches each for a total panel thickness of .04 inches.

For all but the 2"x2" notch, a symmetric set of boundary conditions were used. The top of the panel was clamped with only the u displacement free. The vertical edges of the panels had the u and v displacements (x and y direction displacements, respectively) and rotation about the x axis, Ru, free. The bottom of the panel was clamped with no free degrees of freedom (DOFs). Refer to Figure 2.5 for displacement and rotation vectors.

The 2"x2" notch was used for the boundary condition study in which unsymmetric sets of boundary conditions were evaluated in addition to the symmetric boundary conditions used for the other cutouts. The four sets of unsymmetric boundary conditions evaluated are listed in Table 2.2.

Table 2.2

Unsymmetric Boundary Conditions for the 2"x2" Cutout

Boundary Condition	1	2	3	4
Top of panel	u free	u free	u free	u free
Right side of panel	u, v, Ru free	Top half: u,Ru free; Bottom half: u, v, Ru free	u, v, Ru free	u, v, Ru free
Bottom of panel	clamped	clamped	clamped	clamped
Left side of panel	Top half u,Ru,free Bottom half: u, v, Ru free	u, v, Ru free	Top edge: u, v ,Ru free Middle: Ru free Bottom half: u, v, Ru free	Top 1/4: u,Ru free Bottom 3/4 u, v, Ru free

ALL OTHER DOFs WERE FIXED

Element Selection

The element selected for this analysis is a quadrilateral plate element referred to as the QUAF 411 in the STAGSC-1 documentation [25]. This is the same element used by Janisse [23]. The QUAF 411 has 32 DOFs; 3 translational rotations, 2 in plane rotations and 2 independent normal rotations at each corner node, plus tangential displacements at each of the four midside nodes. Figure 2.6 shows the QUAF 411 with its DOFs. The QUAF 411
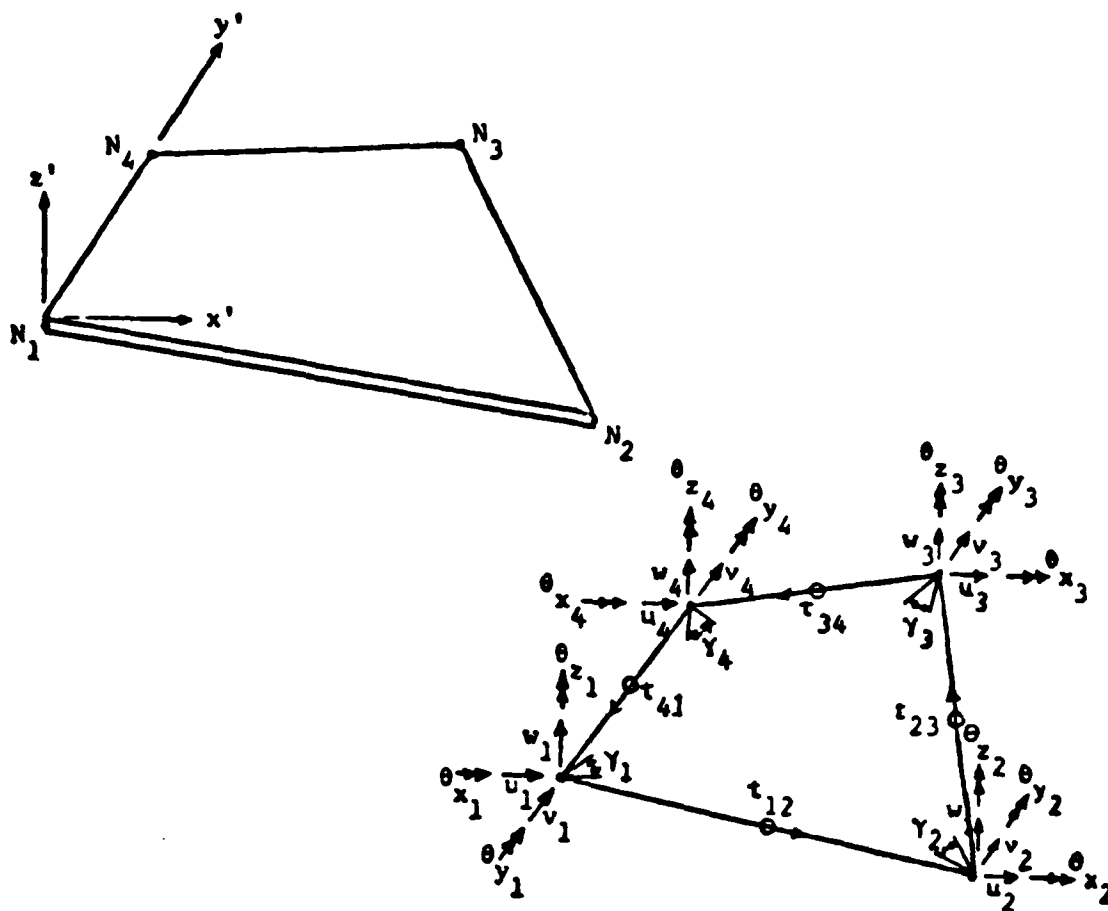
Figure 2.6. Quadrilateral 411 Plate Element with
Local Coordinate System

element was developed to remove the displacement
incompatibility which exists when flat shell elements do not
lie in the same plane [27]. If the edge displacements are
to be compatible, the transverse displacement shape
functions must be of the same order as the in-plane shape
functions which are cubic. Element 411 has two rotations
at each corner node which permit individual rotation of each
adjacent side and therefore allow shear strain at the
corners. The shape functions for the 411 element are cubic
parallel to the edge and quadratic perpendicular to the edge

for in-plane displacements. The bending shape functions are cubic in both directions [27]. Since the panels studied in this thesis require the nonlinear collapse analysis branch of STAGSC-1 which uses large displacement theory and moderate rotations, the extra DOF at the corner node and the translational DOF at the midside node make the QUAF 411 element the best available element. A drawback to the QUAF 411 element is that there is no transition element in the STAGSC-1 library, so a constant grid size must be used [27].

III. DISCUSSION AND RESULTS

Finite Element Mesh Refinement

A mesh refinement study was conducted on the panel with the 2"x2" notch to determine an optimal finite element mesh arrangement. A viable tradeoff between improved results due to an increased number of data points and the corresponding increase in computer time had to be considered. The results from this convergence study were then applied to the design of the finite element mesh for other panels.

Initially, a finite element mesh consisting of 13 rows and 13 columns of one inch square QUAF 411 elements was tested. This mesh is referred to as the coarse mesh. In a finite element method for solving a continuum mechanics problem, the approximation improves as more elements are used [28]. Therefore, the 13x13 mesh provides the roughest approximation for the panel's behavior. The coarse mesh was then refined by cutting the elements immediately around the cutout into one half-inch square elements. Due to the fact that there is no transition element for the QUAF 411 element, some elements in the mesh are rectangular when the mesh is refined.

The rectangular elements have aspect ratios that are not unity. Aspect ratio will be defined as the length of the element in the x (axial) direction, divided by the length of the element in the y (circumferential) direction. An element with an aspect ratio of one does not experience

24

TABLE 3.1

Mesh Refinement Results for a 2" x 2" Notch

	13x13	17x19	19x17	19x19	21x19	25x25
NDOF (Active)	1203	2381	2395	2705	3029	5029
Bandwidth	97	129	128	145	145	192
CPU Time to Collapse Load (sec)	545	1156	925	1097	1582	4852
Collapse Load (lbs/in)	217.6	208.1	217.3	207.3	207.6	191
Difference From 25x25 Grid (%)	12.2	8.2	12.1	7.9	8.0	—
Number of Load Steps	28	26	21	20	26	22

the biases introduced when using elements with different magnitudes of length in the x and y directions. Cook [28] states that a desirable, but not mandatory, requirement for convergence is that an element should have no preferred directions. In other words, the element should be geometrically invariant. Various mesh refinement arrangements were tested to determine how elements with aspect ratios other than unity affected the behavior of the panel.

The results of the mesh refinement study can be found in Table 3.1. In this table, CPU (Central Processing Units) time is the amount of computer time used to reach collapse load. The bandwidth is the full bandwidth used for matrix storage in the finite element analysis. The number of load

steps is the number of times a load increment was applied. As collapse load is approached, the computer program cuts the load increment to achieve convergence. The results, as shown in this table, for the 25x25 grid (consisting entirely of one half-inch square elements) are taken from Janisse [23]. The coarse grid had a collapse load that was 12.2% higher than the 25x25 grid but took 88% less computer time. Janisse [23] also found that the collapse load for a coarse grid was 18% higher than experimental results, referred to subsequently, (experimental collapse load was 2121 lbs) whereas the 25x25 mesh had a collapse load that was only 7.5% higher than the experimental collapse load. The mesh refinement study is a method for determining the best way to more closely approximate experimental results, without using an unreasonable amount of computer time.

Figure 3.1 shows the refined mesh in the vicinity of the cutout for each of the different mesh arrangements studied. By comparing the results for the 17x19 and 19x17 grid, one can observe that the 17x19 grid more closely approximates experimental collapse load but uses 20% more computer time than the coarse mesh. The 19x17 mesh does not show an improvement in collapse load, indicating that elements with an aspect ratio of .5 hinder the advantages that are expected when refining a mesh. The 19x19 mesh had half-inch square elements a uniform distance of 2 inches from the opening. This refinement was found to more closely approximate the collapse load while using 23% less computer time than the 25x25 grid. A further grid refinement to a
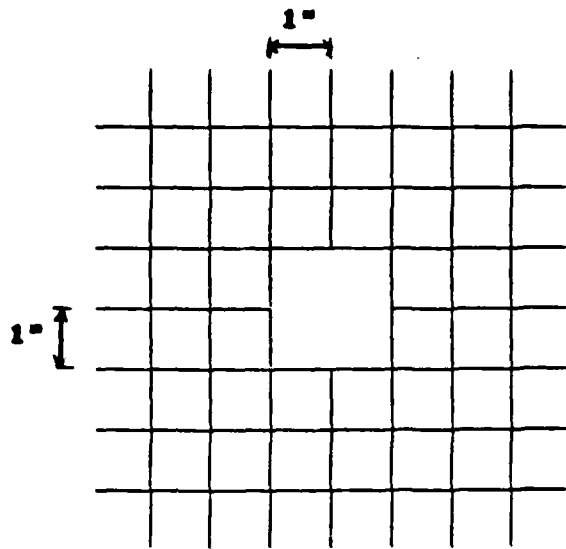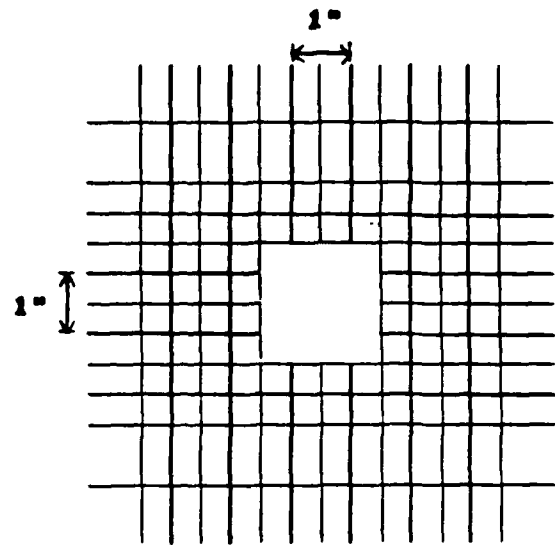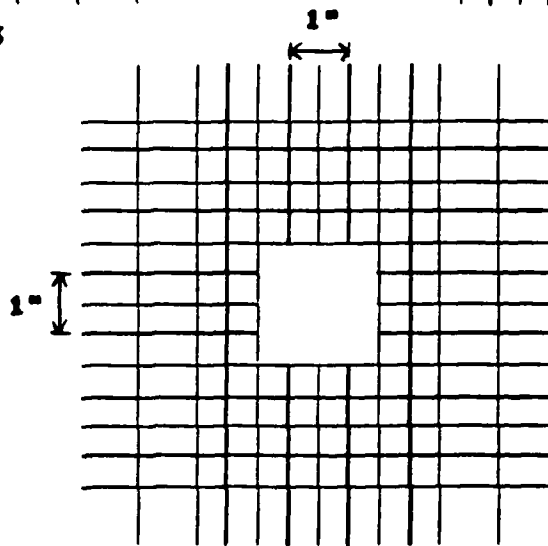
Figure 3.1. Refined Meshes for 2" x 2" Notch

21x19 mesh did not improve the collapse load approximation over values obtained for the 19x19 mesh, but used almost 500 seconds more computer time than the 19x19 mesh. From a collapse load approximation point of view, the 19x19 mesh is the best refined mesh to choose.

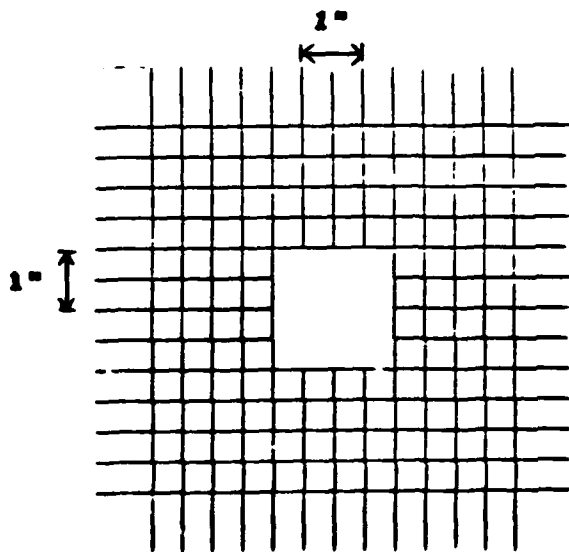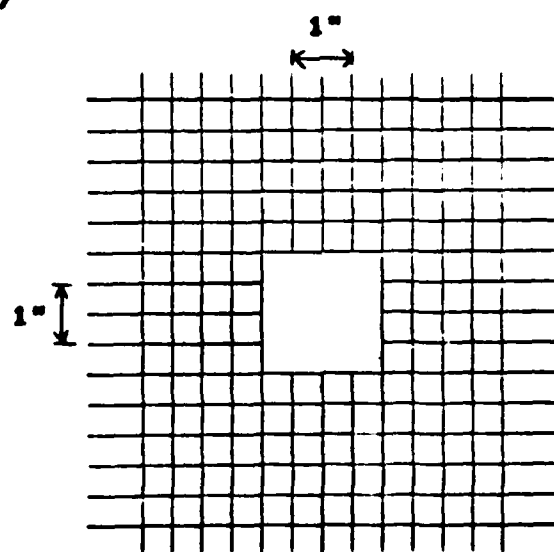To further analyze the meshes, the values for the moments, M_y and M_x, and force N_y, were compared in the vicinity of the notch. (Refer to Figure 2.3 for the individual forces and moments acting on a laminate). These force parameters were chosen for analysis because they are important components in a collapse analysis. Each functional value was compared along rays at different angles extending from the upper left corner of the notch. Figure 3.2 is a comparision of M_y versus distance from the corner of the notch for all five meshes along an outward ray at 135° from the upper left corner of the notch. The 13x13 mesh provides the least accurate approximation for behavior because it has fewer elements. As the mesh is refined, the values of M_y for each of the cases tested begin to cluster together. The 19x17 mesh does not follow the convergence pattern of the other three refined meshes. Over 1.5 inches from the opening where the rectangular elements start, the values for M_y diverge. The elements with a .5 aspect ratio are only an inch away from the opening thus not allowing an improvement in results as would be expected with a refined mesh. The .5 aspect ratio elements are longer in the circumferential direction and therefore the moment about the x axis, M_y, appears to be adversely affected by the
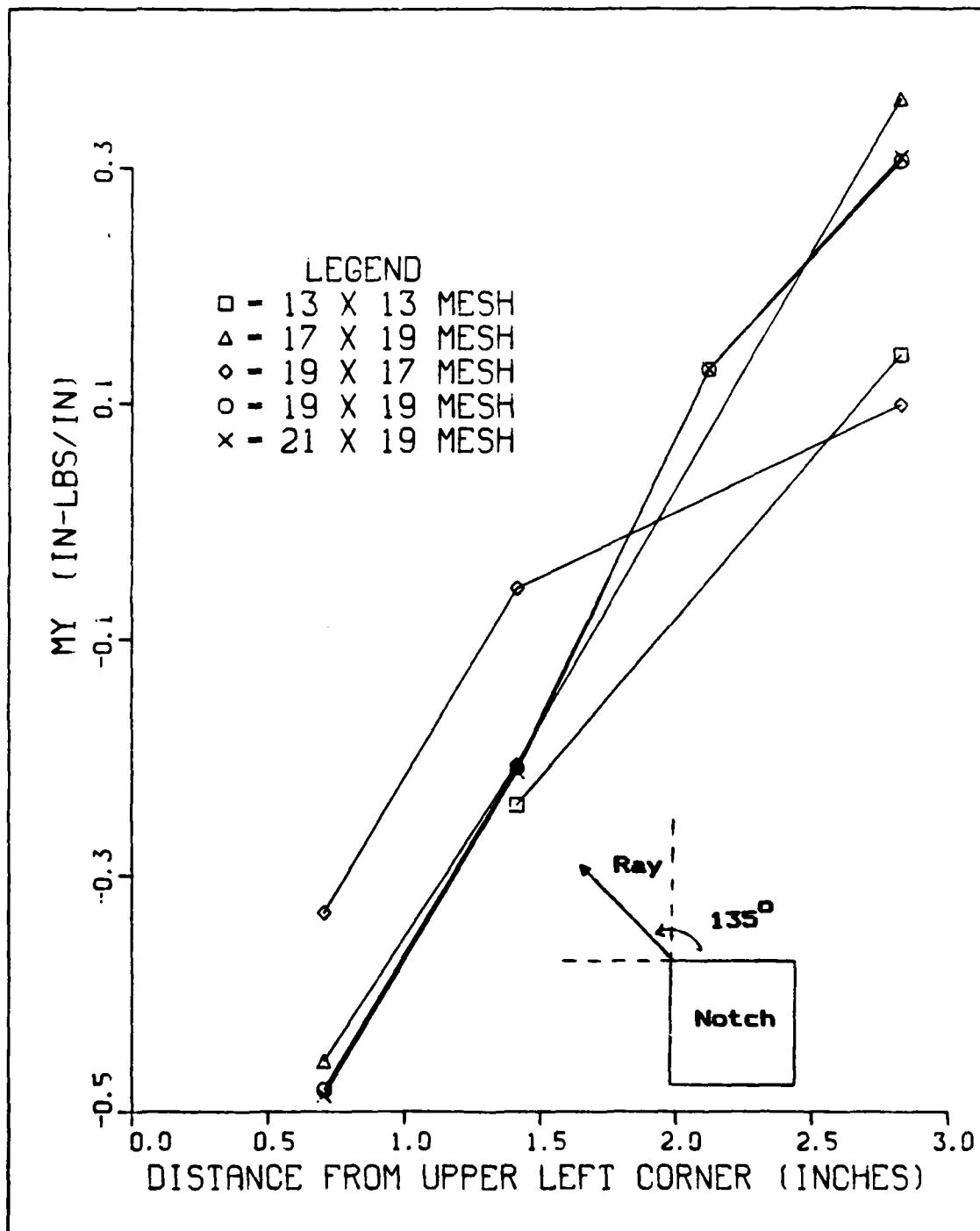
Figure 3.2. Moment about X Axis versus Distance from
Corner along a Ray at 135°

shorter dimension in the axial direction. An element with an aspect ratio of 1 does not seem to experience the difficulties associated with an oblong element. The results for the 19x19 and 21x19 mesh do not differ significantly.

To examine the meshes further, values for M_x along a line at 45° from the corner are compared in Figure 3.3. Even though the magnitude of the moment is small, the values for each of the meshes are consistent from a finite element model point of view. As the mesh is refined, the values for M_x begin to cluster together except for the coarse mesh. The 17x19 mesh diverges from the others over 1.5 inches from the corner where elements with an aspect ratio of 2.0 start appearing in the mesh. The divergence for the 17x19 mesh is noted in Figure 3.3 whereas it did not happen in Figure 3.2. This is due to the fact that Figure 3.3 is a plot of moment about the y axis, M_x, so elements with the longer dimension in the vertical direction affect the behavior of the panel. This leads to the conclusion that the mesh should be refined equidistant around the cutout, as can be seen from the 19x19 mesh arrangement in Figure 3.1.

A further refinement, the 21x19 grid, does not improve the results for M_x or M_y over the 19x19 mesh. The 21x19 also does not adversely affect the values for M_x or M_y. This is because the oblong elements are far enough away from the cutout so as not to cause problems with the results. Since the 21x19 mesh does not improve results but uses more computer time, the 19x19 mesh appears to be the optimum finite element mesh for the 2"x2" notch.
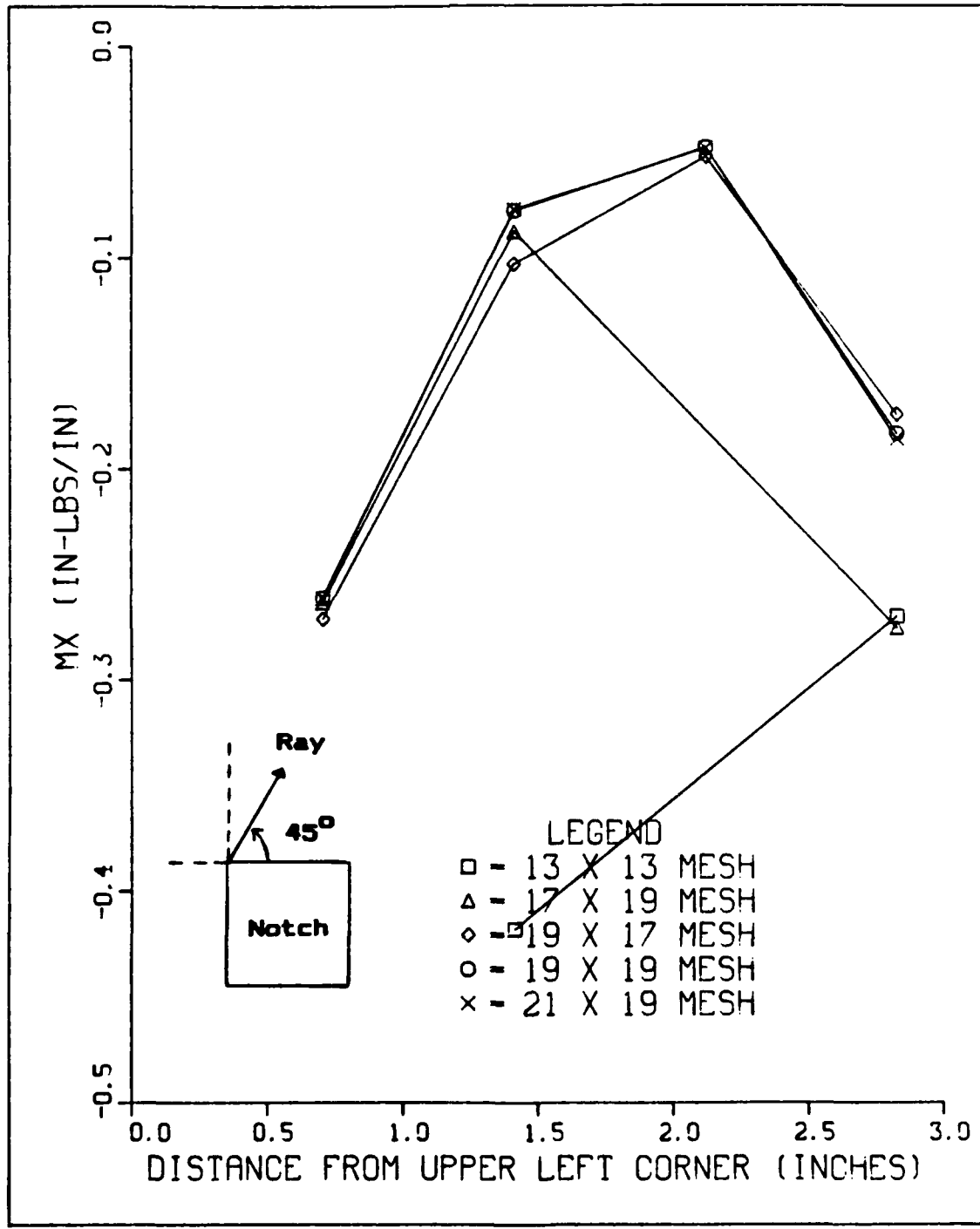
Figure 3.3. Moment about Y Axis versus Distance from Corner along a Ray at 45°

31

One additional parameter, force in the y direction, N_y, was examined (Figure 3.4) along a ray at 90°. The mesh characteristics follow the refinement in a similar fashion to the moment function comparisons. All of the refined meshes are good approximations over the coarse mesh for the force function.

From examining the mesh parameters, the 13x13 mesh is the least accurate due to the fewer number of elements used in the numerical approximation. With the 17x19 and the 19x17 meshes, difficulties arise when considering the moments about axes in the direction of the shorter dimension of the oblong element. The 19x19 mesh has elements with an aspect ratio of 1 over a uniform distance from the opening. This mesh experienced no irregularities when approximating moments. A more refined mesh (21x19) gave no significant improvement for values in the vicinity of the notch. Oblong elements greater than 2 inches from the cutout had no adverse effects on the buckling behavior of the panel.

The results from the mesh refinement study were next applied to the finite element mesh for the other panels tested. As stated earlier, it is best to refine the mesh evenly around the cutout. If this is not possible due to the size or positioning of the cutout, elements with an aspect ratio other than unity should be at least four square elements from the cutout. Elements with aspect ratios of .5 adversely affect M_y and collapse load, and should be at least 2 inches from the cutout. Elements with aspect ratios of 2 affect M_x and should be at least 1.5 inches from the
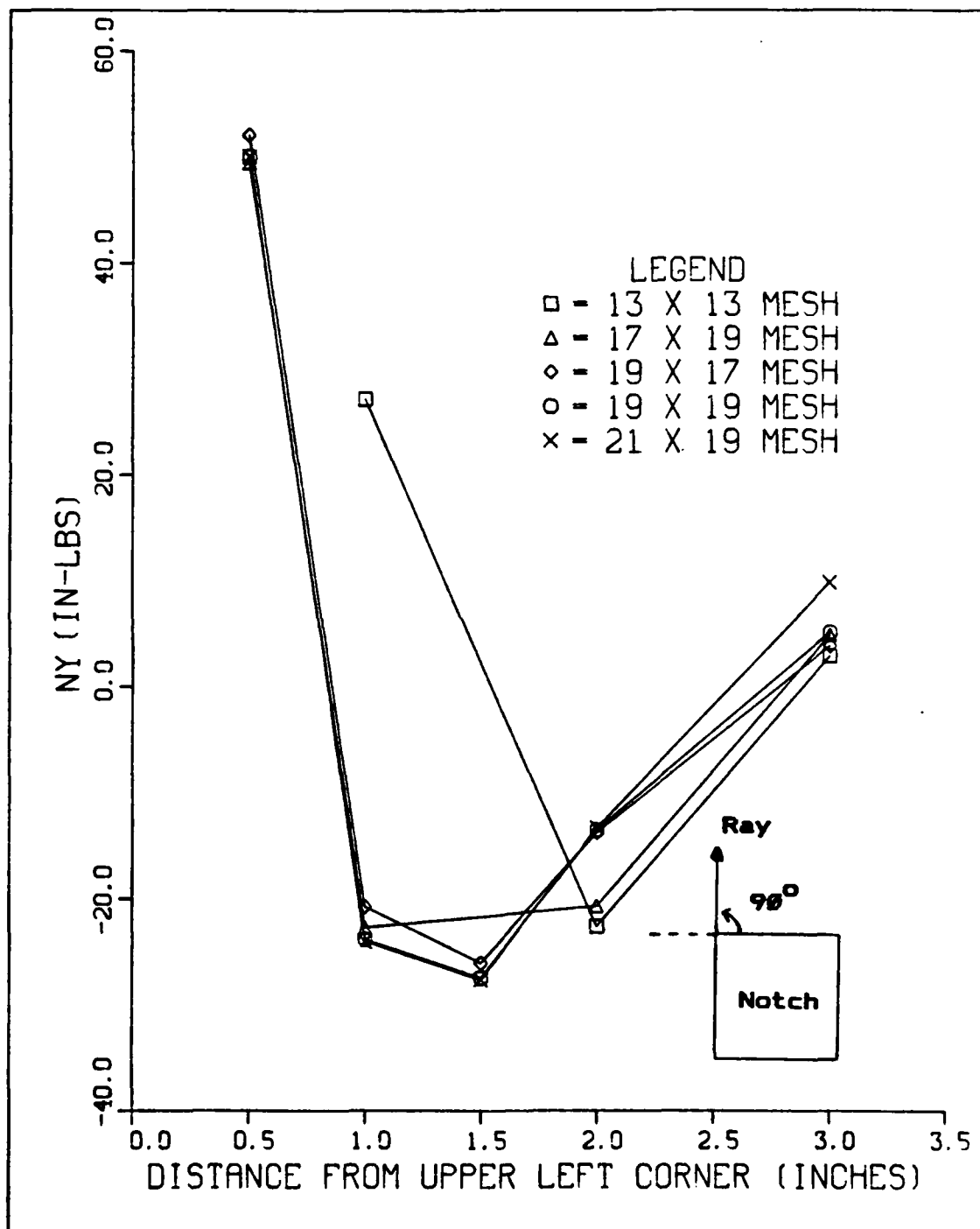
Figure 3.4.   Axial Force, N_y, versus Distance from

Corner along a Ray at $90°$

cutout. The mesh arrangements chosen for each of the notches will be discussed later in this thesis.

Boundary Condition Study

An experimental study has previously been carried out by the Fatigue, Fracture and Reliability Group of the Air Force Wright Aeronautical Laboratories at Wright-Patterson AFB considering a 2"x2" notch within the same type of grapite-epoxy panel described previously. An attempt to simulate a simple support boundary condition along the vertical edges, and clamped at the top and bottom was carried out. Results from this study, referred to in subsequent paragraphs, indicated that the experimental boundaries were not acting as originally assumed, yet collapse load was within approximately 10% of the experimental value. Thus, the author conducted a finite element study of varieties of boundaries to try to approximate the actual boundaries present within the experiment. It is, to the best of the author's knowledge, the first attempt at numerically simulating an experimental set of boundaries for a composite panel with a given size notch.

Several different boundary condition cases were studied for the 2"x2" notch with the refined mesh in an attempt to more realistically model the experimental results. Four different sets of unsymmetric conditions were modeled (Table 2.2) along with the symmetric boundary conditions described

34
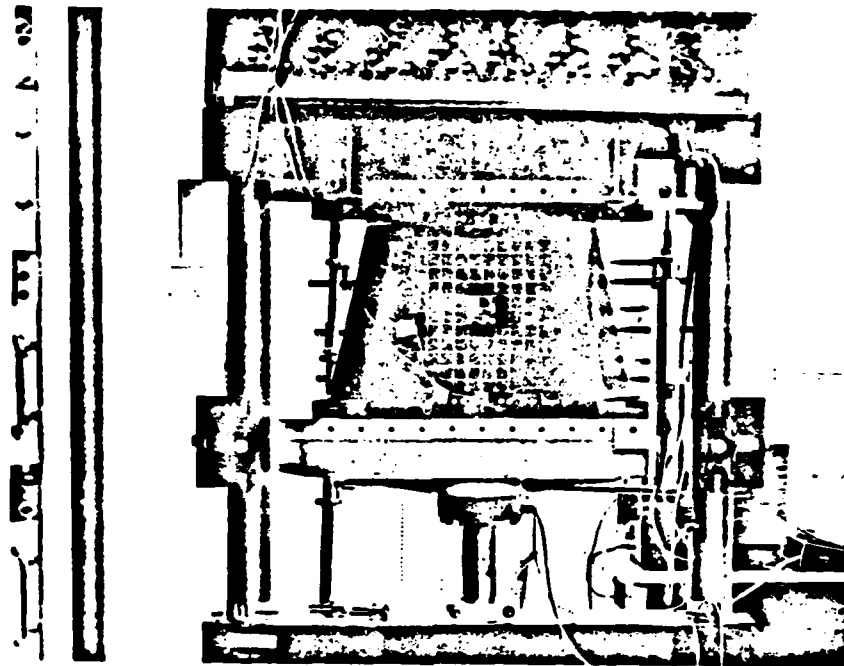
Figure 3.5. Test Apparatus with Panel

in Section II of this thesis.

The experimental text fixture (Figure 3.5) was similar to that used by Hebert [22] and Janisse [23]. The panel was fabricated from NARMCO T300/5208 graphite-epoxy. A two inch square hole was cut out of the center of the panel. The corners of the cutout were machined to be slightly rounded (1/16 inch radius) rather than a perfect square cutout so that there are no singularities at the corners. For a more detailed description of the test apparatus, see Reference [22]. The experimental apparatus was modified for this testing by placing Linear Variable Differential Transformers (LVDTs) at various locations on the panel to measure out-of-

2.5"　　2.5"　　1"　1"　　2.5"　　2.5"

2.5"

5
(-.0165")

2   # 3   # 4
•   •   •
(.00245")   (-.0171")   (-.0125")

2.5"

6
(-.0350")

5   # 6

10
(-.0112")

1"

7   # 10   # 11   # 12
•   •

11
(-.0006")

1"
(-.0244")   (-.0035")

14   # 16

14
(-.0098")

2.5"

16
(-.0101")

13   # 15   # 17
•   •   •
(-.0013")   (.0051")   (.0045")

2.5"
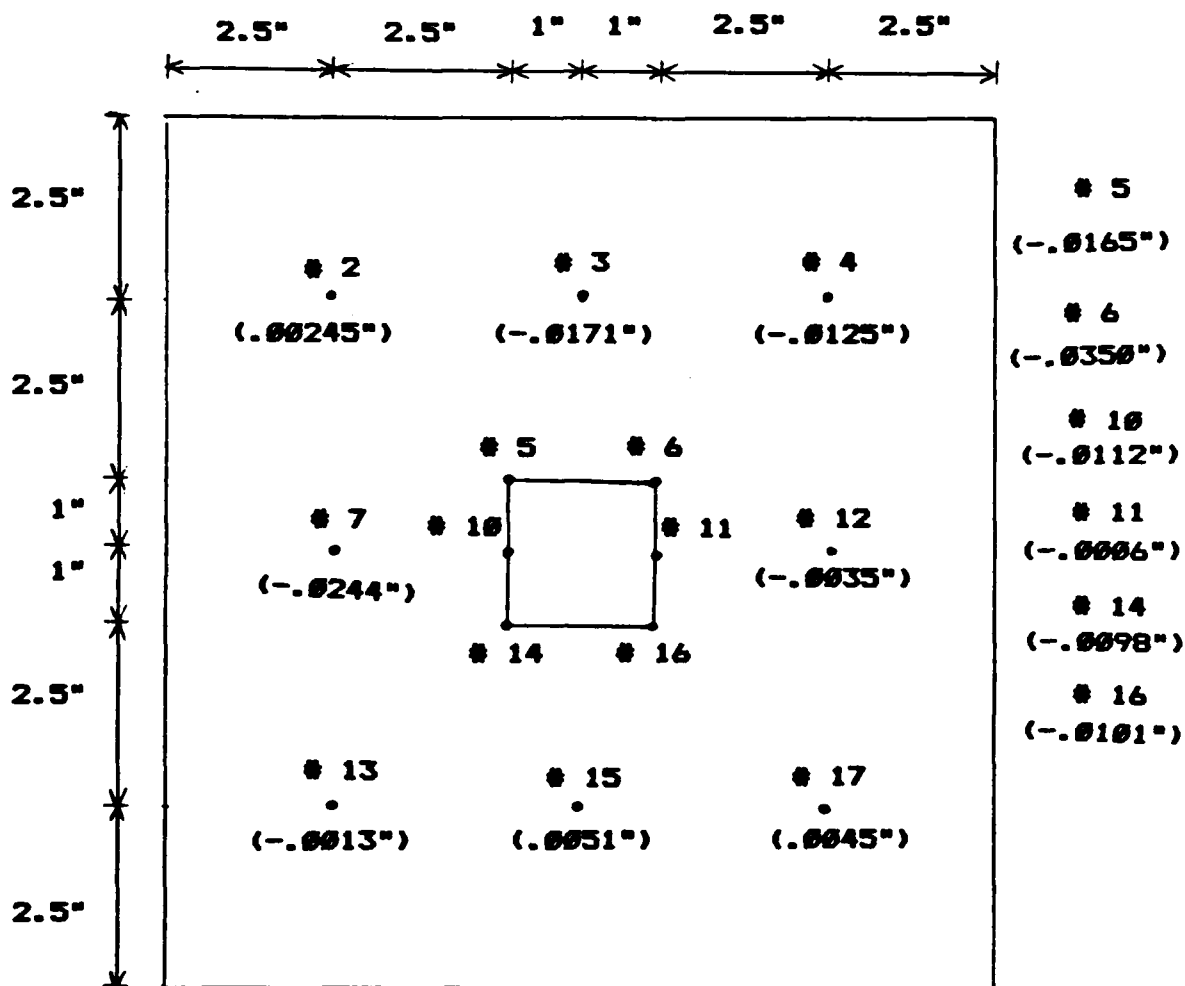
Note: 0.0 inch initial displacement along top and
      bottom edges

Key: •   LVDT Location
        ( ) Initial Radial Displacement or
             Surface Imperfection

Figure 3.6. LVDT Location and Initial Radial Displacement

on Experimental Panel

plane (radial) displacements. Figure 3.6 shows the locations of the LVDTs on the panel as viewed from the front of the panel (panel radius into the page).

Various analytic boundary conditions were examined in addition to the symmetric boundary conditions, because previous studies did not model experimental results precisely. During the experimental testing, depressions in the teflon tape that held the panel into the side restraints were noted. The teflon tape on the left side of the panel had the largest depressions. This indicated that the experimental boundary conditions were changing from the initial conditions. An attempt at modelling this phenomena, was carried out by fixing the v displacement first on the upper half of the left side of the panel, and then on the upper half of the right side. Next, the v displacement was held on the upper quarter of the left side of the panel. Finally, both the u and v displacements were fixed between 1 inch to 6 inches down the left edge of the panel. These results, along with the results for the symmetric boundary, were compared to the experimental findings. Radial displacements at several different LVDT locations were compared as a function of load.

The experimental panel was also examined in order to see if there was any initial eccentricity or displacements introduced into the panel by the test apparatus prior to the loading. The initial radial displacements of the panel were measured by use of a set of dial vernier calipers. This device was also used by Hebert [22] to measure surface

37

imperfections. Using 0.0 as a datum surface, positive displacement is measured radially outward. The top and bottom of the panel were designed to be at a displacement of 0.0. Theoretically, if the panel is manufactured and mounted perfectly, the entire panel would have an initial radial displacement of 0.0. Figure 3.6 shows the initial radial displacements at each of the LVDT locations.

At the point corresponding to LVDTs 2 and 17 there is an outward bulge, whereas in the vicinity of the cutout, there is a negative displacement. These eccentricities can mainly be attributed to initial inaccuracies introduced by the test facility when mounting the panel in the test apparatus. The effect that these initial eccentricities have on the actual panel as compared to analytic results can be seen in Figures 3.7 through 3.11. In these figures, boundary conditions 1, 2, and 3 are as listed in Table 2.2. Boundary condition 4 in Table 2.2 was considered but not plotted because the results did not differ significantly from the results for boundary condition 1.

Analytical and experimental results for the radial displacement at LVDT location 2 are compared in Figure 3.7. One can observe that the variety of boundary conditions tested fall significantly away from experimental data. The author notes that the boundary condition in itself does not solely affect the displacement of the panel. The effect that the overall initial negative displacement has on the experimental results at LVDT location 2 can be seen in Figure 3.7. The experimental data shows that the panel at

38

point 2 is initially displaced outward, but as the load is applied, the point starts to bow out and then appears to reverse its motion and maintains an almost linear relation as a function of load. A possible course for this phenomena may be explained by the fact that the negatively displaced area around the cutout acts as a restraining force analagous to a support. The area absorbs moments and acts similar to a depressed clamped edge. This appears to cause a constant displacement function of experimental data for point 2 because the cutout area is holding the panel and preventing it from moving in the direction of its initial displacement. The analytic results for all of the boundary conditions tested are very similar and do not approximate the experimental results at point 2 as well as one would like.

By comparing analytic and experimental results for radial displacement at LVDT location 3, Figure 3.8, one can see that the results for boundary condition 3 better approximate with experimental data. At point 3, the results for boundary condition 3 show almost no radial displacement. This implies that the effect of boundary condition 3 is to physically create a counterflexure point at the given LVDT location and therefore will theoretically have no moment in the y direction. The effect of the eccentricities can also be observed in Figure 3.8. The cutout area is more depressed than the panel around point 3 and therefore restrains the point. One would expect point 3 to move inward, but the panel in the vicinity of the cutout restrains the movement and as the applied load reaches 500
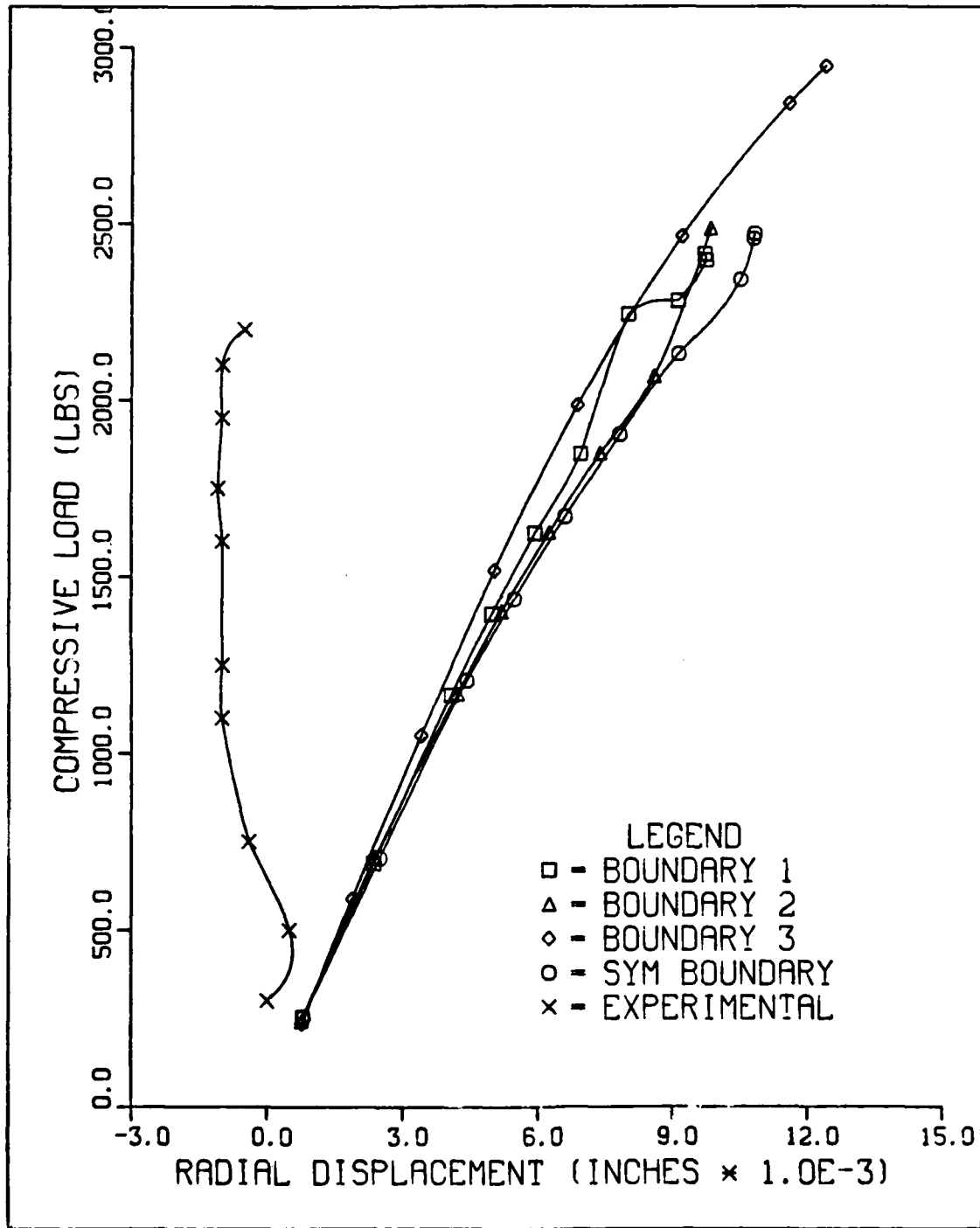
39

Figure 3.7. Radial Displacement Plot, for Boundary Conditions Studied, at LVDT Location 2
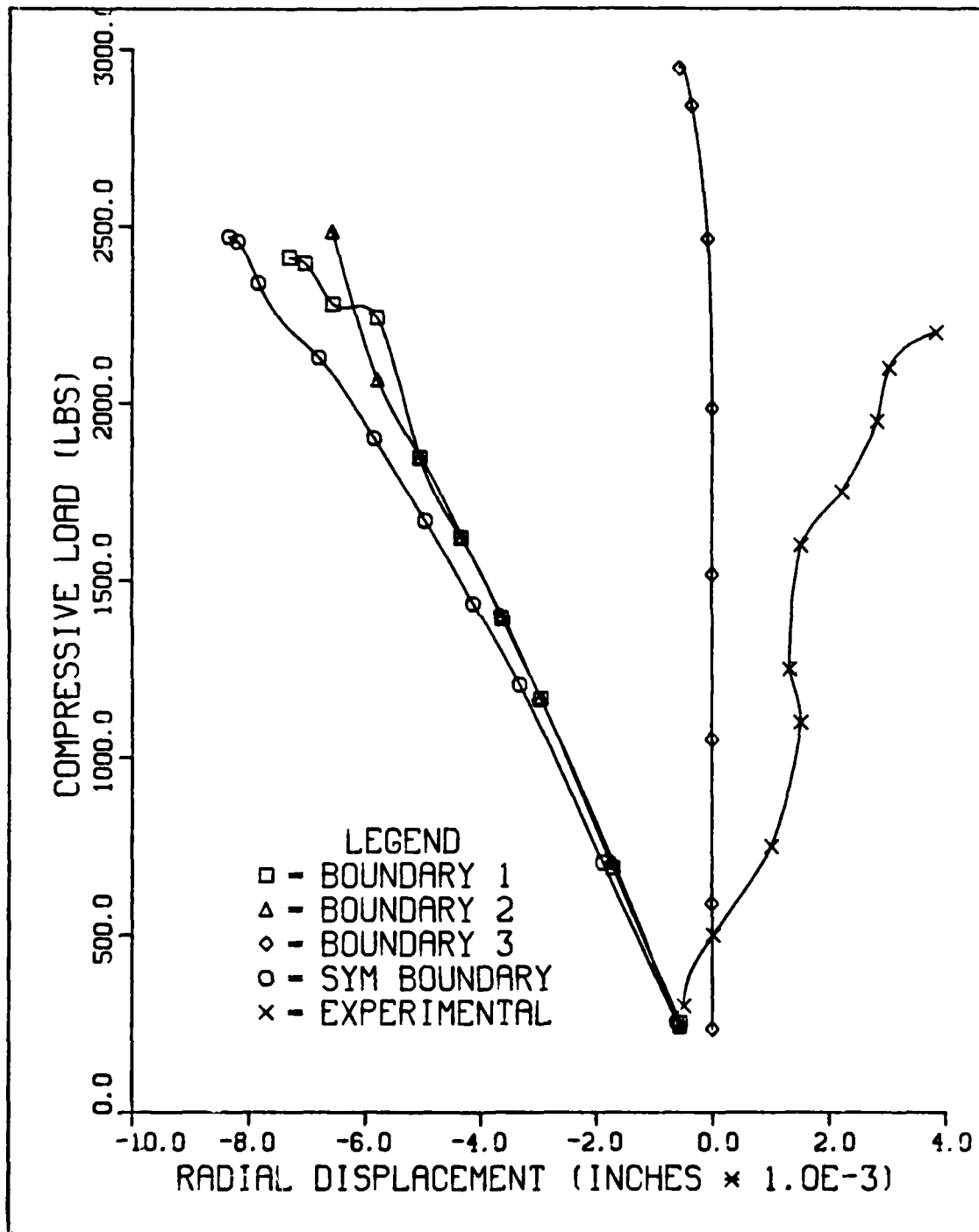
Figure 3.8.   Radial Displacement Plot, for Boundary

Conditions Studied, at LVDT Location 3

41

lbs, the displacement reverses since the area around the cutout is acting analogous to like a support. It therefore appears that point 3 is experimentally undergoing displacement as a function of surface imperfections and a change in boundary condition similar to analytic bounary condition 3 which is a restrained edge.

If one examines the panel at LVDT 4 in Figure 3.9, it is observed that the large initial displacements at the upper right corner of the cutout (corresponding to LVDT 6) acts analogous to a folded plate and causes point 4 to displace outward. There is a tendency for the area of the cutout to restrain areas of the panel. Although there is no applied force at the cutout, the restraint generated is due to the radial location of the cutout. The area of the cutout is initially displaced inward more than LVDT location 4. This causes more moment restraint to act on point 4 with increasing load as the area around the cutout acts similar to a folded plate. This phenomena can only be modeled analytically if the surface eccentricity is precisely incorporated into the finite element model. These displacement characteristics appear to be happening experimentally. At an applied load of about 1500 lbs, the experimental data shows that point 4 starts shedding or redistributing its load and begins to move radially inward. Boundary conditions 1, 2, and the symmetric conditions approximate the behavior well up to about 1500 lbs. Boundary condition 3 bounds the experimental data on the other side. This seems to indicate the boundary conditions
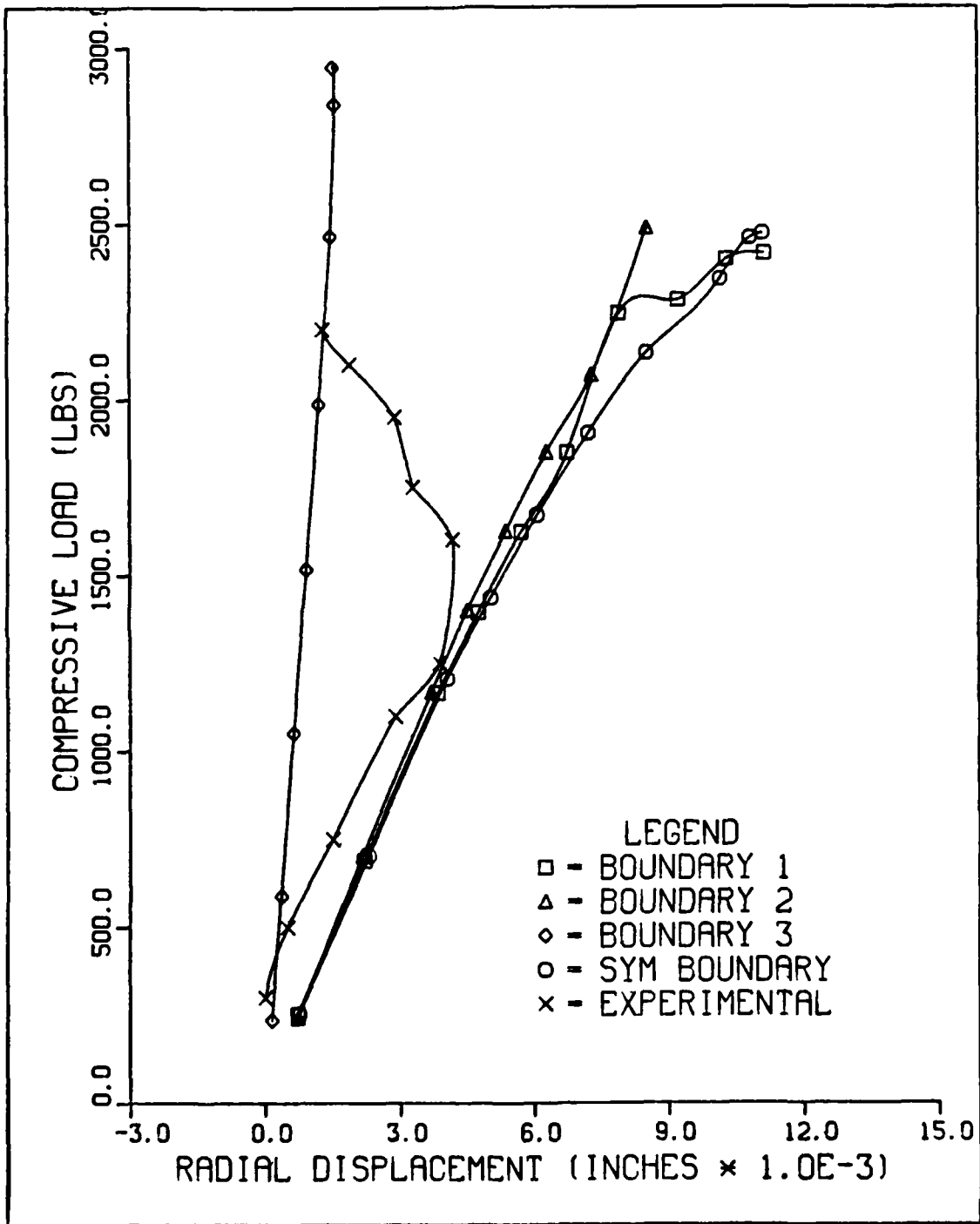
42

Figure 3.9. Radial Displacement Plot, for Boundary
Conditions Studied, at LVDT Location 4

tested in this thesis for point 4 bound the experimental displacement data, and the actual conditions to be applied analytically are somewhere in between these cases. This is due to the fact that boundary condition 3 was applied from the onset of the load application process. The experimental results indicate that there is some sort of restraint affecting point 4. Boundary condition 3 best models this at higher loads when the change begins to occur experimentally.

Figure 3.10 compares the analytic and experimental results for radial displacement at LVDT location 11. Boundary condition 3 generally shows the same trend of displacement as experimental results. When the effect of the boundary condition is considered along with initial surface imperfections, the translation between the two curves can be attributed to the effect of the initial eccentricities.

Boundary condition 3 does not affect the results for displacement at point 17 (Figure 3.11) as it did for the other points considered. This is largely due to the fact that point 17 is a greater distance from the changing boundary than the other points. All the analytic boundaries approximate the radial displacement at point 17 to the same degree because the point is so far removed from the boundary that the action of the restraint is not felt.

In addition to the initial eccentricities causing the test panel to behave differently from analytic results, it is noted that each point on the test panel does not start at a datum of 0.0, but rather at an amount of the initial
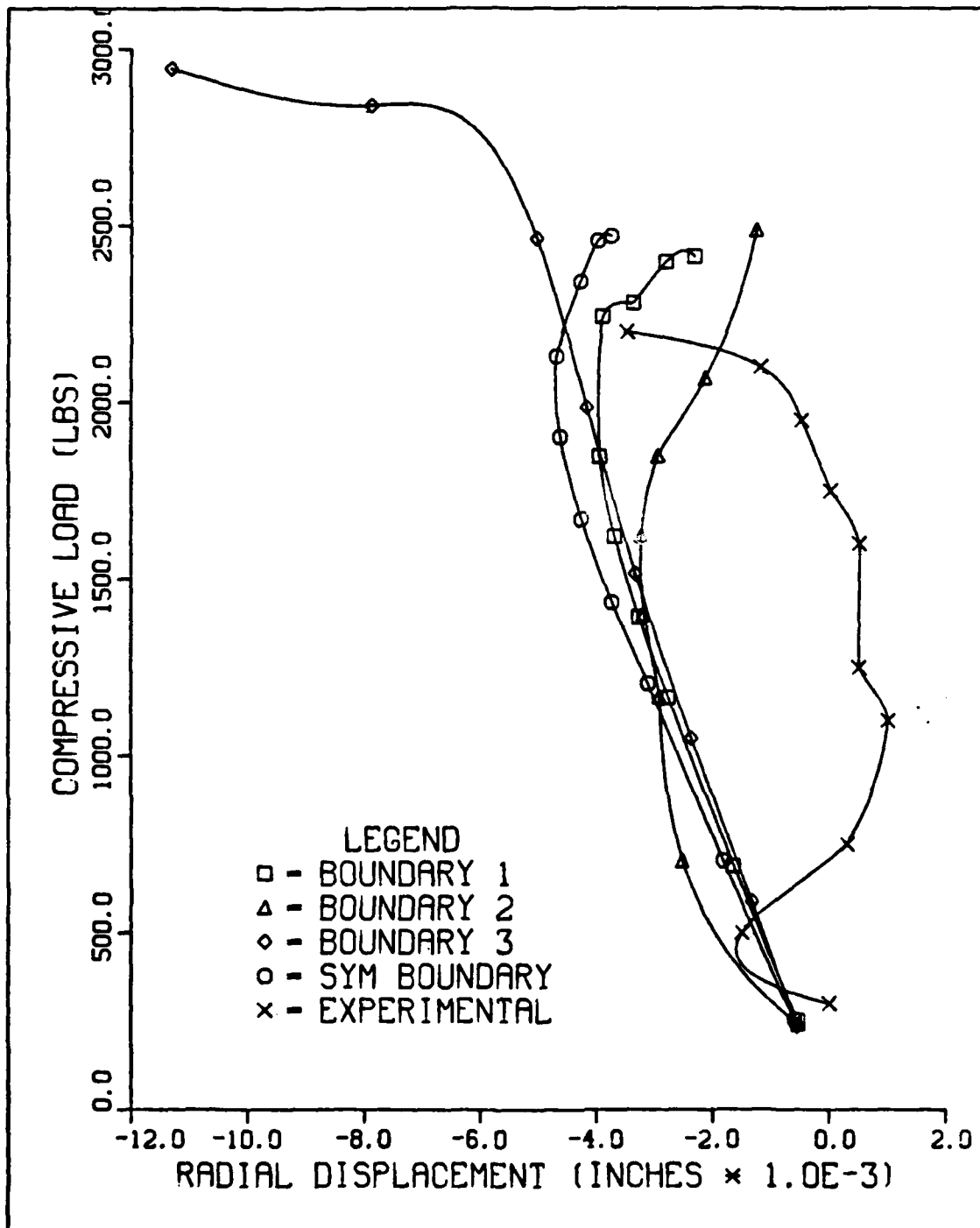
44

Figure 3.10. Radial Displacement Plot, for Boundary
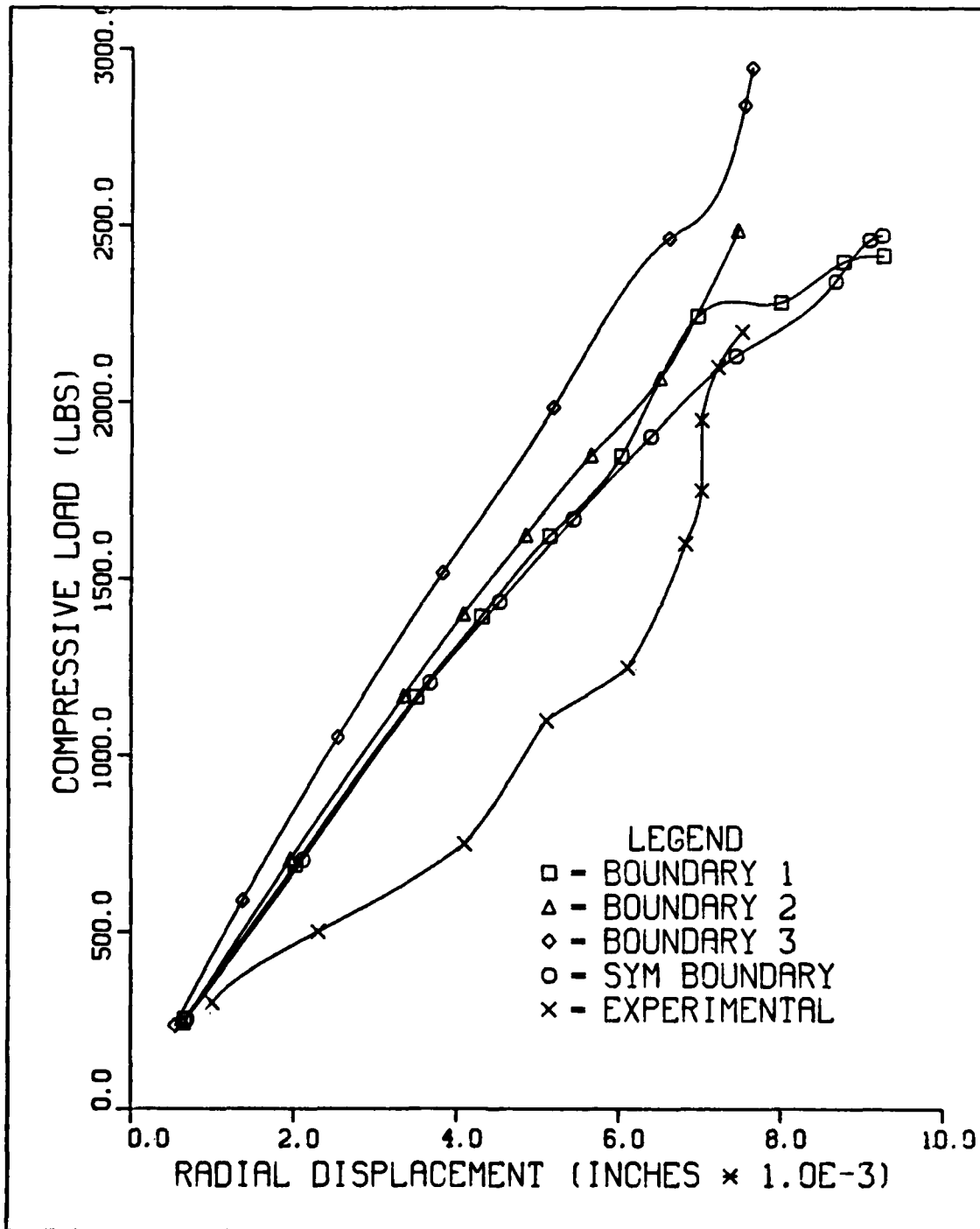Conditions Studied, at LVDT Loacation 11

45

Figure 3.11. Radial Displacement Plot, for Boundary Conditions Studied, at LVDT Location 17

displacement from as the datum. This means that each of the experimental curves on Figures 3.7 through 3.11 should be shifted by the amount of the initial displacement at each of the respective LVDTs. This would mean that the analytic results for boundary condition 3 better approximate experimental displacement results.

Boundary condition 3 attempts to model some friction appearing in the v direction depicted by small depressions registering on the teflon tape in the test apparatus. Analytically, a portion of the left side of the panel was held rigidly with rotation about u permitted. The right side was free to move in the analytic simulation. The results for LVDTs 3 and 4 (using boundary condition 3) compared more favorably because the left edge boundary condition more accurately models what was happening experimentally. There is more displacement allowed further from the simulated rigid body than near it (LVDT 2). A clamped boundary acts as a fold which produces bending moment as load increases, thus causing smaller displacements near the edge. As the applied load increases experimentally, the radial displacements become large and the boundary conditions change as the panel buckles outward. Portions of the panel surface come in contact with the side restraints causing friction. The results at LVDTs 11 and 17 are not affected as dramatically because their location is farther away from the changing boundary. Boundary condition 3 is not a true approximation of the experimental boundary but rather appears to be an upper bound. The true boundary

47

is a function of load and displacement. To better model experimental results analytically, this clamped boundary condition should not be applied at the beginning of loading but rather when the displacements start getting large and the depressions form in the teflon tape.

One difference that occurred with boundary condition 3 is that the collapse load was 16% greater than for the other conditions tested (Figure 3.12). Boundary condition 3 has a collapse load of greater than 3000 lbs whereas the other boundaries tested had collapse loads of approximately 2500 lbs. The higher collapse load is due to boundary condition 3 producing a greater stiffness (slope of load versus end shortening curve) in the panel by restraining the u displacement. This stiffness, which is twice that for the other boundary conditions, leads to a 17% higher collapse load. The experimental panel has initial eccentricities which result in a collapse load of only 2200 lbs. The geometrically perfect panels used in the analytical work therefore have consistently higher collapse loads than the experimental panel. Another reason that the collapse load for boundary condition 3 is higher than experimental results is that analytically the u restraint was applied at the beginning of the load application process. Experimentally, the boundary condition changes as a function of applied load.

The reader may notice that an attempt to improve the analytic radial displacement function in comparison to experimental values did not improve the collapse load
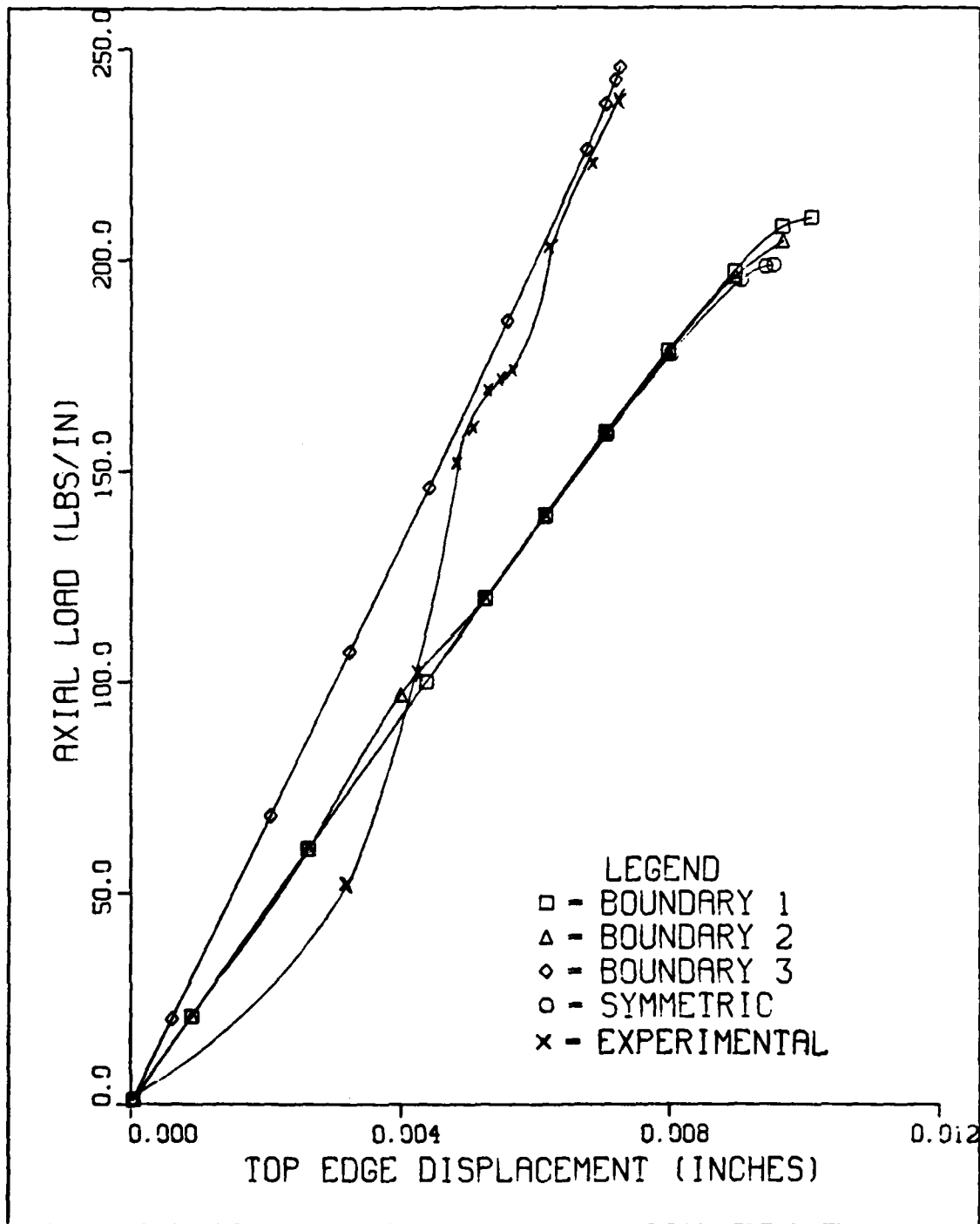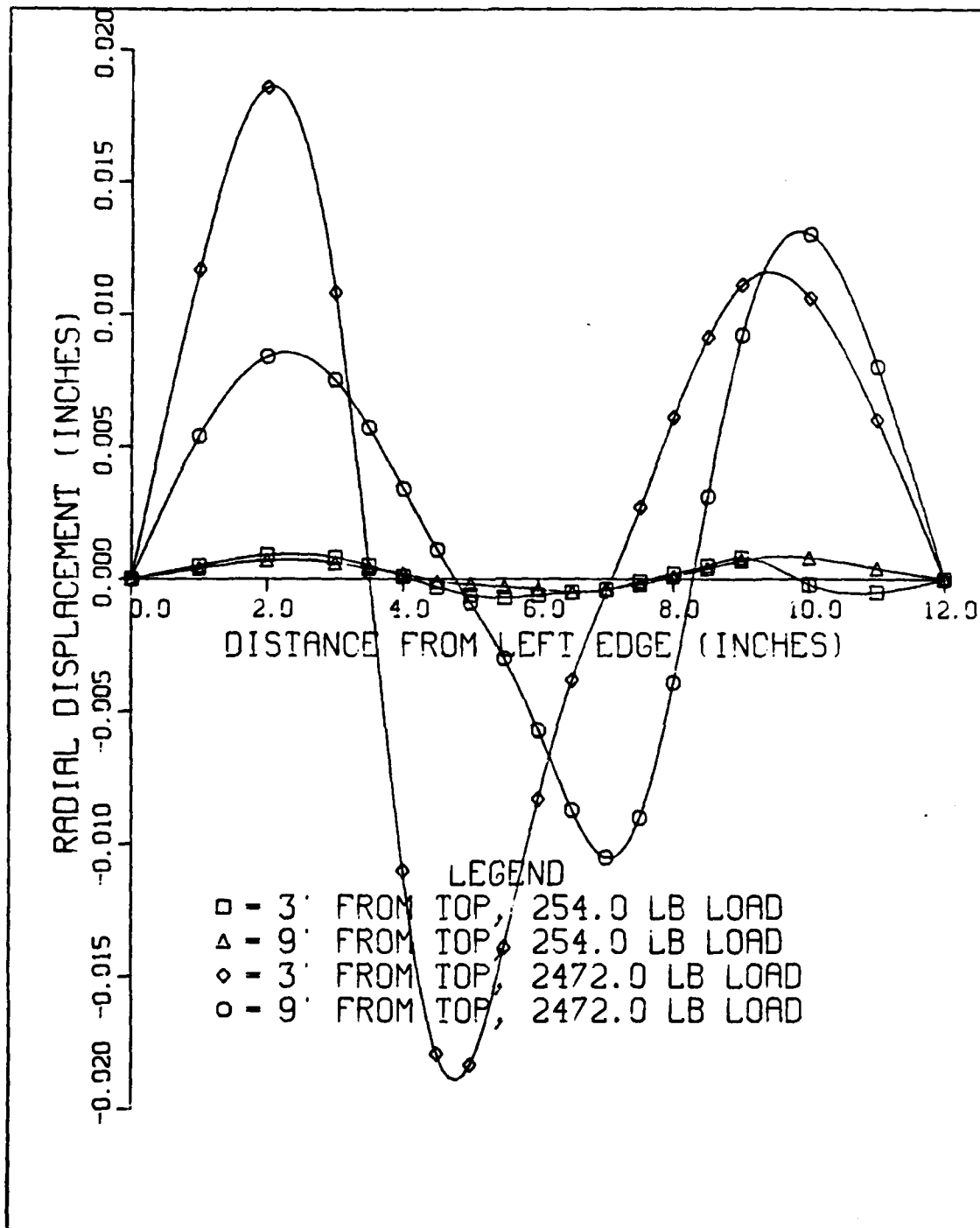
Figure 3.12. Top Edge Displacement, U, as a Function
of Applied Load

49

representation. In fact, the boundary condition which best represented the experimental displacement yielded a collapse load approximately 30% greater than the test value. This appears to indicate the fact that collapse is, considering this particular geometric case, a function of axial load which is comparatively independent of radial displacement. Thus, one appreciates the statement that buckling is an averaging phenomena in which most secondary effects are unimportant. Of course, it is required to keep in mind that the problem just described relates to a small cutout within a cylindrical panel. The relative movement within the panel is primarily linear. A subsequent section (Notch and Cutout Study) of this thesis, considers several larger cutouts which yield truely nonlinear phenomena.

Discussion up to this point has been involved with comparing analytic and experimental results. Now, this thesis will deal with a strict analytic comparison. Moments and displacements will be examined in order to gain a better understanding of the behavior of a cylindrical panel with the various boundary conditions previously compared. The radial displacement was plotted as a function of distance from the left edge of the panel along two lines, 3 inches and 9 inches from the top of the panel. The displacement along each of these lines was plotted for a low load level and also for a collapse load for each of the boundary conditions tested (Figures 3.13 through 3.16). From Figure 3.13 it can be seen that the top of the panel deflects more near the left edge of the top of the panel than it does
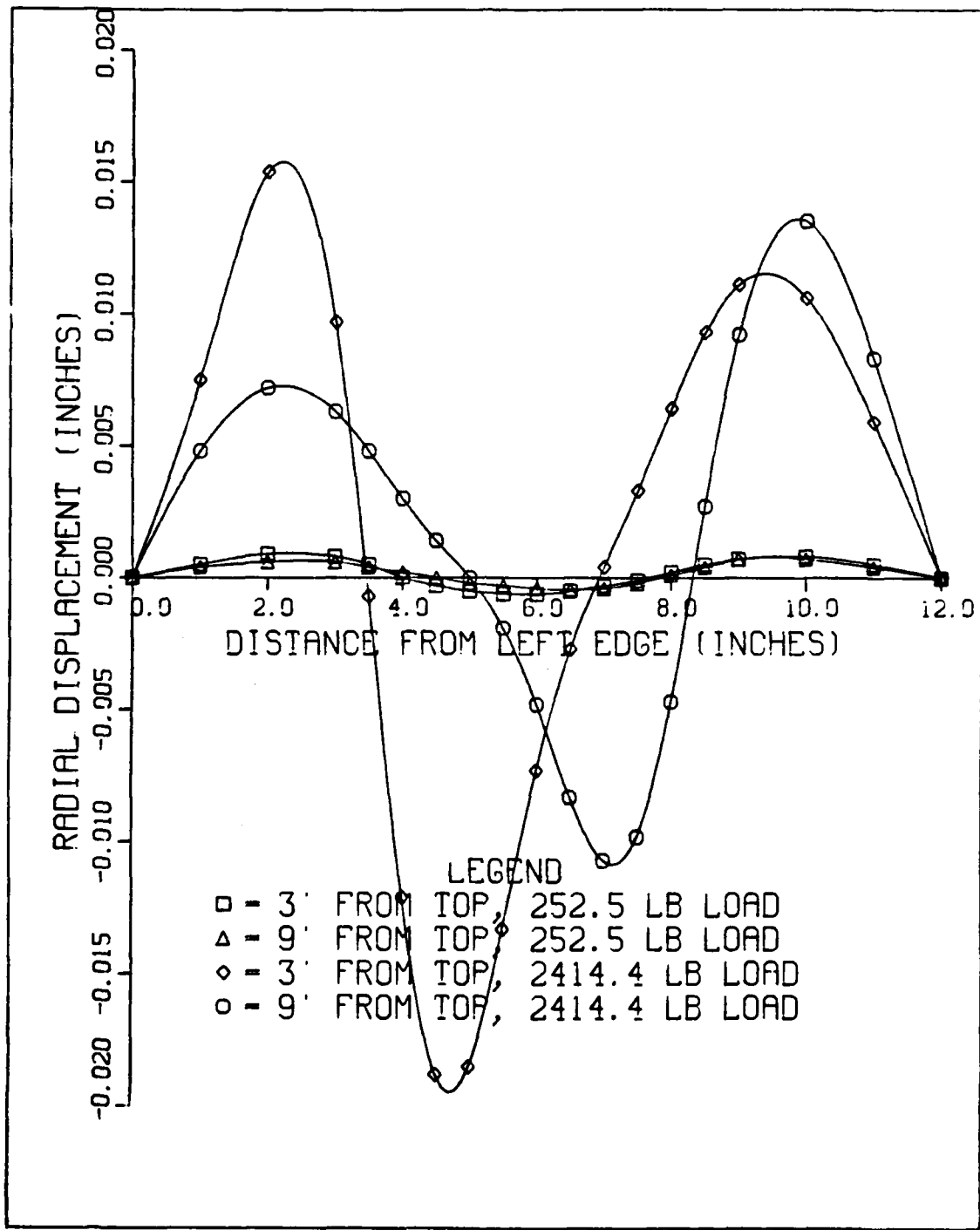
Note: Displacements taken along lines 3" and 9" from top edge of panel.

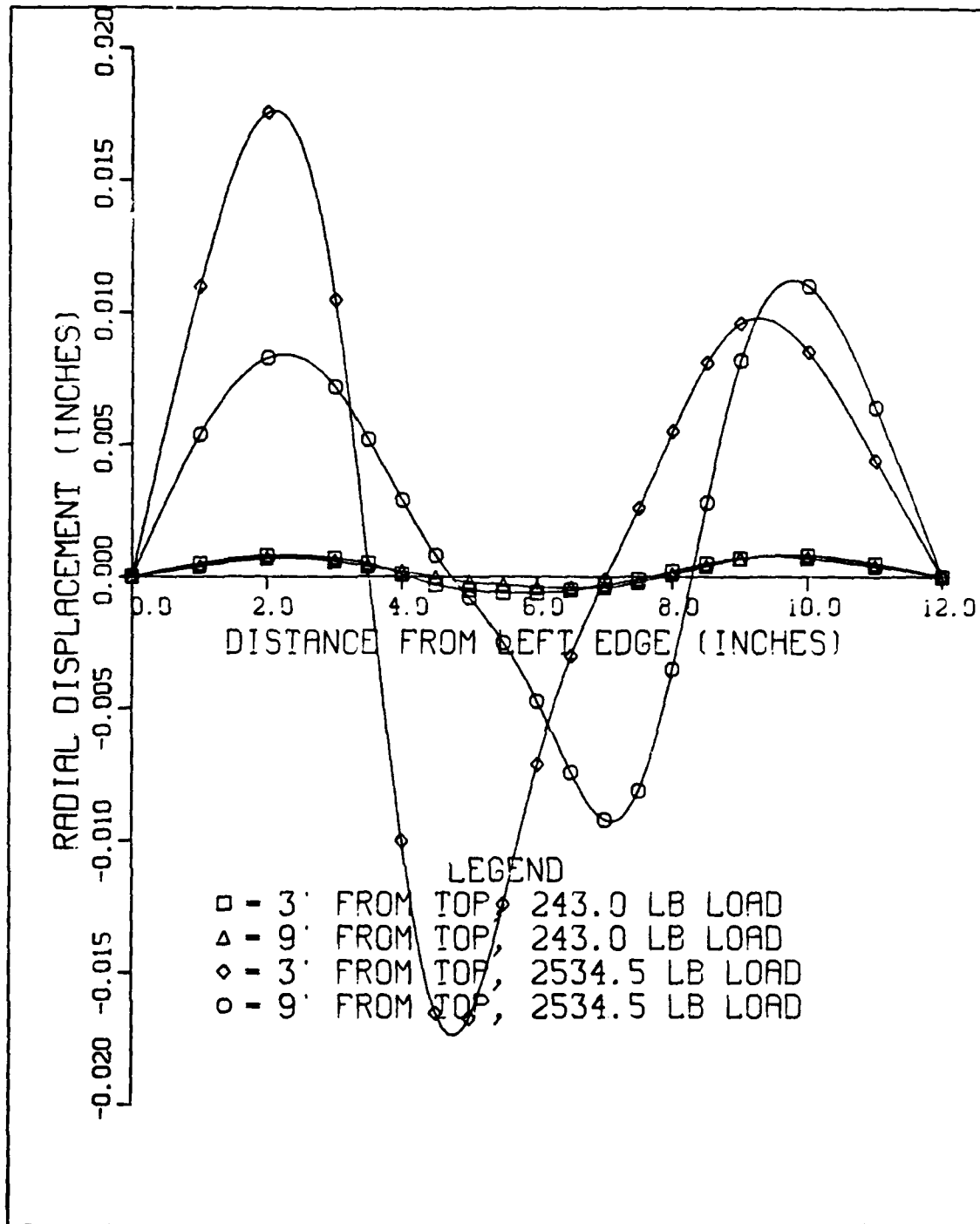**Figure 3.13.** Radial Displacement as a Function of Panel Location for Symmetric Boundary Conditions

51

along the line 9 inches down. There is a trough forming radially inward from the upper left edge of the cutout to below the lower right edge of the cutout. Figures 3.14 and 3.15 show that when v is restrained on one edge, the radial displacement is not affected significantly except to lessen the radial displacement slightly near the restrained edge. By restraining u displacement (boundary condition 3) the radial displacement is less near the left edge as can be seen in Figure 3.16. The trough of radial displacement has shifted dramatically when compared to the other three boundaries studied. By restraining the u displacement, the trough starts above the upper right edge of the cutout and extends diagonally to below the lower left edge of the cutout.

The values for M_x and M_y, for each of the boundary conditions were compared along lines 2.5 inches and 9.5 inches from the top of the panel. The moment about the y axis for symmetric boundary conditions (Figure 3.17), boundary condition 1 (Figure 3.18), and boundary condition 2 (Figure 3.19) are very similar, and have no significant differences. The maximum and minimum moments correspond to the points of greatest outward or inward radial displacement. Restraining the v displacement on the upper half of the panel does not affect M_x significantly. Examining M_x for boundary condition 3 (Figure 3.20) shows that the moment is smaller for the 2946 lb load near the semi-clamped left edge. The moments near the center of the panel are nearly the same in magnitude even though boundary
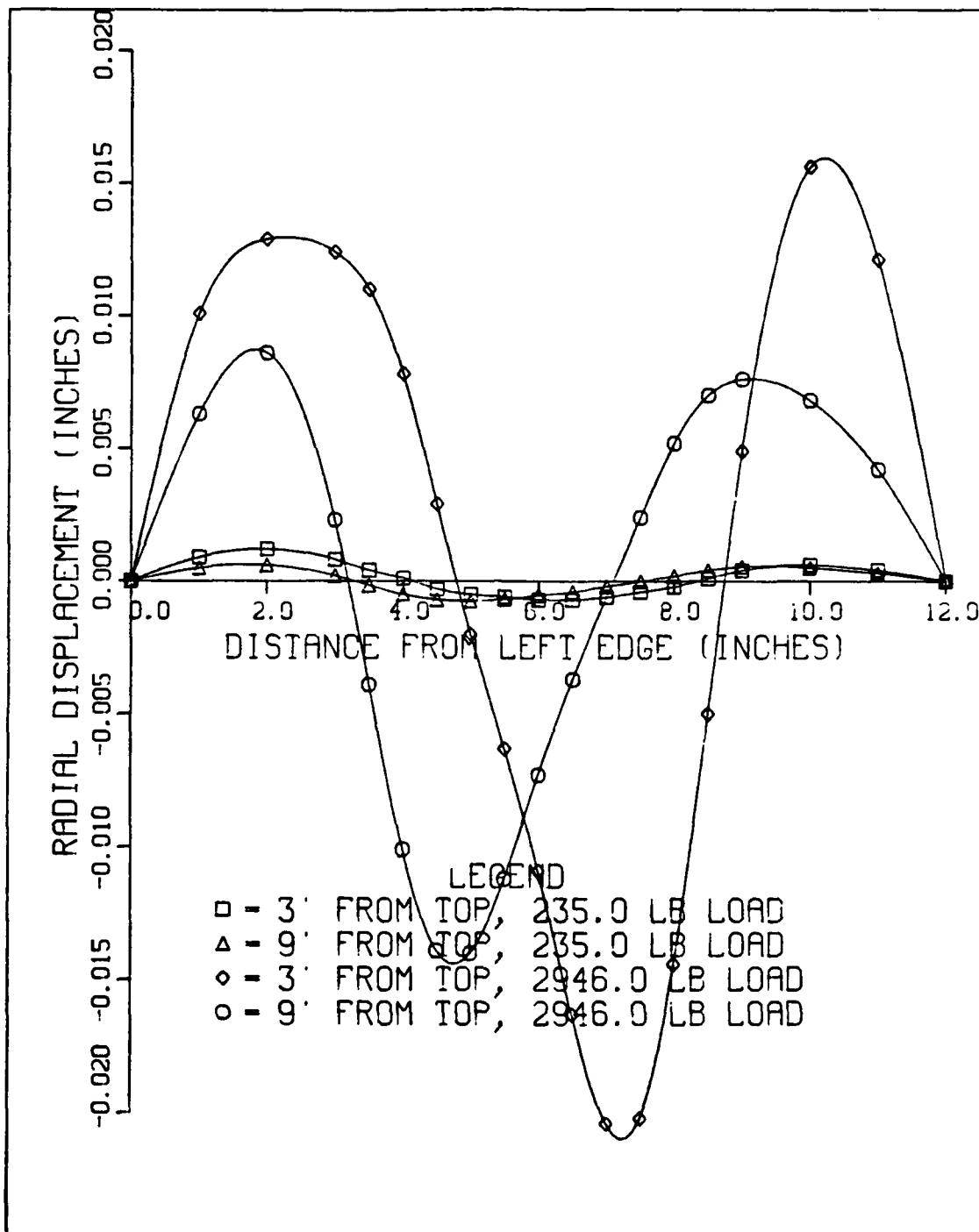
52

Note: Displacements taken along lines 3" and 9" from top edge of panel.

Figure 3.14. Radial Displacement as a Function of Panel
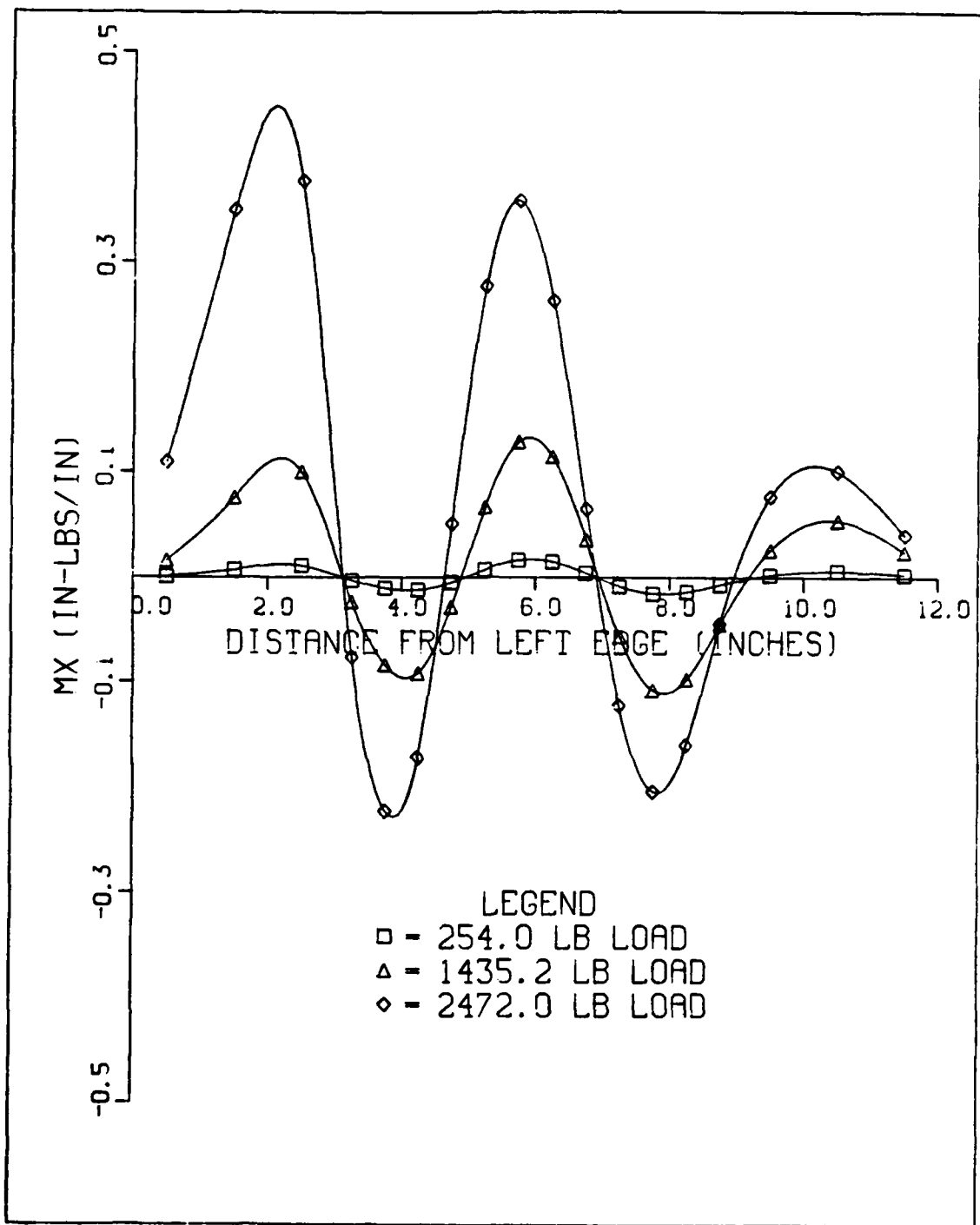Location for Boundary Condition 1

Note: Displacements taken along lines 3" and 9" from top edge of panel.

Figure 3.15. Radial Displacement as a Function of Panel Location for Boundary Condition 2
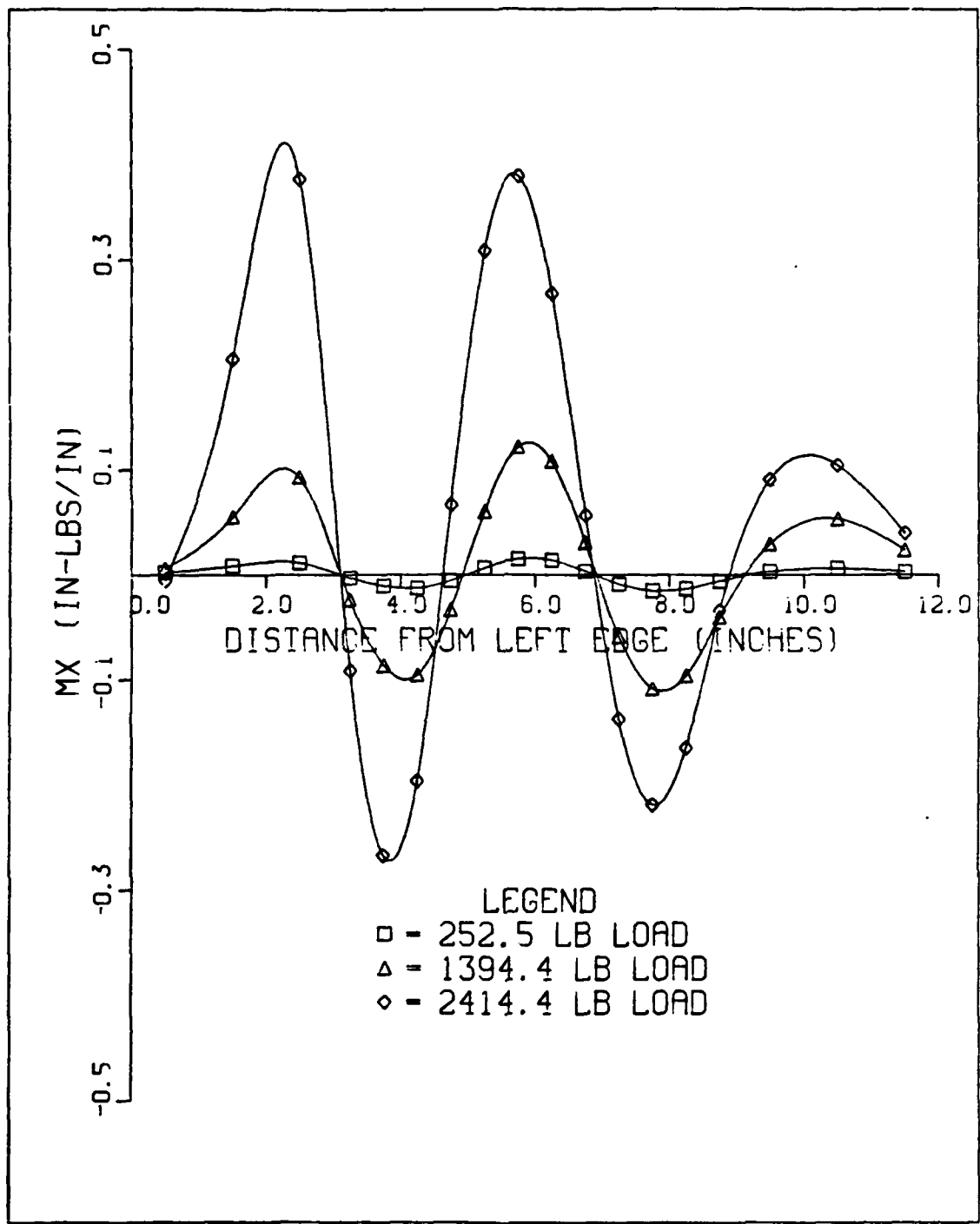
Note: Displacements taken along lines 3" and 9" from top edge of panel.

Figure 3.16. Radial Displacement as a Function of Panel Location for Boundary Condition 3
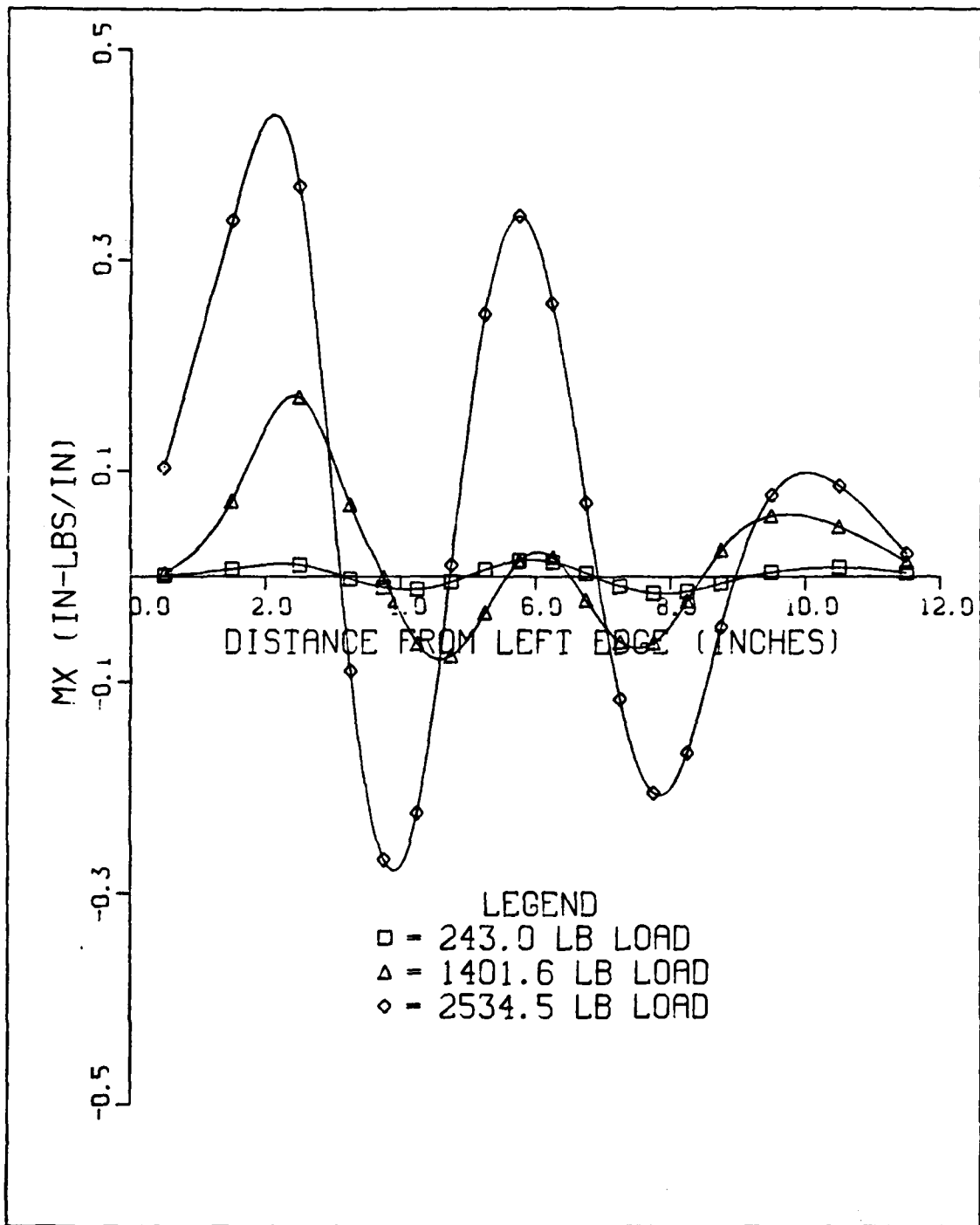
Note: Moments taken along a line 2.5" from top edge of panel.

Figure 3.17. Moment about Y Axis, M_x, versus Distance from Left Edge of Panel for Symmetric Boundary Conditions
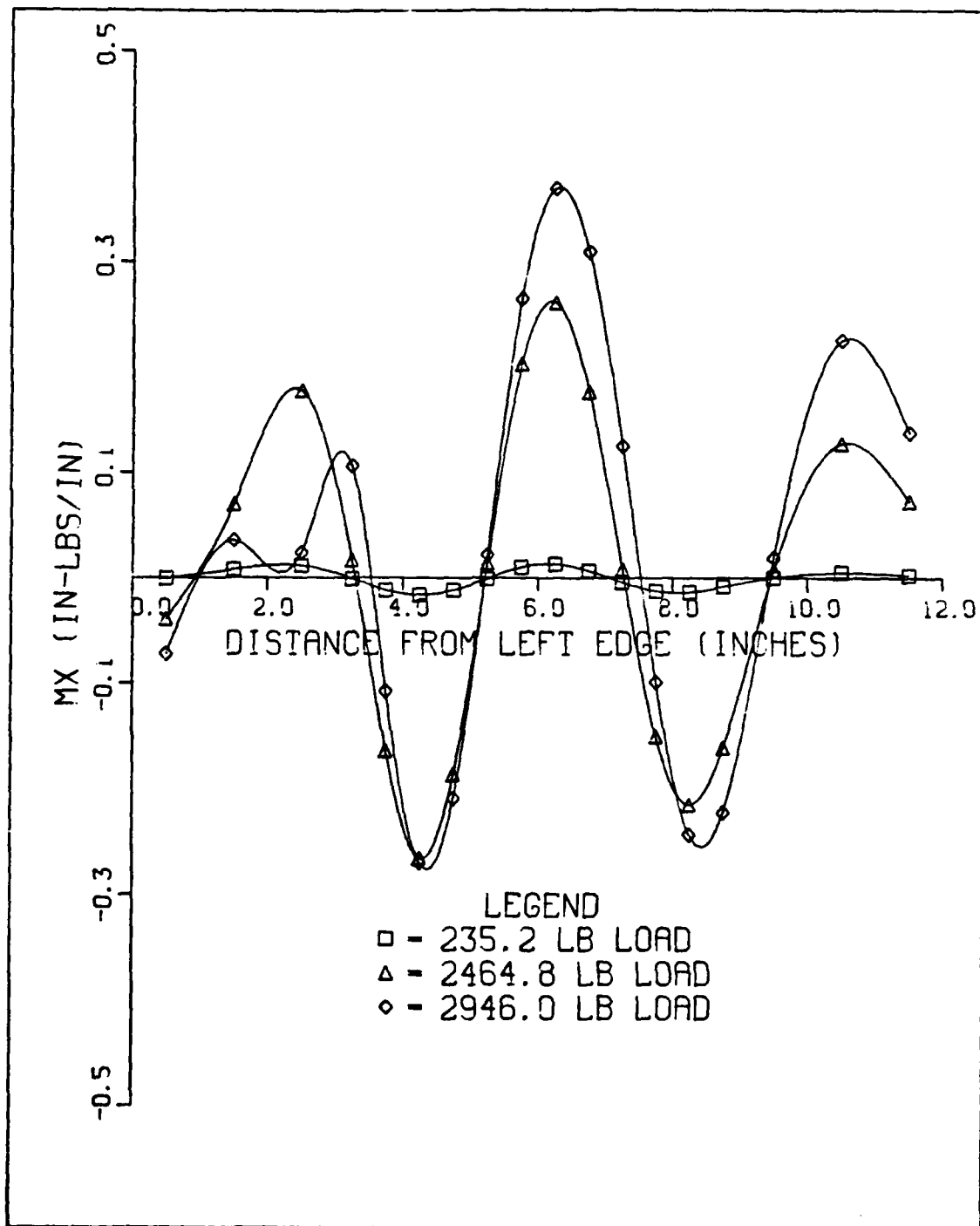
Note: Moments taken along a line 2.5" from
top edge of panel.

Figure 3.18.   Moment about Y Axis, M_x, versus Distance
from Left Edge for Boundary Condition 1

Note: Moments taken along a line 2.5" from top edge of panel.

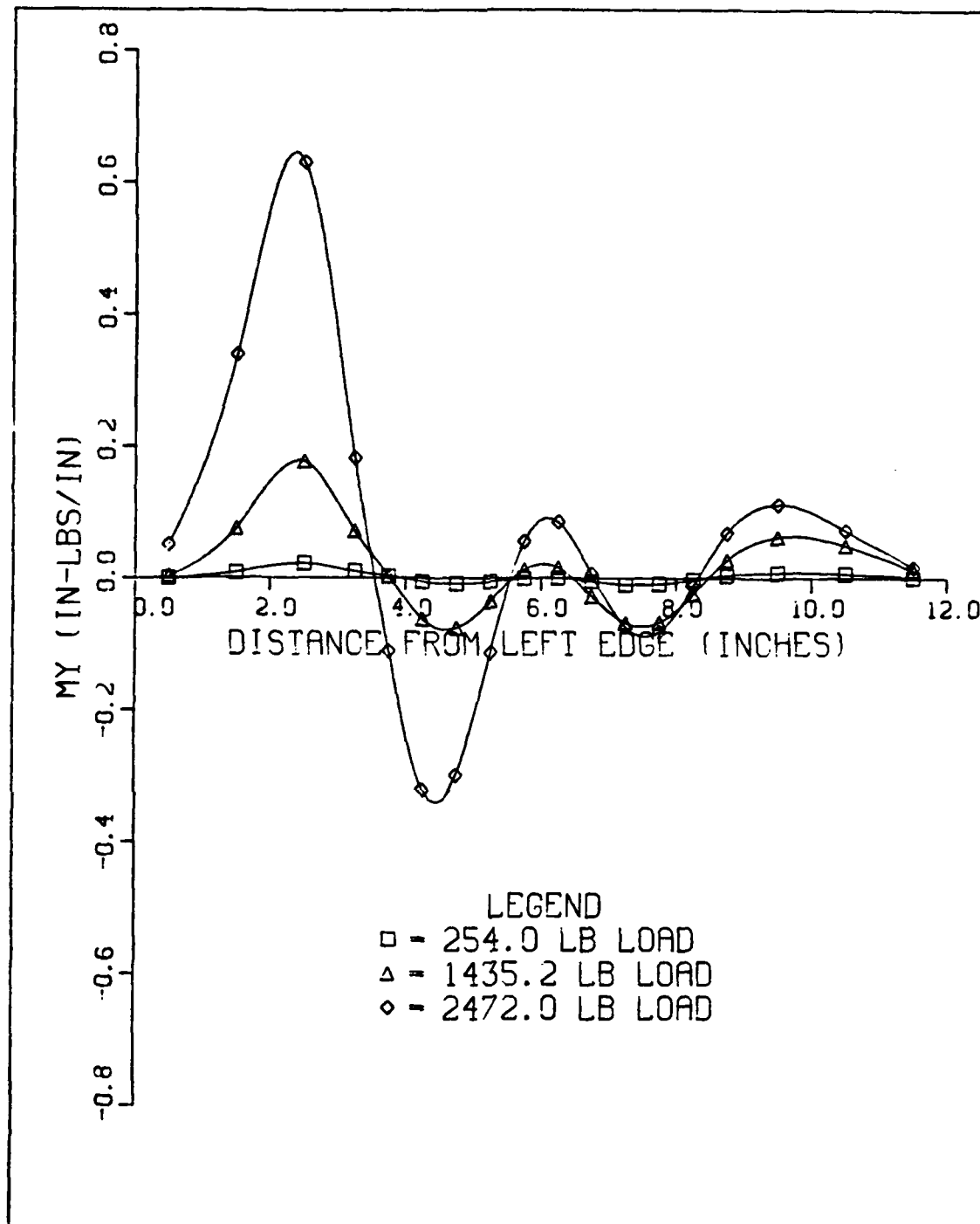Figure 3.19. Moment about Y Axis, M_x, versus Distance from Left Edge for Boundary Condition 2

58

Note: Moments taken along a line 2.5" from top edge of panel.

Figure 3.29. Moment about Y Axis, M_x, versus Distance from Left Edge for Boundary Condition 3

condition 3 had a higher collapse load than the other cases. This is due to the restraint on the left edge which correspondingly reduces M_x near the panel's center. The values for M_x near the right edge of the panel for boundary condition 3 are greater than the corresponding moments for the other boundary conditions. This is caused by the right edge being freer to move as compared to the left edge. The moments at collapse have the same trend for the symmetric boundary and boundaries 1 and 2 because the moments are not large enough to be affected by the restraint in the v direction. Boundary condition 3 produces moments that are negative at the left edge.

The moment about the x axis was also compared along the upper line (Figures 3.21 through 3.24). Once again there is no significant effect introduced by restraining the v displacement on the upper half of the panel. For boundary condition 3, Figure 3.24, the values for M_y are much less than for the other boundaries. The negative values for M_y are also much greater between 7 and 9 inches than for the previous boundary conditions. This occurs because the restrained displacements act similar to a clamp such that displacements farther away oscillate more freely, yielding larger negative moments about the x axis. The large peak in M_y in Figures 3.21 through 3.23 at 2.5 inches from the left edge corresponds to LVDT location 2. Boundary condition 3 more accurately models experimental results, yet there should be physically less moment build up near the left edge in the experimental panel than the amount computed
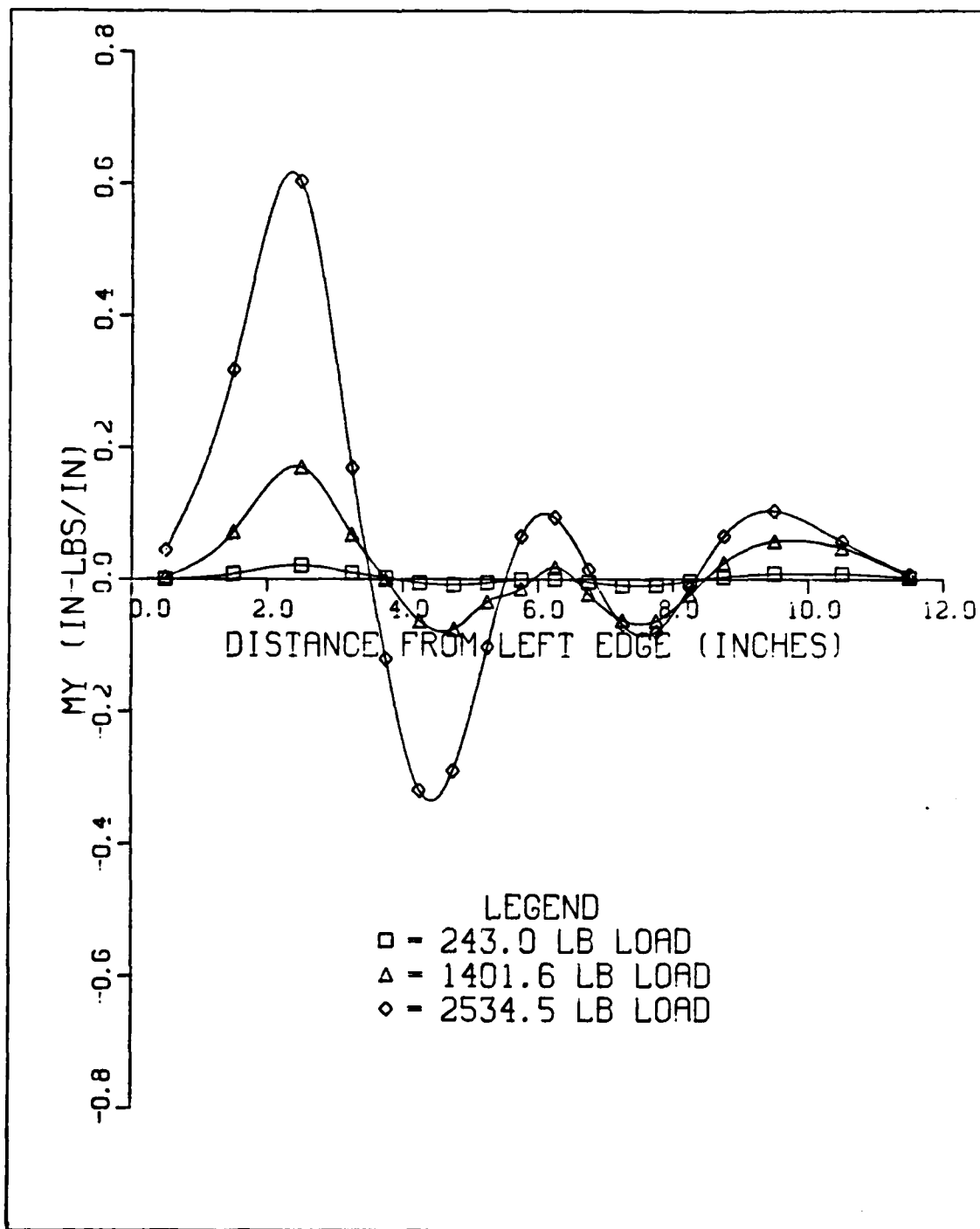
60

Note: Moments taken along a line 2.5" from top edge of panel.

Figure 3.21. Moment about X Axis, M_y, versus Distance from Left Edge of Panel for Symmetric Boundary Condition
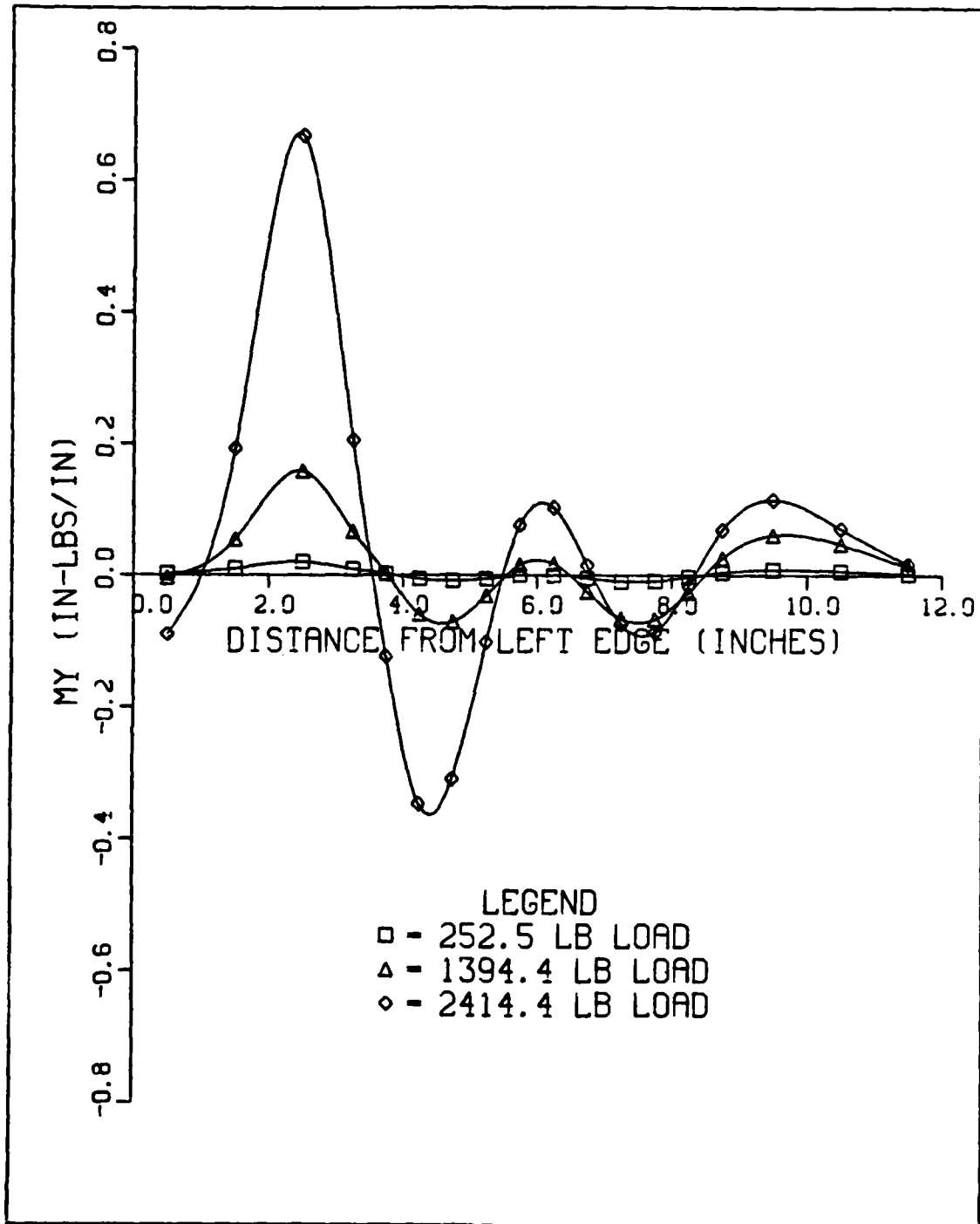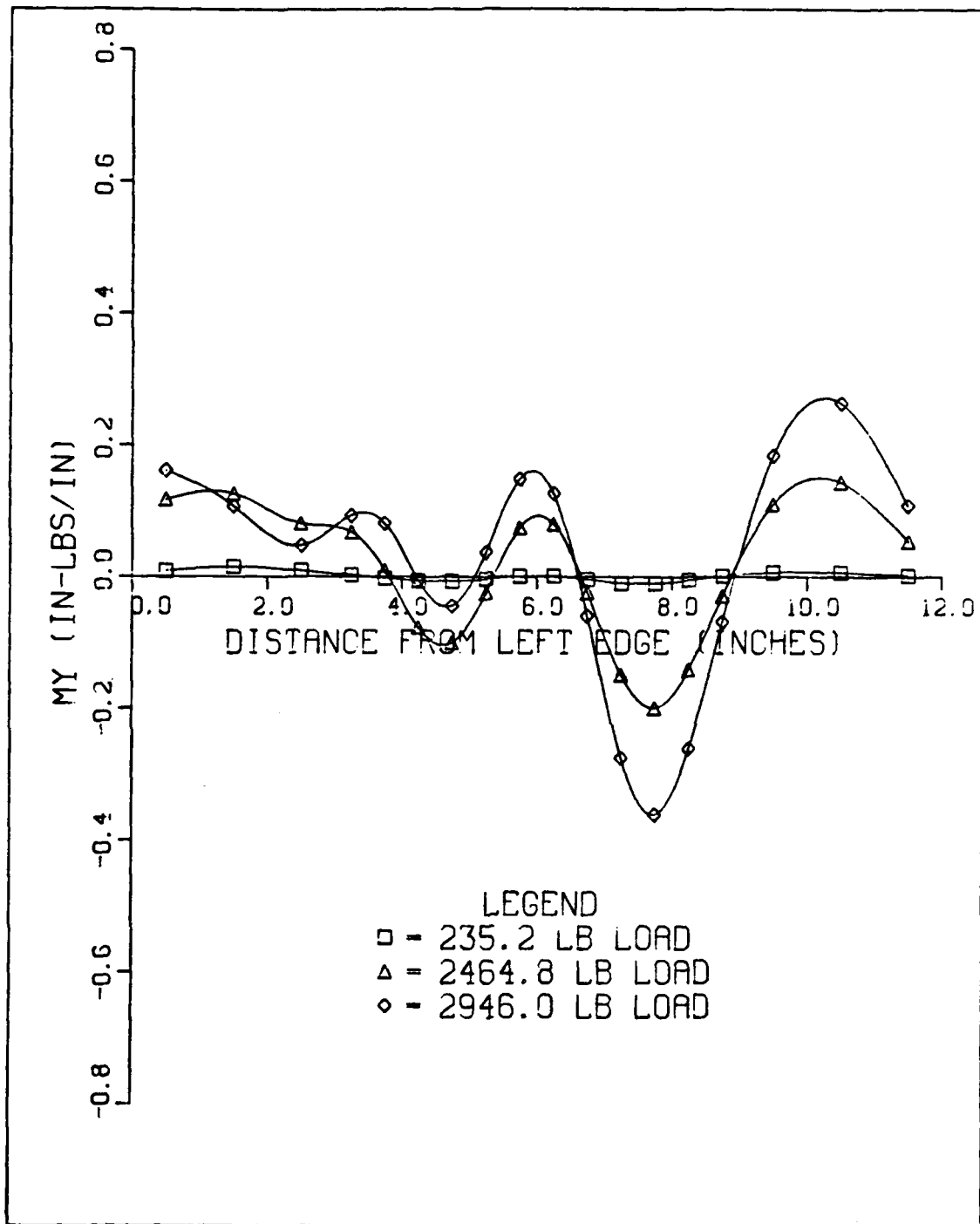
Note: Moments taken along a line 2.5" from top edge of panel.

Figure 3.22. Moment about X Axis, M_y, versus Distance from Left Edge for Boundary Condition 1

Note: Moments taken along a line 2.5" from top edge of panel.

Figure 3.23. Moment about X Axis, M_y, versus Distance from Left Edge for Boundary Condition 2
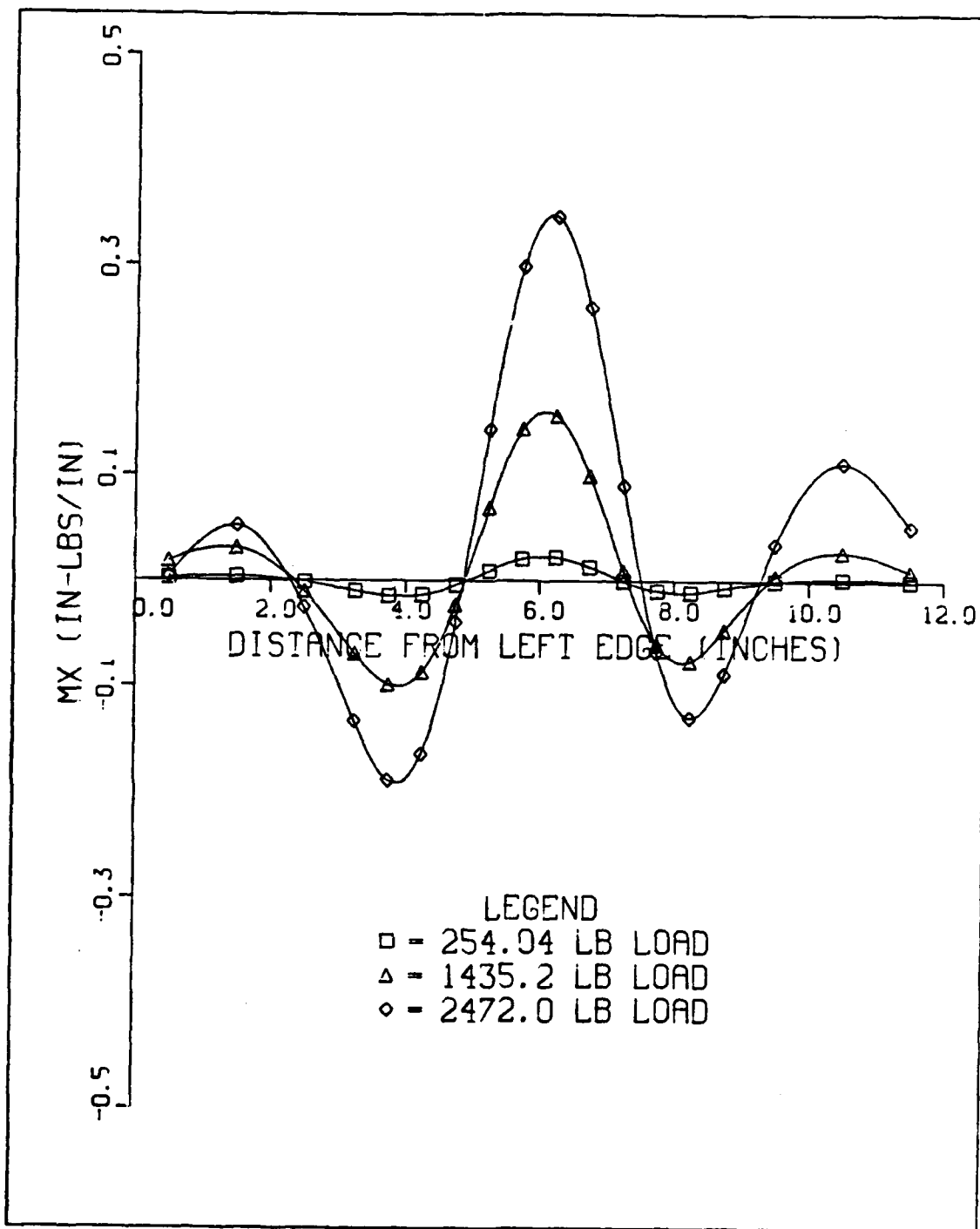
Note: Moments taken along a line 2.5" from top edge of panel.

Figure 3.24. Moment about X Axis, M_y, versus Distance from Left Edge for Boundary Condition 3

64

analytically because the experimental boundary condition changes with applied load. In each of these figures, the values for moment in the y direction go to zero at the edges of the panel.

The values for M_x and M_y were also compared along a line 9.5 inches from the top of the panel. This line is far enough away from the changing boundaries so that one would expect little change between the values. M_x for the symmetric boundary condition (Figure 3.25) does not differ significantly from the values for M_x with boundary condition 1 (Figure 3.26) or 2 (Figure 3.27). These two unsymmetric boundary conditions show a slight increase in moment at collapse load 10 inches from the left edge of the panel. A slight influence from the restained u displacement is experienced by M_x values along the lower line for boundary condition 3 (Figure 3.28). The moment has peaks at approximately the same locations as with symmetric boundary conditons, but the magnitudes are slightly less.

Moment about the x axis, M_y, was also examined at the three load levels along the lower line. Figure 3.29 shows the results for the symmetric boundary conditions. Comparing boundary condition 1 (Figure 3.30) to these values shows an increase in M_y near the right edge of the panel. This is due to the fact that the entire right edge of the panel is freer to move in the y direction as compared to the left edge of the panel. Figure 3.31 shows this same result for boundary condition 2 except the phenomena is observed along the left edge of the panel. The magnitudes for M_y are
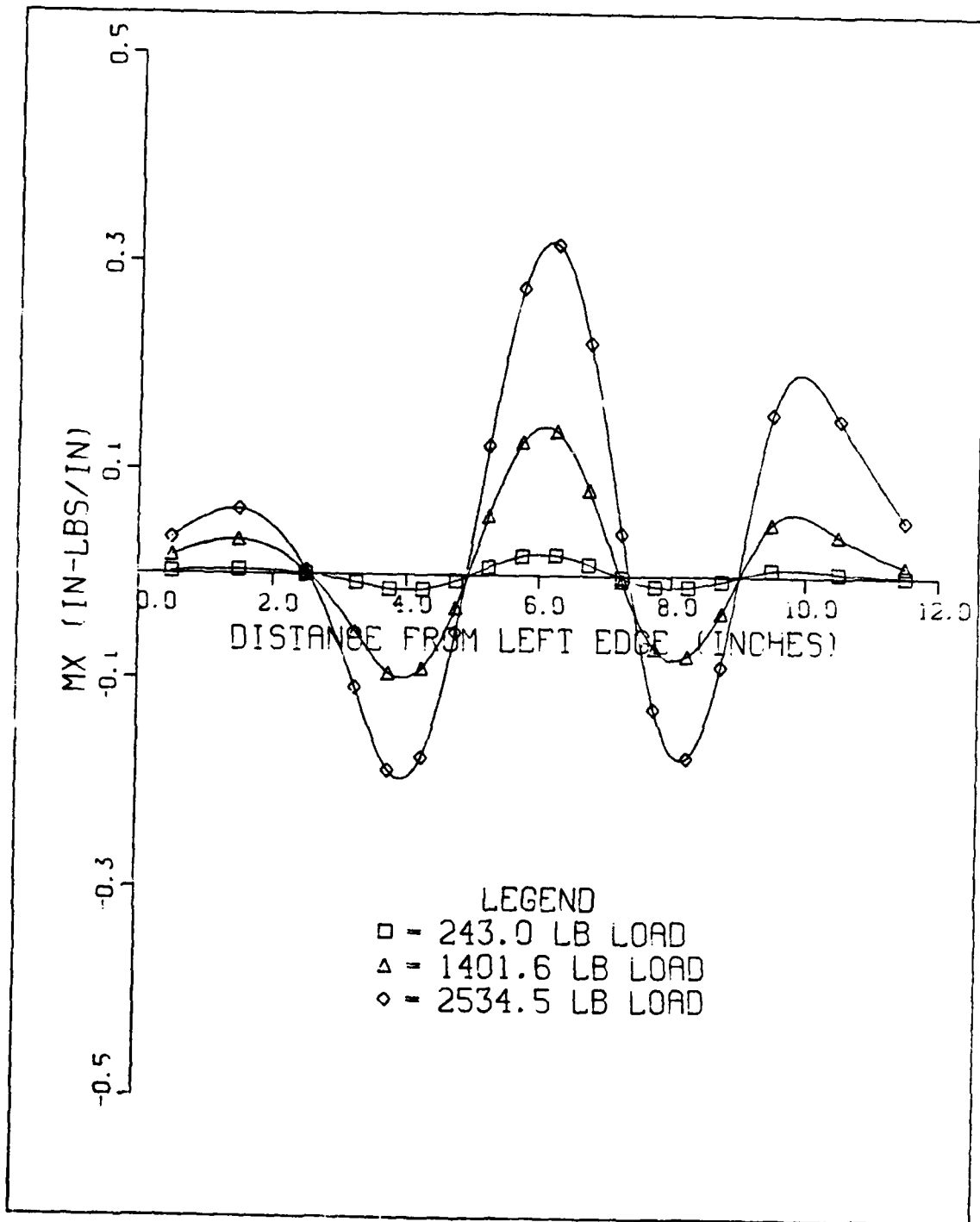
65

Note: Moments taken along a line 9.5" from
top edge of panel.

Figure 3.25. Moment about Y Axis, M_x, versus Distance
from Left Edge of Panel for Symmetric
Boundary Condition

66
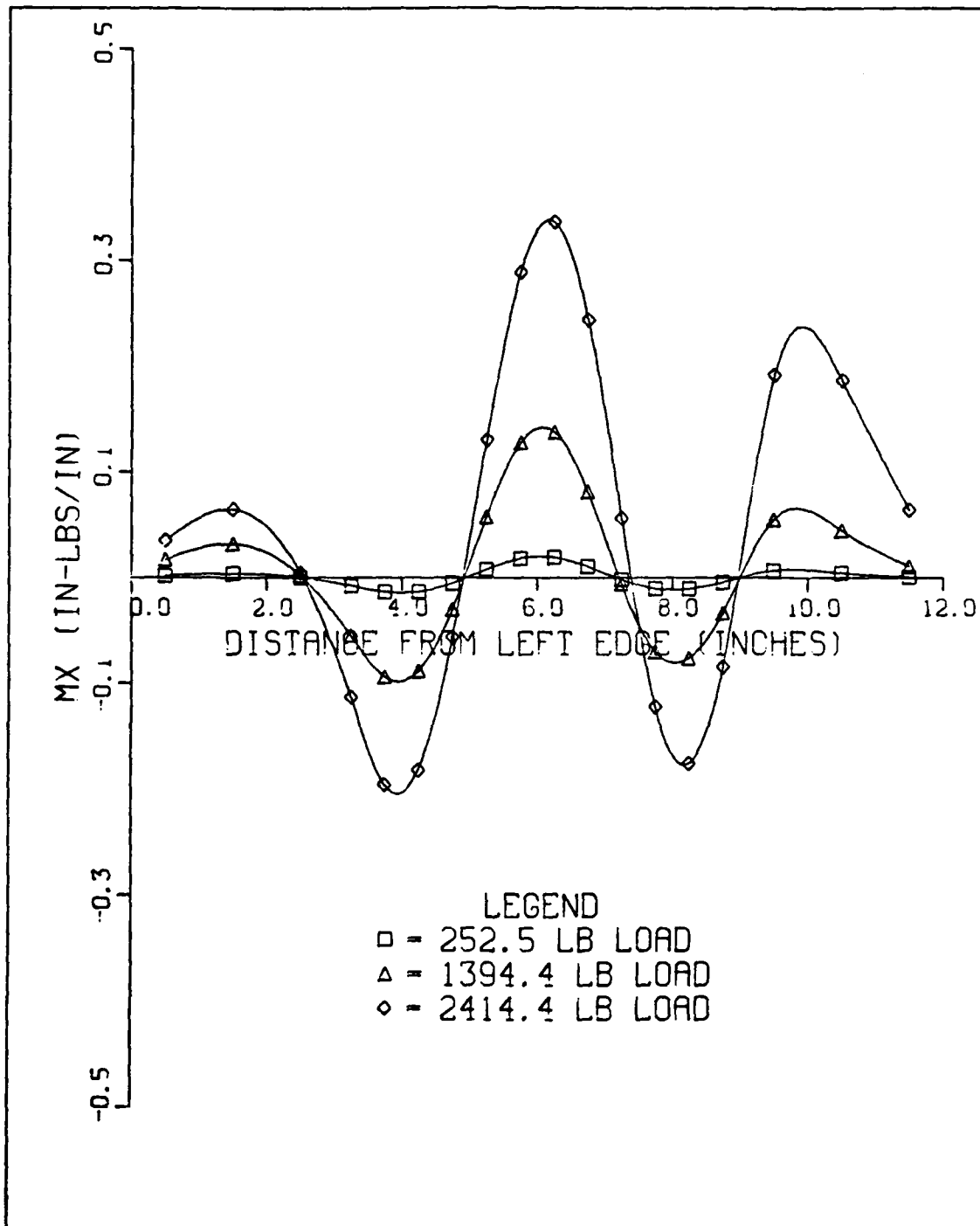
Note: Moments taken along a line 9.5" from top edge of panel.

Figure 3.26. Moment about Y Axis, M_x, versus Distance from Left Edge for Boundary Condition 1
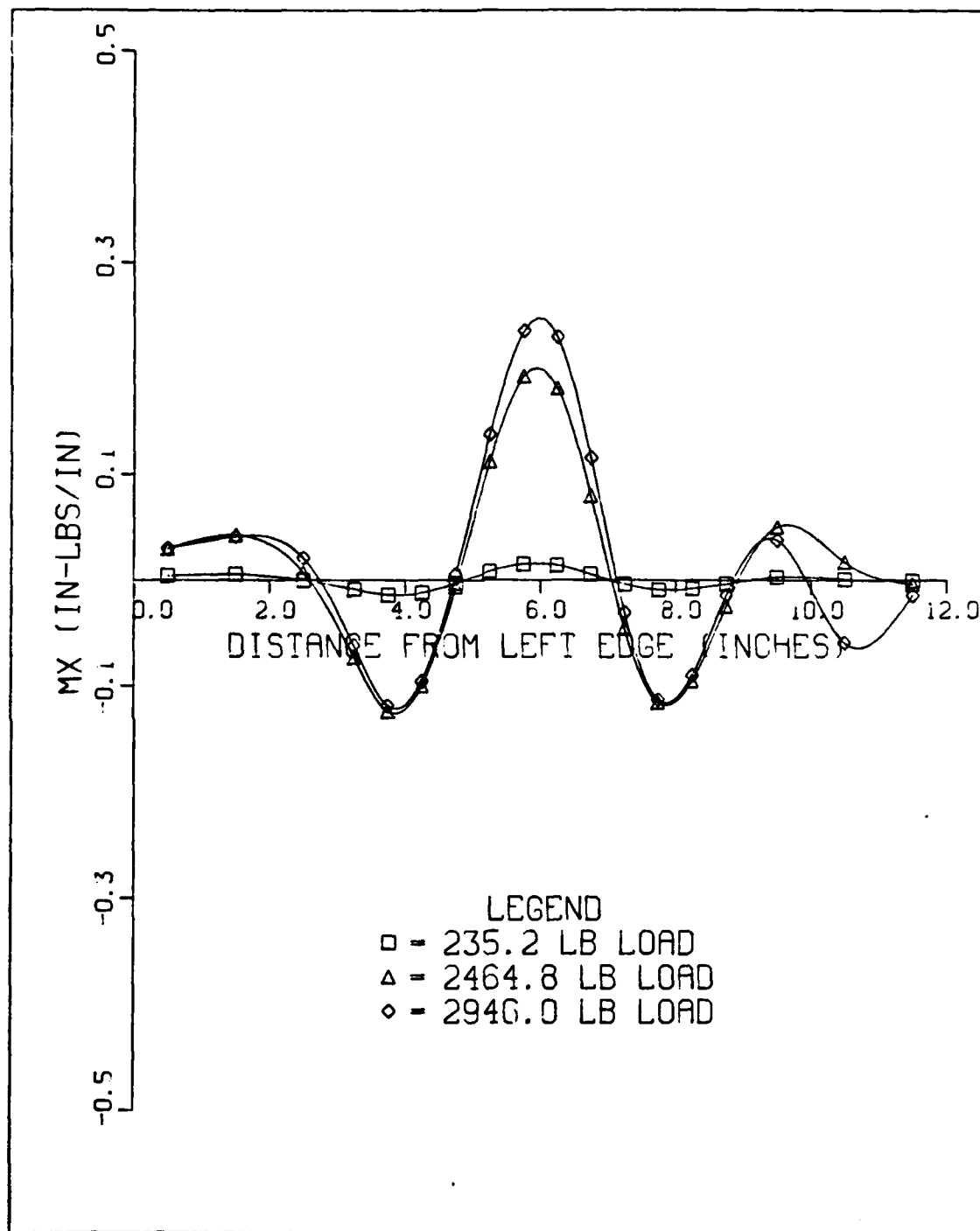
Note: Moments taken along a line 9.5" from
top edge of panel.

Figure 3.27. Moment about Y Axis, M_x, versus Distance
from Left Edge for Boundary Condition 2

68

Note: Moments taken along a line 9.5" from top edge of panel.

Figure 3.28. Moment about Y Axis, M_x, versus Distance from Left Edge for Boundary Condition 3

Note: Moments taken along a line 9.5" from
        top edge of panel.

Figure 3.29.   Moment about X Axis, M_y, versus Distance
               from Left Edge of Panel for Symmetric
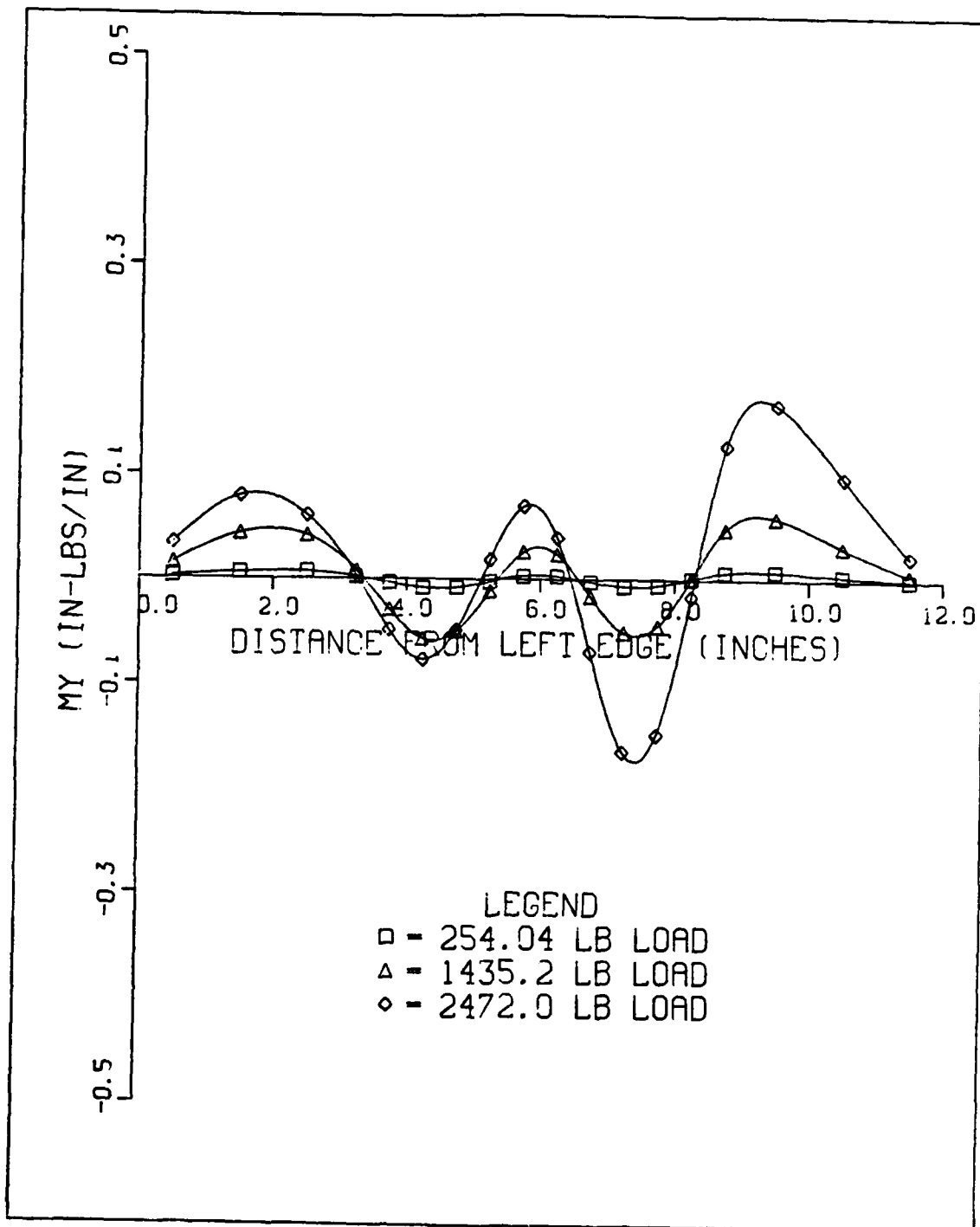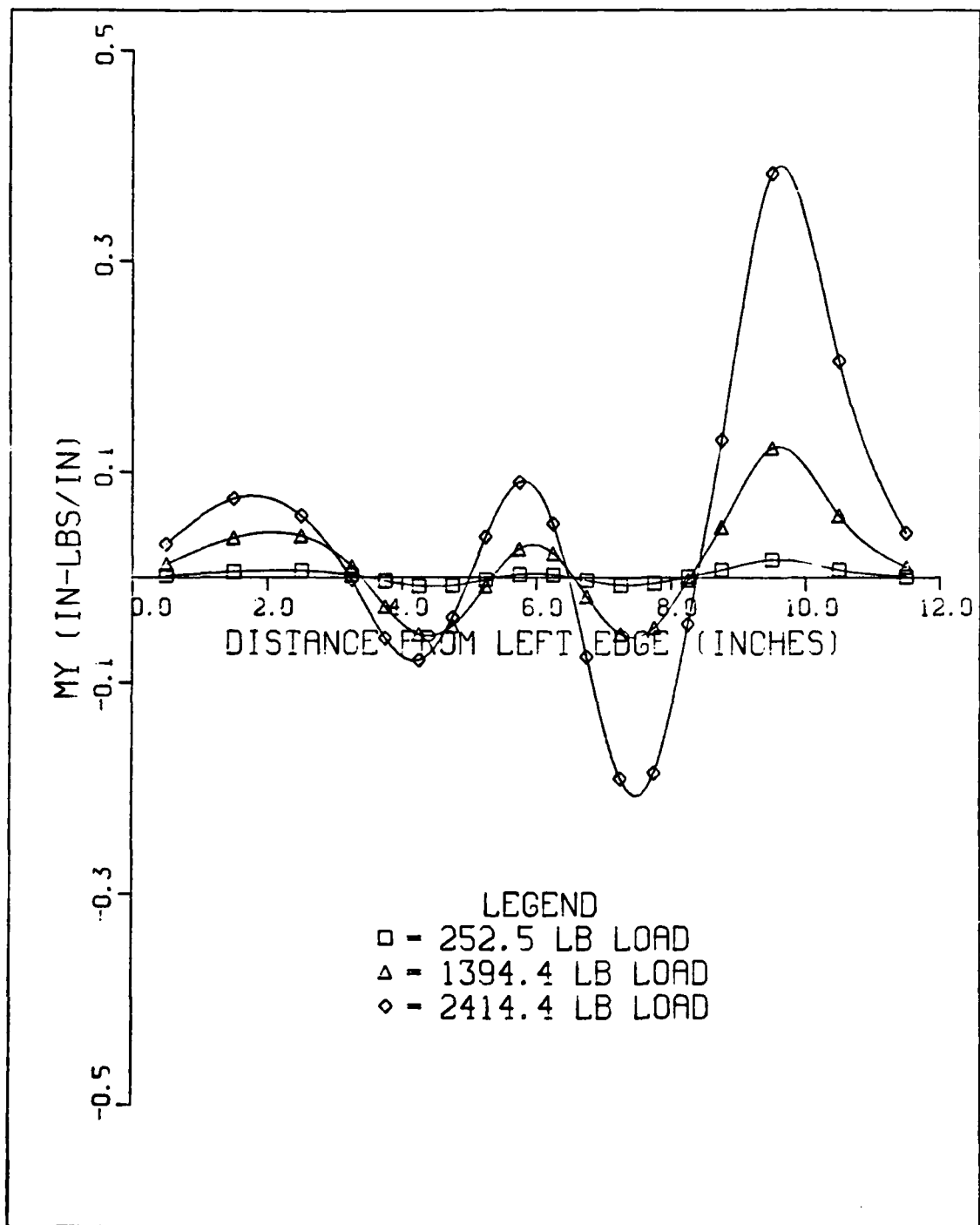   Boundary Condition

70

Note: Moments taken along a line 9.5" from
top edge of panel.

Figure 3.30. Moment about X Axis, M_y, versus Distance
from Left Edge for Boundary Condition 1

Note: Moments taken along a line 9.5" from top edge of panel.

Figure 3.31. Moment about X Axis, M_y, versus Distance from Left Edge for Boundary Condition 2

Note: Moments taken along a line 9.5" from top edge of panel.

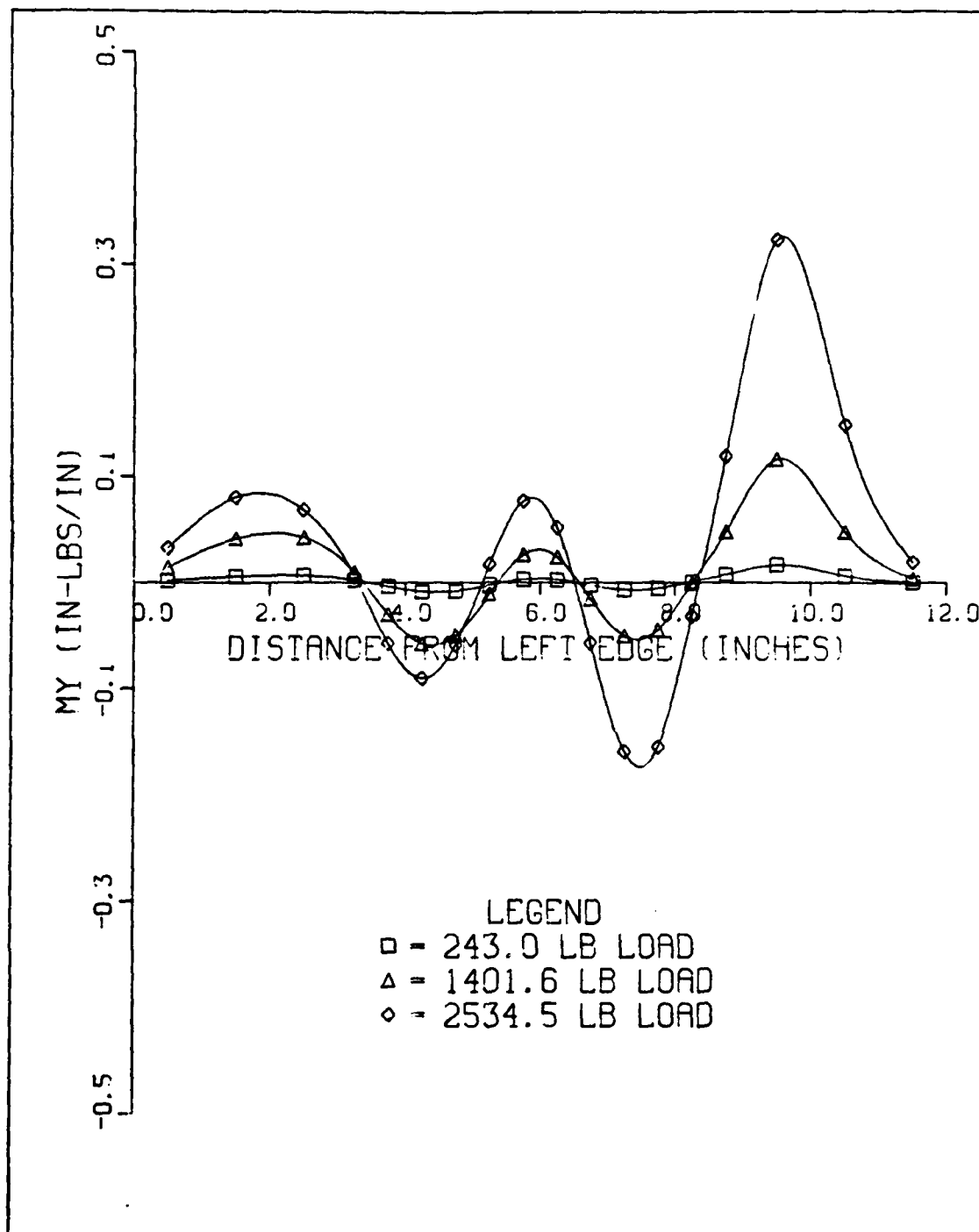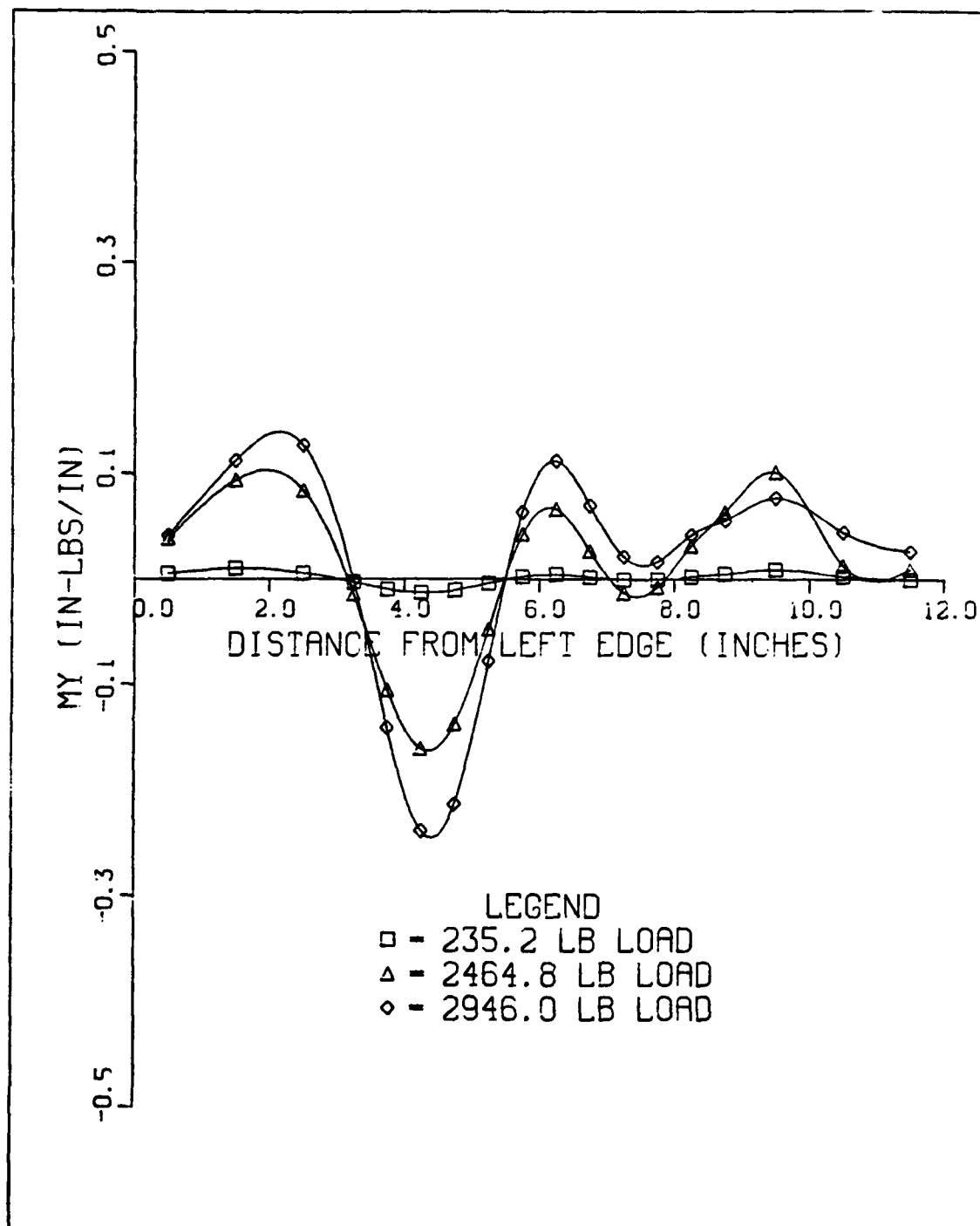Figure 3.32. Moment about X Axis, M_y, versus Distance from Left Edge for Boundary Condition 3

greater for boundary condition 3 (Figure 3.32) except along the right edge of the panel where they are slightly less.

The large peaks in the moment about the y axis along both lines near the middle of the panel correspond to the location of the cutout. Along the upper line, the moments about the y axis are negative near the center of the panel, whereas the moments are positive at the center of the panel along the bottom line. The moments are symmetric about the center of the panel except for boundary condition 3 at the lower load levels.

Notch and Cutout Study

The focus of the notch analysis involved examing the effect that different size cutouts have on the buckling behavior of cylindrical panels. Six different cutout sizes were studied as listed in Table 2.1. The 2"x1" and 1"x2" cutouts, along with the 2"x2" cutout will be considered notches for this thesis because the area of the cutout is less than 5% of the total panel area. Of particular interest were the rectangular cutouts with aspect ratios of 0.5 or 2.0. The boundary conditions used for this part of the analysis is the symmetric boundary condition listed in Table 2.2. It may be recognized that under the definition used in this thesis to define a notch, the resulting phenomena of collapse tends to be linear contrary to nonlinear behavior for cutouts as will be shown subsequently.

The procedures developed previously have been used to model the finite element mesh for each of the cutouts. Figure 3.33 shows the cutout region's refined mesh. As was noted in the mesh refinement section of this thesis, the mesh should be refined equidistant around the cutout. Due to the size and positioning of the 1"x2" and 2"x1" notches, this was not possible. For the 1"x2" notch the mesh was refined 2 inches to each side and 1.5 inches to the top and bottom of the notch. This refinement kept elements with a 0.5 aspect ratio the desired minimum distance from the cutout. Elements with an aspect ratio of 2 were allowed to be slightly closer to the cutout because their influence on the buckling behavior was not as critical. In order to keep the elements with a .5 aspect ratio the minimum distance from the opening, the mesh for the 2"x1" notch was refined 2.5 inches in the circumferential direction. Since the 2"x4" and 4"x2" cutouts and the square cutouts have even dimensions, the mesh was refined evenly around each cutout.

A summary of the grid selection data for each of the cutouts is presented in Table 3.2 The grid selection data for the 2"x2" notch with the 19x19 mesh can be found in Table 3.1. As can be noted from Table 3.2, the 4"x4" cutout took the most computer time, yet had the lowest collapse load. This time function occurred because there were over 3000 active degrees of freedom for this cutout.

The first parameter examined in this notch comparison study was the collapse load for each panel. The top edge displacement as a function of applied load is plotted in
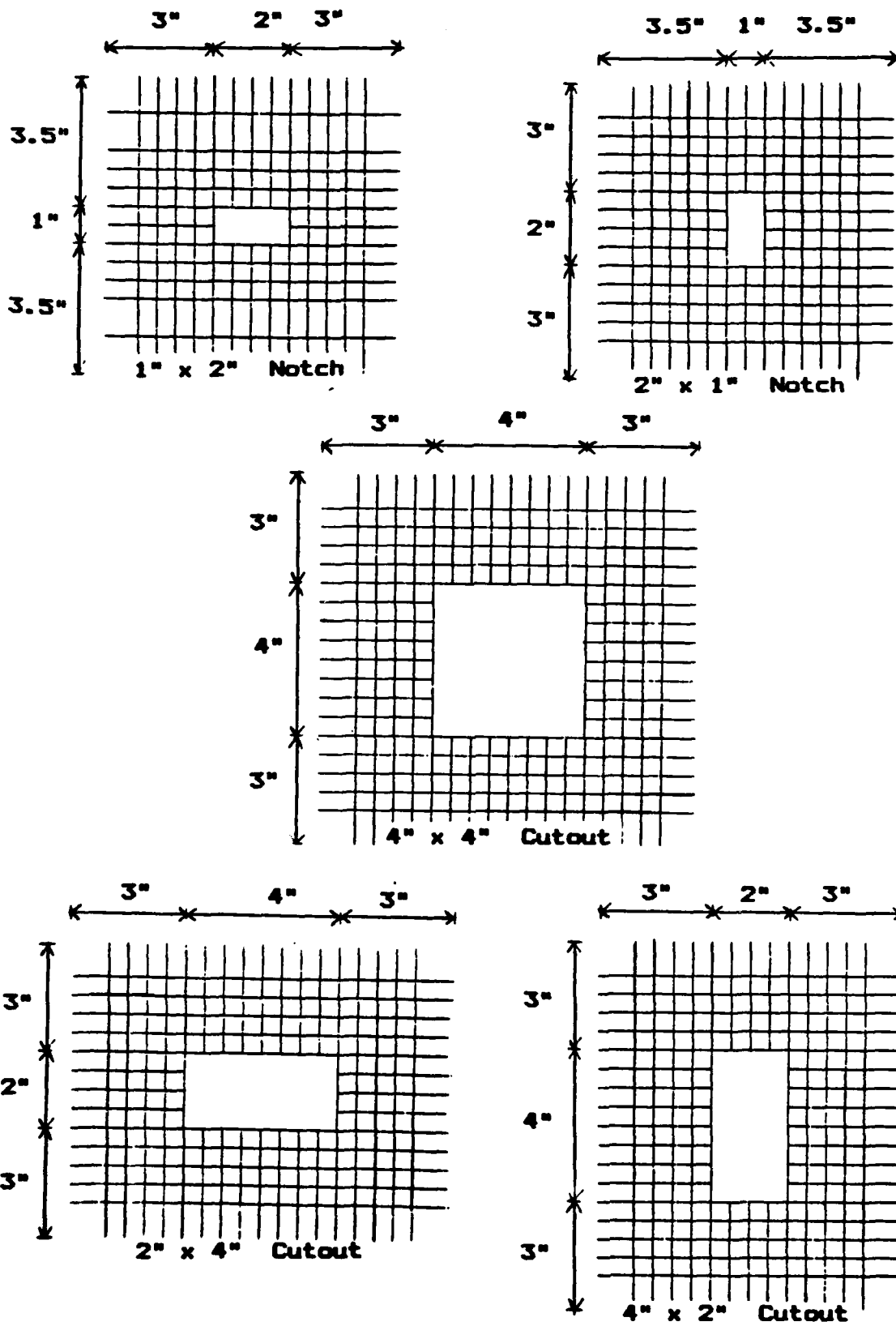
75

Figure 3.33. Refined Mesh in Vicinity of Cutouts

Table 3.2

Grid Selection Data for Panels

Size of Cutout	2"x1"	1"x2"	4"x4"	2"x4"	4"x2"
Grid Size	19x19	17x19	21x21	19x21	21x21
Number of Active DOFs	2761	2437	3007	2903	2917
CPU Time (sec)	2532	1294	4018	2888	3214
Collapse Load (lbs/in)	292.9	249.3	122.0	162.3	180.4
Number of Load Steps	21	33	49	32	34

Figures 3.34 and 3.35. The panels with the 2"x1" and 1"x2" notches have higher collapse loads because there is less material cut from the panel. The 2"x1" notch produces the highest collapse load because its smallest direction is perpendicular to the applied load. This is a stiffer panel than the 1"x2" notch panel because the 1"x2" notch has higher stress concentrations at its corners. The higher stress concentrations can be correlated to higher strains which results in greater displacements. The 4"x4" cutout has the lowest collapse load because it has the most material removed. The 4"x2" cutout, which has an aspect ratio of 2, has a higher collapse load than the 2"x4" cutout. This is due again to the high stress concentrations at the corners of the cutout when considering the 0.5 aspect ratio. These figures show that notches with an aspect
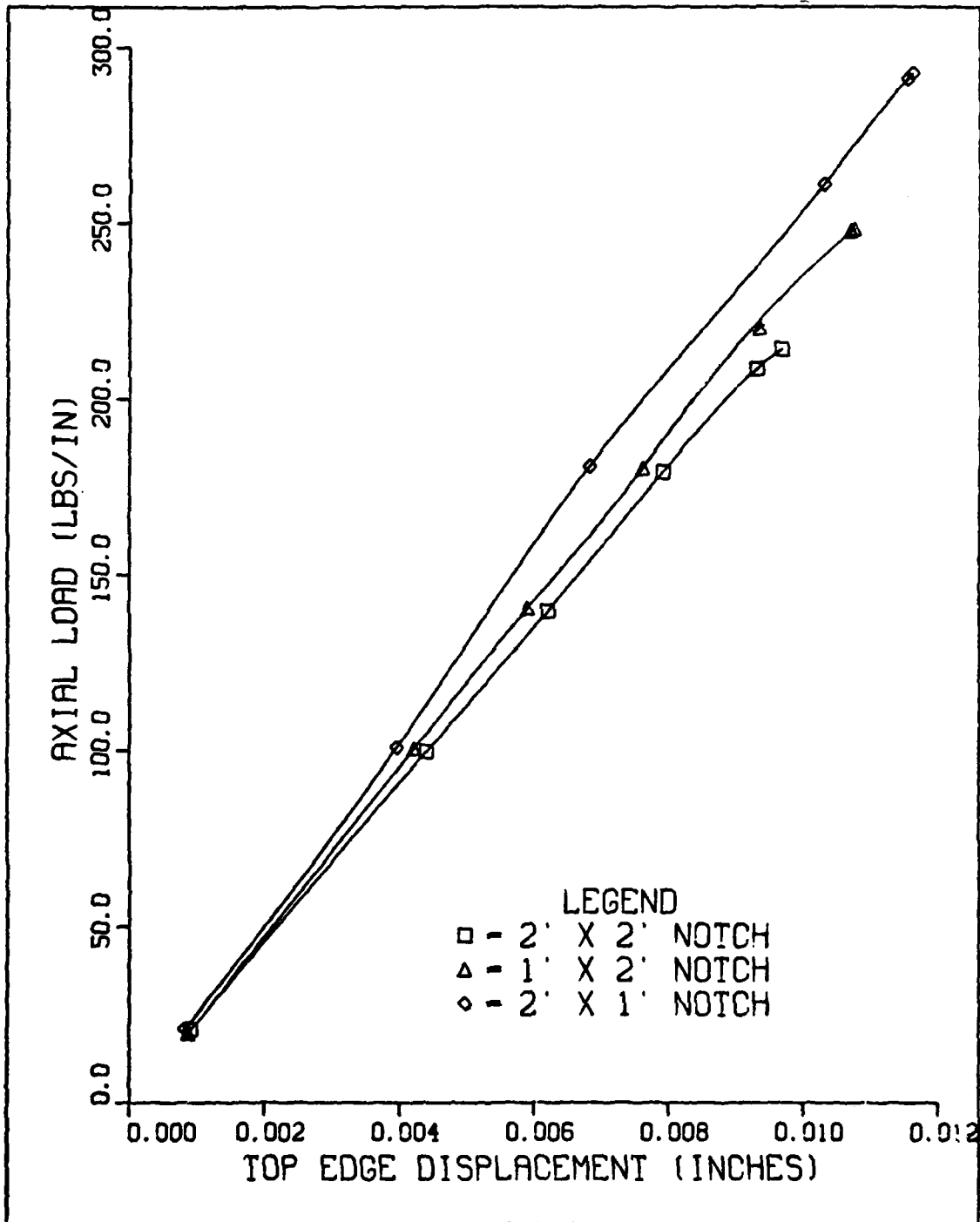
77

Figure 3.34. Load Displacement Curves for Panels with 1"x2", 2"x1", and 2"x2" Notches
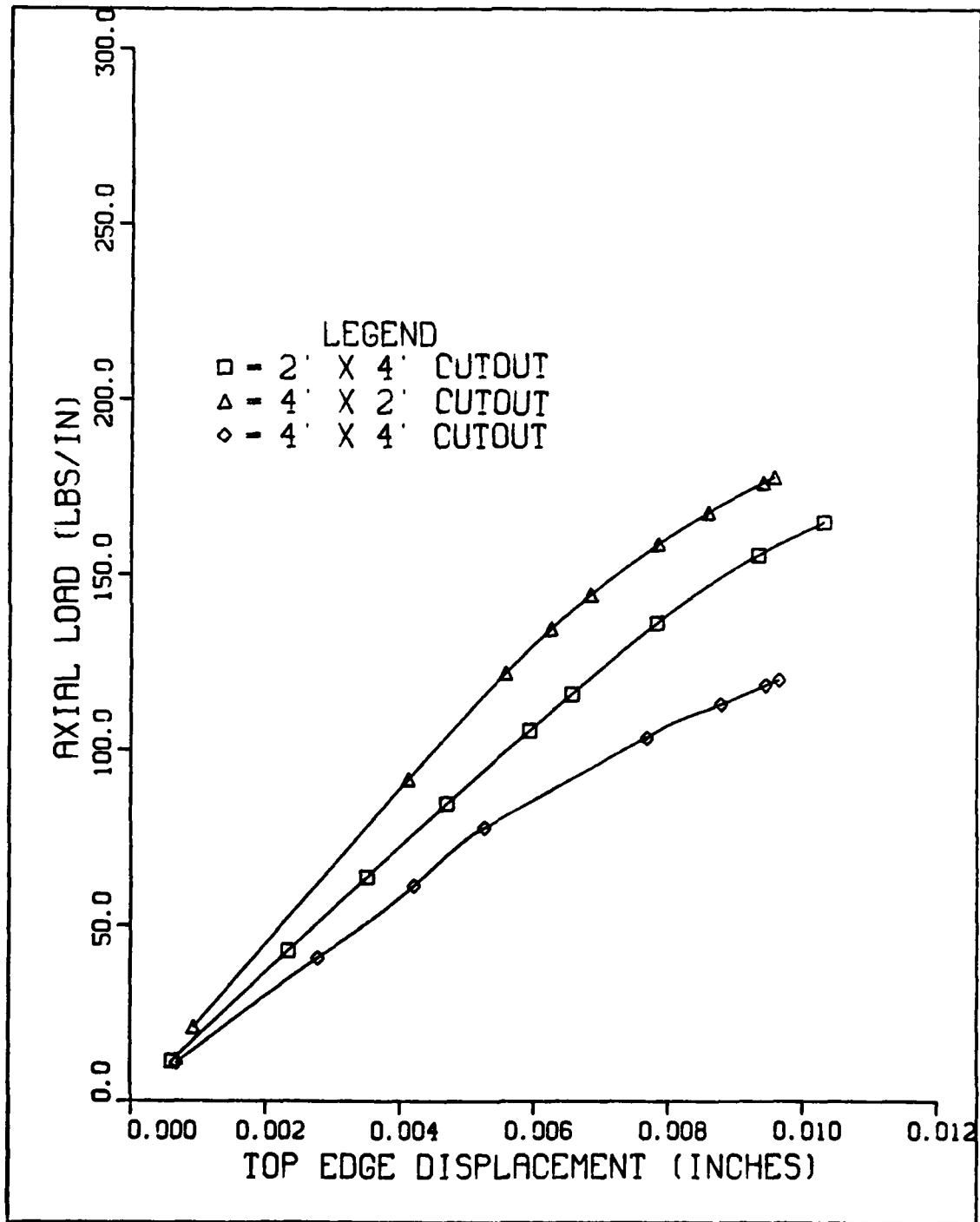
Figure 3.35. Load Displacement Curves for Panels with 2"x4", 4"x2", and 4"x4" Cutouts

79

ratio of 2 can withstand greater loads than cutouts of the same area with aspect ratios of either 0.5 or 1. Furthermore, these figures show that those cutouts defined as notches resist load linearly relative to displacement.

As mentioned previously, the area around cutouts with 0.5 aspect ratios deflect more than notches of the same area with aspect ratios of 2 at equivalent loads. This can be seen in Table 3.3 which lists the maximum and minimum radial displacements corresponding to applied loads. For the 2"x1", 1"x2" and 2"x2" notches, the point of minimum radial displacement is basically the same. It occurs at the center of the upper edge of the cutout in all cases. The point of maximum radial displacement shifts from the upper right edge of the cutout at lower load levels to the upper left quarter of the panel at collapse load. This same pattern can be seen for the 4"x2", 2"x4" and 4"x4" cutouts. Minimum radial displacement occurs near the center of the top edge of the cutout. Maximum radial displacement at collapse load is at the upper left quarter of the panel. The 2"x1" notch produces the least amount of radial displacement at collapse load. The panel with the 4"x4" cutout has the greatest amount of surface area removed which results in a more flexible structure. Therefore, this panel has the largest radial displacement at collapse load of all the panels tested.

To analyze the displacement pattern over the entire panel, contour plots at collapse load are presented in Figures 3.36 through 3.41. For the 2"x1", 1"x2" and 2"x2"

80

Table 3.3

Locations of Points of Maximum and Minimum Radial Displacement for Cutouts Studied

CUTOUT SIZE (in)	LOAD (lbs/in)	WMAX (in)	COORDINATE LOCATION OF WMAX		WMIN (in)	COORDINATE LOCATION OF WMIN	
			X(in)	Y(in)		X(in)	Y(in)
2 x 1	101.1	.00361	6.0	9.5	-.00345	5.0	6.0
	271.0	.01264	6.0	9.5	-.01526	5.0	6.0
	292.9	.01660	5.0	3.0	-.02680	5.0	5.5
1 x 2	100.7	.00703	6.0	9.0	-.00129	5.5	6.0
	236.0	.02717	5.0	3.0	-.03995	5.5	5.5
	249.3	.02547	5.0	2.0	-.05377	5.5	5.5
2 x 2	99.9	.00826	6.0	9.0	-.01412	5.0	6.0
	160.3	.01429	5.5	3.0	-.02467	5.0	6.0
	207.3	.02143	5.5	3.0	-.04591	5.0	5.5
4 x 2	90.5	.00902	5.5	3.5	-.01401	4.0	6.0
	147.3	.04715	6.0	5.0	-.03059	4.0	6.0
	180.4	.07917	6.0	7.0	-.04535	4.0	6.0
2 x 4	40.7	.00893	5.5	3.0	-.01814	5.0	6.0
	100.3	.02464	5.5	3.0	-.05033	5.0	6.0
	162.3	.04360	5.5	9.0	-.08688	5.0	6.0
4 x 4	70.5	.03015	5.5	4.0	-.04093	4.0	6.0
	113.2	.08645	6.0	4.0	-.07824	4.0	6.0
	122.0	.09572	6.0	4.0	-.08487	4.0	6.0

END
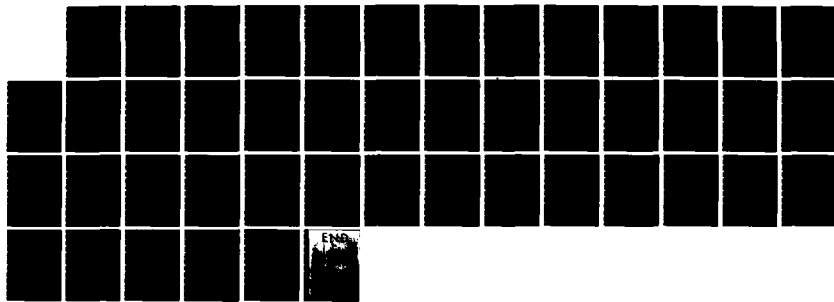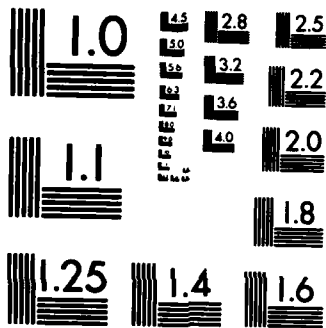
MICROCOPY RESOLUTION TEST CHART
NATIONAL BUREAU OF STANDARDS-1963-A

notch plots, there is a definite inward deflected trough of radial displacement which extends from the upper left edge of the cutout to the lower right edge. For the 2"x1" notch, the trough is almost diagonal from corner to corner whereas the trough for the 1"x2" and 2"x2" begins to shift more towards the center of the panel. Two bulges of positive radial displacement occur along either side of the trough with the maximum displacement being on the upper left quarter of the panel. Refer to Table 3.3 for the coordinate locations of maximum and minimum radial displacement. For the 4"x2", 2"x4" and 4"x4" cutout contours (Figures 3.39 through 3.41), this trough does not extend diagonally but is basically straight up and down the panel. The displacement pattern of the panels with the 4"x2" and 2"x4" cutouts remain almost symmetric at collapse load and the panel with the 4"x4" cutout remains entirely symmetric at collapse. As in the other contour plots the width of the trough corresponds to the width of the cutout. Janisse [23] discusses the fact that the linear eigenvector for a 2"x2" cutout is similar to the collapse contour pattern, thus the small cutout reacts linearly. This is not true with the larger cutouts. This verifies what was stated previously for the definition of a notch in this thesis.

To further analyze the effects of cutout size on the collapse behavior of the panel, radial displacement and moment about the y axis were analyzed. Radial displacement as a function of distance from the left edge of the panel is plotted for the 1"x2" notch in Figure 3.42. Again the
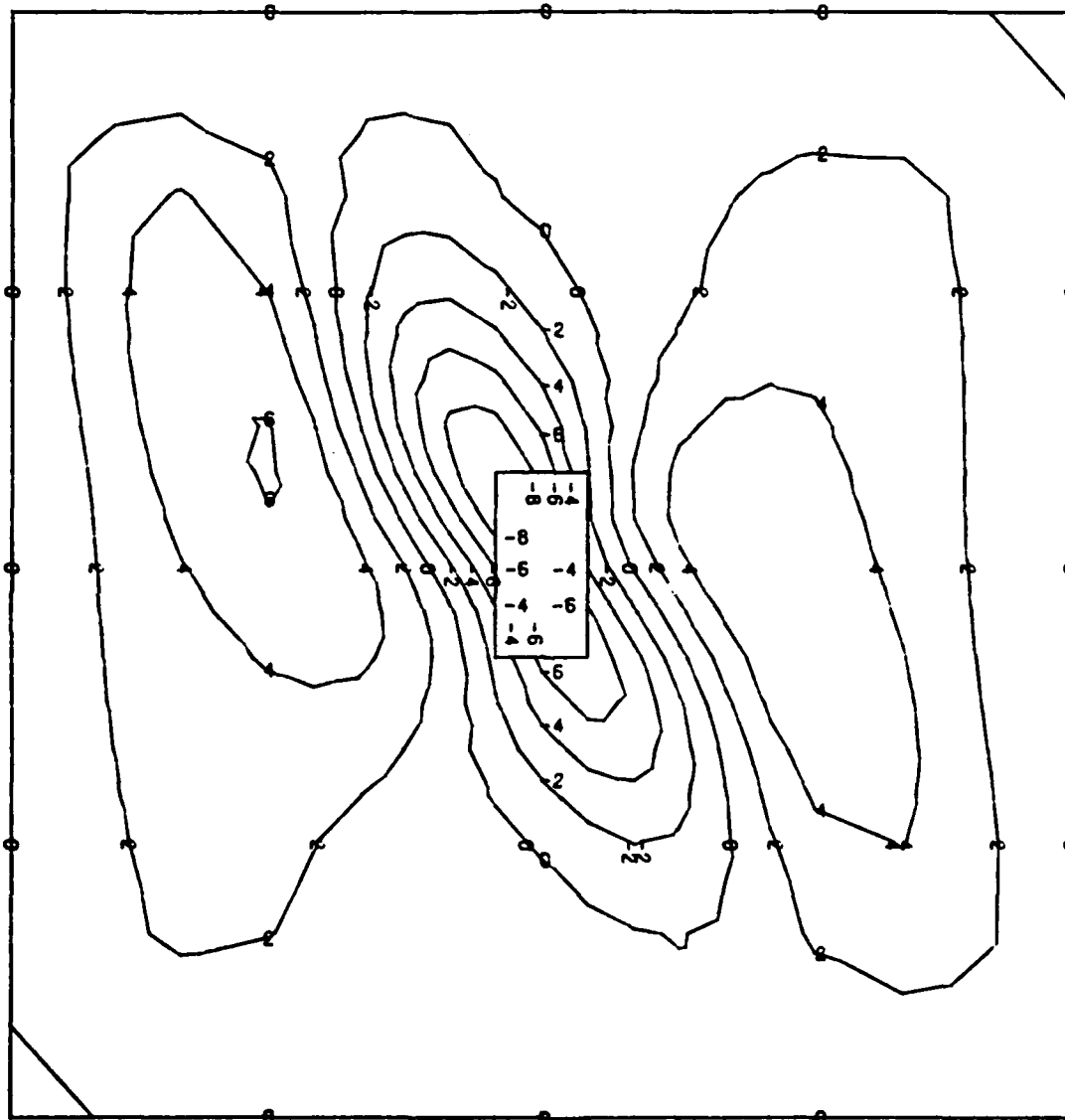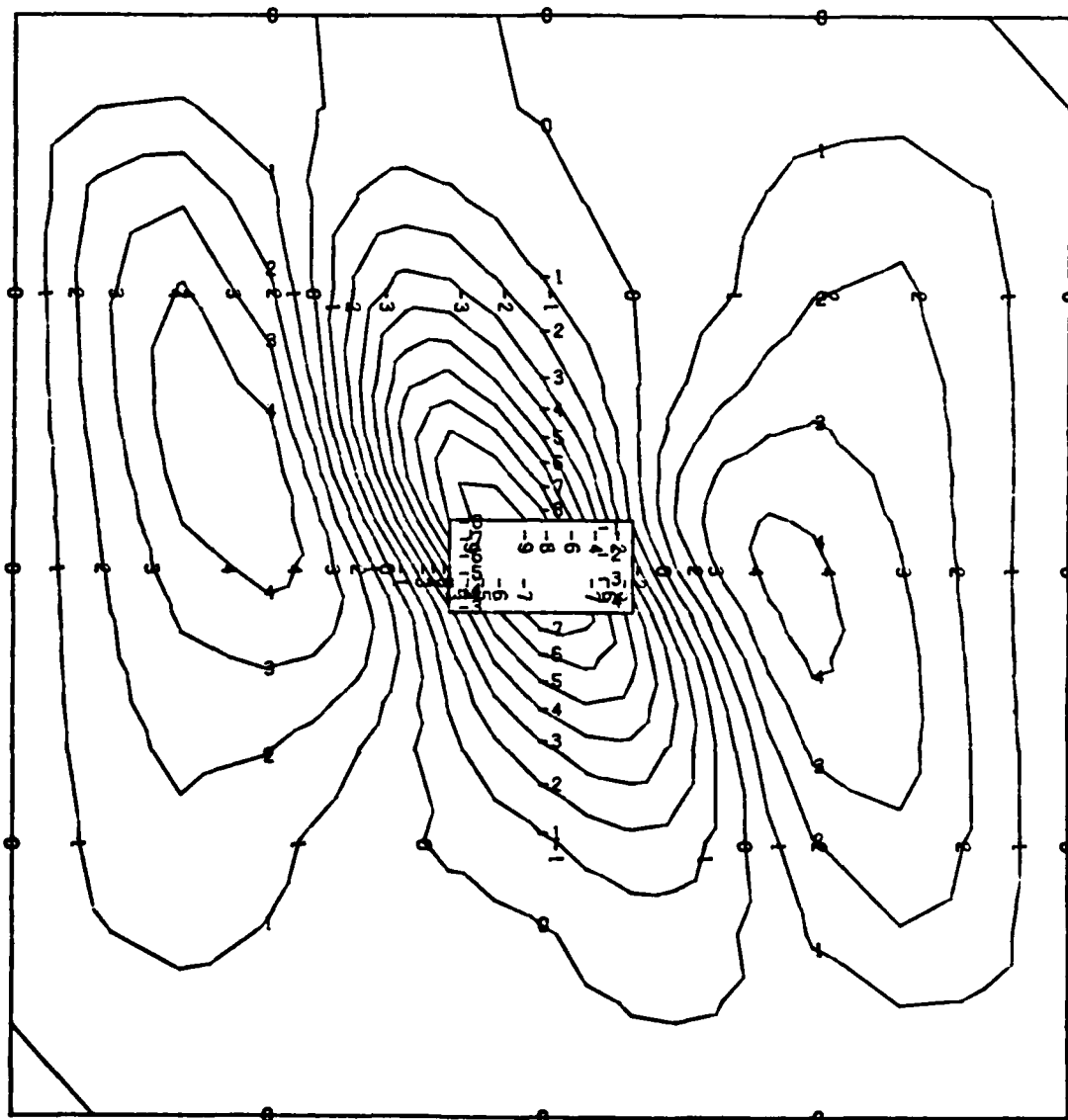
Note: Positive radial displacement is outward.

$$W_{max} = .01660 \text{ inches}$$

$$W_{min} = -.02680 \text{ inches}$$

Figure 3.36. Radial Displacement Contour Plot for 2"x1"
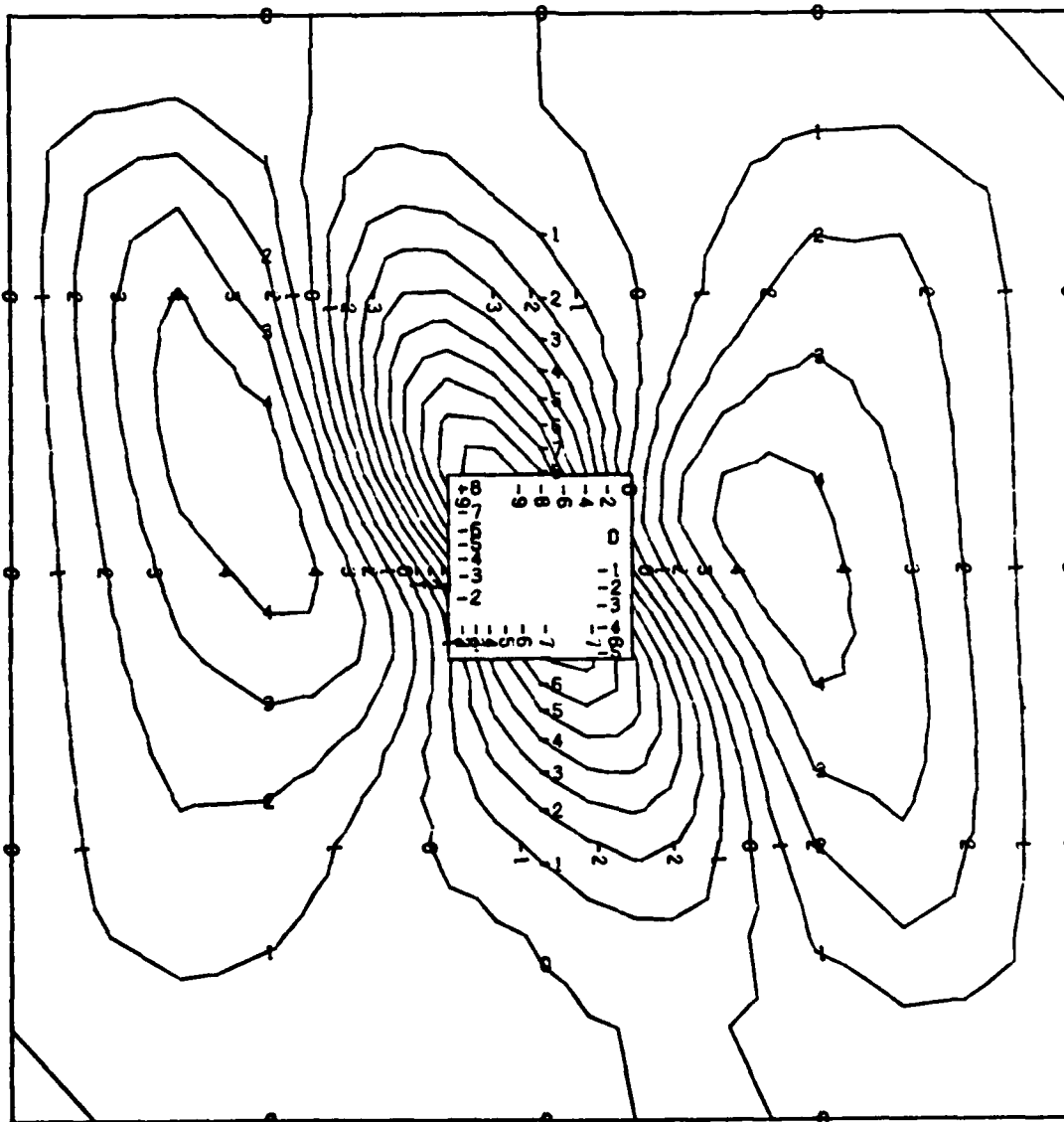
Notch at Collapse Load of 292.9 lbs/in

Note: Positive radial displacement is outward.

W_{max} = .02547 inches

W_{min} = -.05377 inches

Figure 3.37. Radial Displacement Contour Plot for 1"x2"

Notch at Collapse Load of 249.3 lbs/in

Note: Positive radial displacement is outward.

$$w_{max} = .02143 \text{ inches}$$

$$w_{min} = -.04591 \text{ inches}$$

Figure 3.38. Radial Displacement Contour Plot for 2"x2"

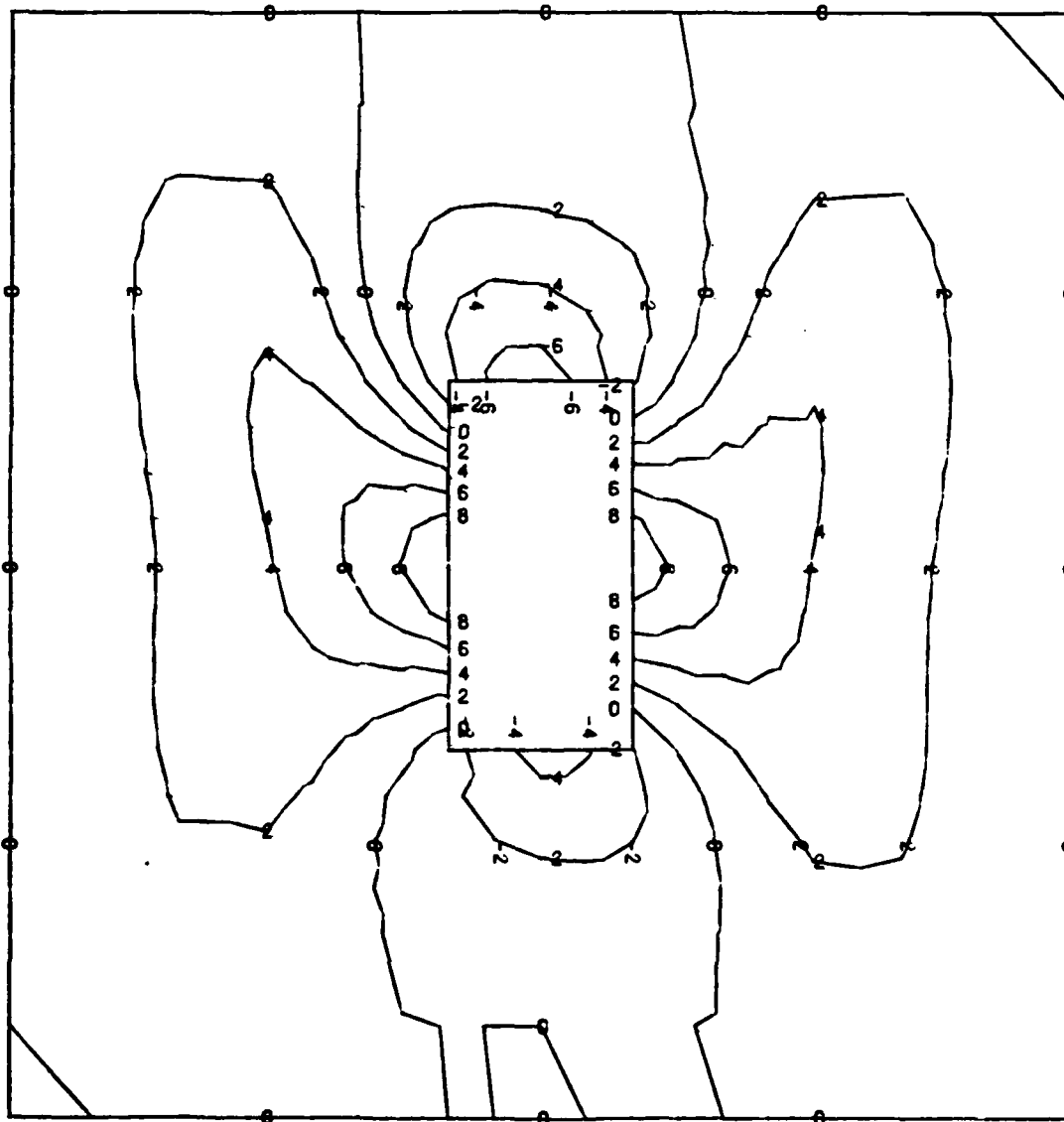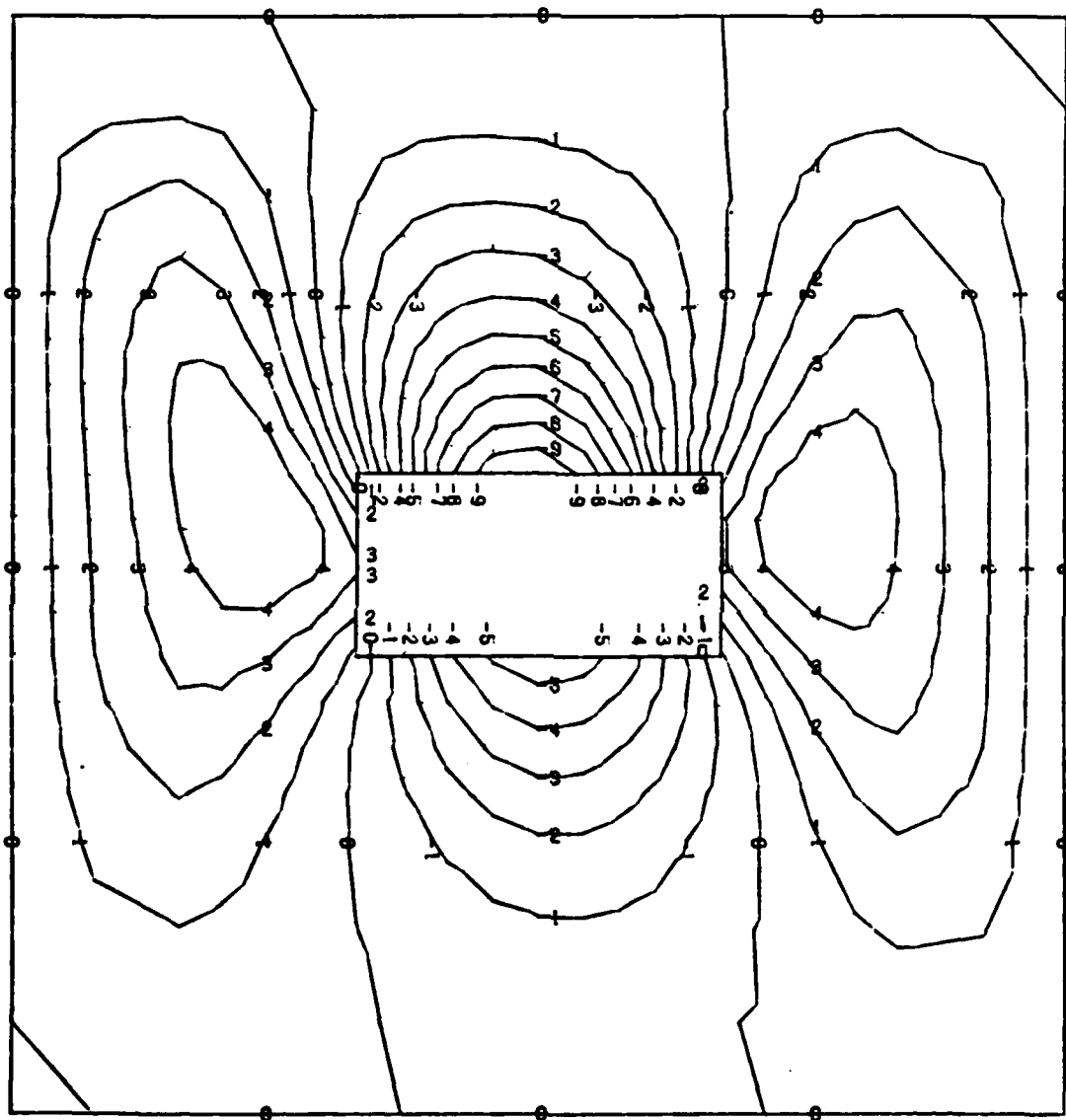Notch at Collapse Load of 207.3 lbs/in

Note: Positive radial displacement is outward.

$$W_{max} = .07917 \text{ inches}$$

$$W_{min} = -.04535 \text{ inches}$$

Figure 3.39. Radial Displacement Contour Plot for 4"x2"

Cutout at Collapse Load of 180.4 lbs/in

Note: Positive radial displacement is outward.

$$w_{max} = .04360 \text{ inches}$$

$$w_{min} = -.08688 \text{ inches}$$

Figure 3.40. Radial Displacement Contour Plot for 2"x4"
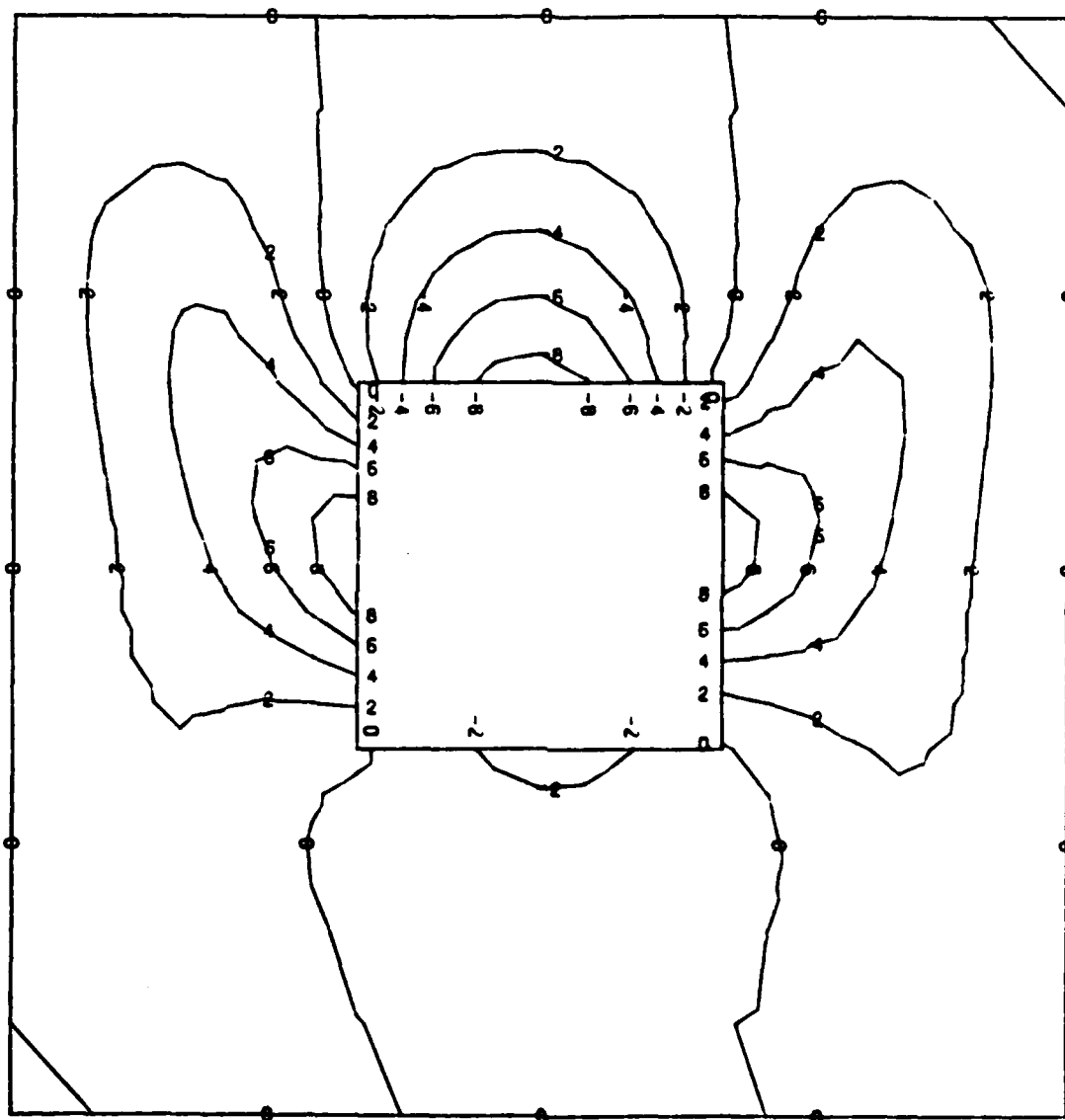Cutout at Collapse Load of 162.3 lbs/in

Note: Positive radial displacement is outward.

W_{max} = .09572 inches

W_{min} = -.08487 inches

Figure 3.41. Radial Displacement Contour Plot for 4"x4"

Cutout at Collapse Load of 122.0 lbs/in.

trough begins to appear with increasing load and the minimum radial displacement shifts from about 4" from the left edge (along the line 3" from the top of the panel) to about 7" from the left edge (along the line 9" from the top of the panel). The moment about the y axis as a function of distance from the left edge is plotted in Figures 3.43 through 3.45 for the 1"x2" notch. The point of minimum M_x along a line 4.25" from the top of the panel corresponds to the same location as the point of minimum radial displacement in Figure 3.42. The moments are greater in magnitude along the area where the trough forms in the panel than M_x near the right edge of the panel. Figure 3.44 is a plot of M_x along a line 5.75" from the top of the panel which passes through the cutout. At collapse load, there is a jump from negative moment on the left edge of the notch to a larger positive moment on the right edge of the notch. Along the line 7.75" from the top of the panel (Figure 3.45), the maximum negative moments occur in the same area that the trough forms. At lower load levels, the values for M_x are symmetric along each of the lines across the panel. At collapse load, the moments are not symmetric and the largest negative moments occur along the radial displacement trough.

The radial displacement and moment in the x direction for the 2"x1" notch are plotted in Figures 3.46 through 3.49. The radial displacement trough seen in Figure 3.46 extends from approximately 5" from the left edge (above the cutout) to 7" from the left edge (along the line below the
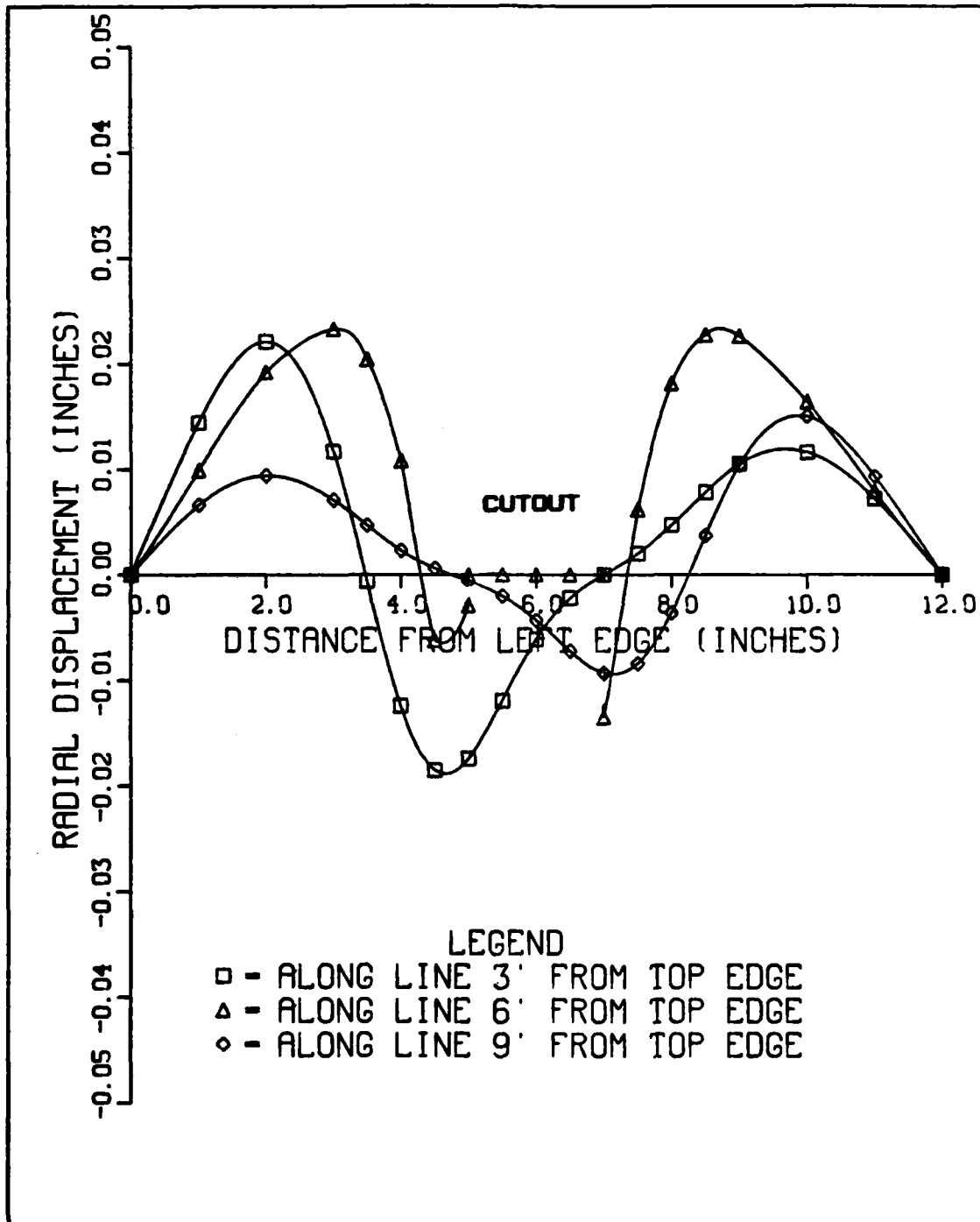
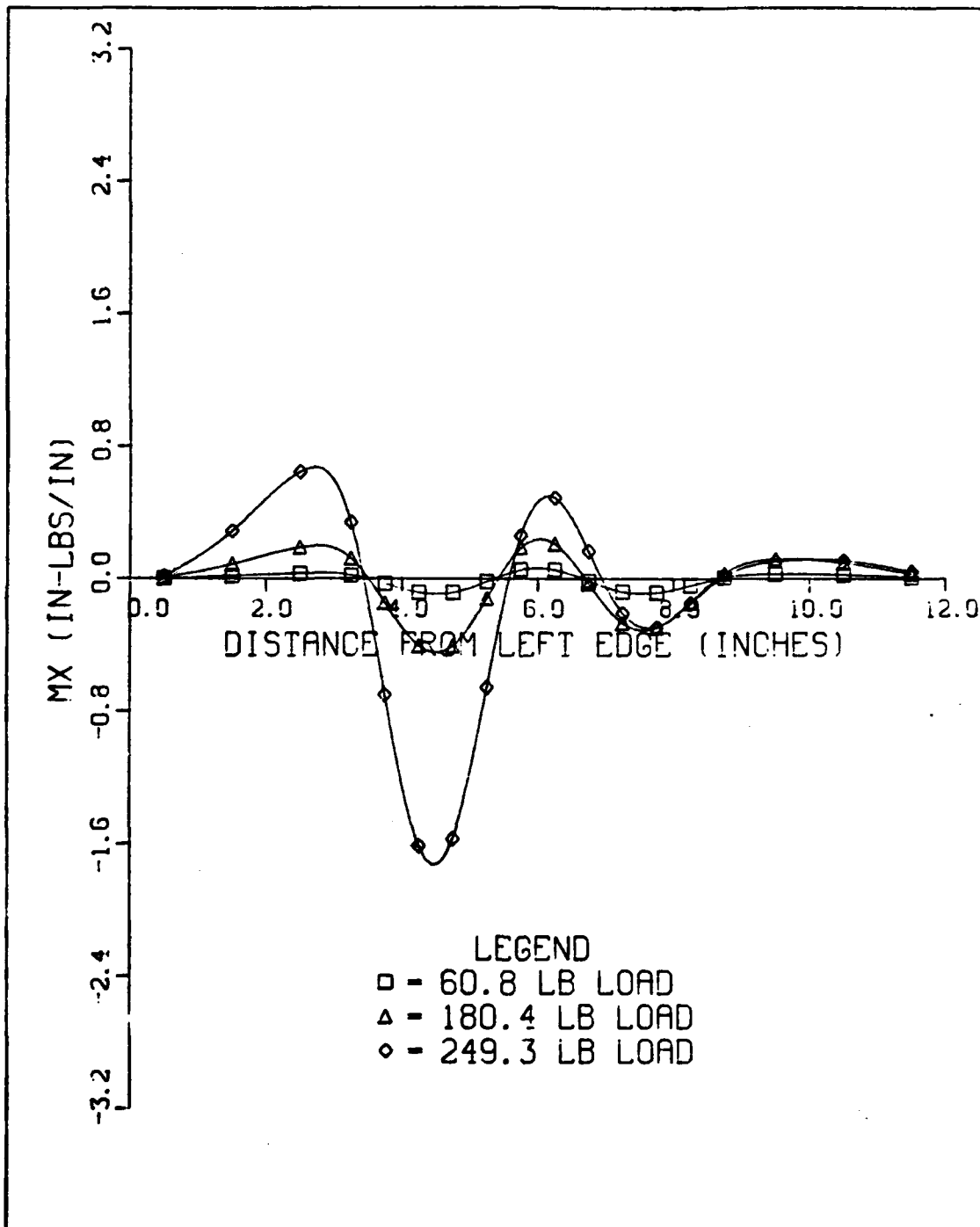**Figure 3.42.   Radial Displacement Profile at Collapse Load for 1"x2" Notch**

Figure 3.43. M_x along a Line 4.25" from Top Edge of Panel for 1"x2" Notch
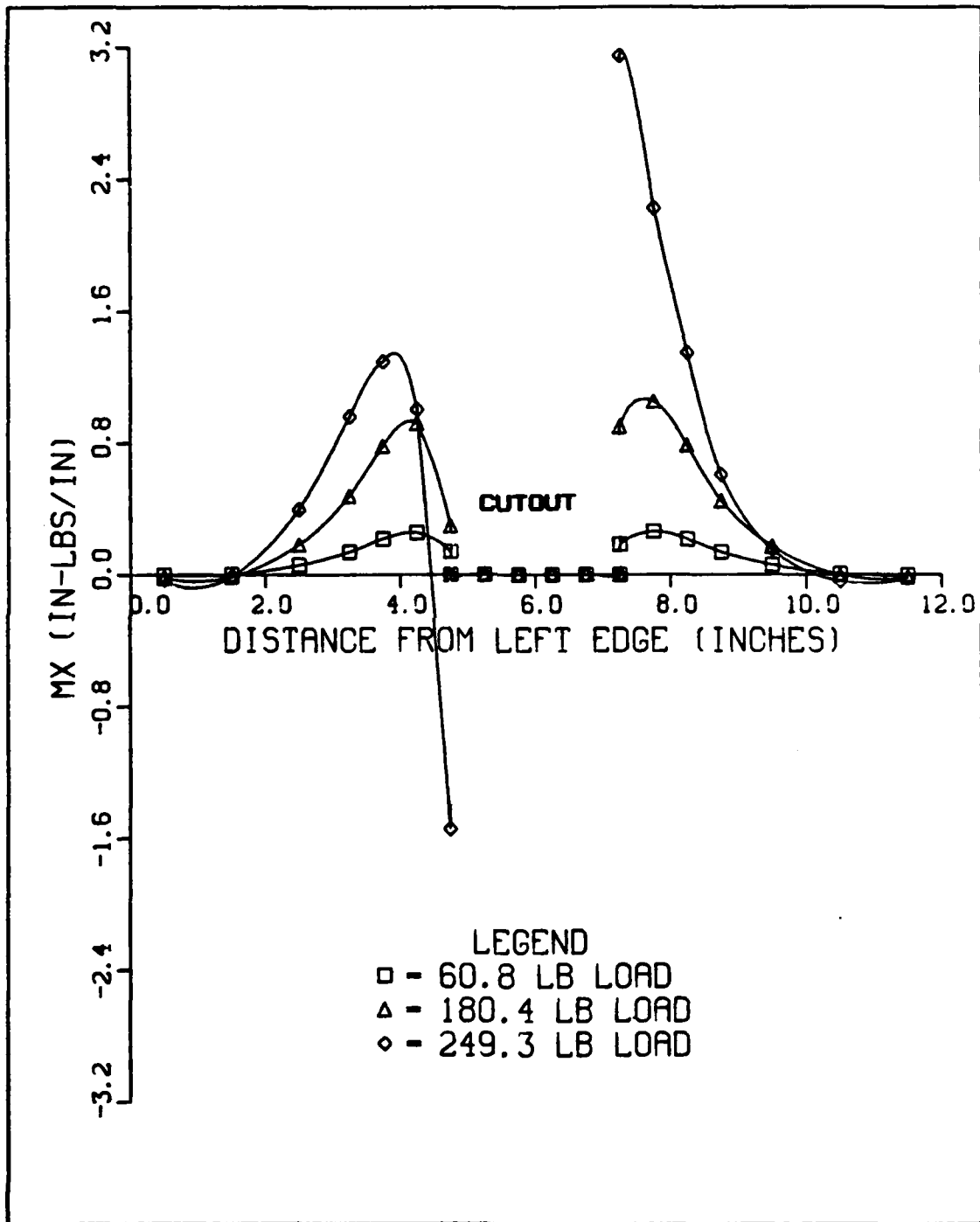
91

Figure 3.44. M_x along a Line 5.75" from Top Edge of Panel for 1"x2" Notch
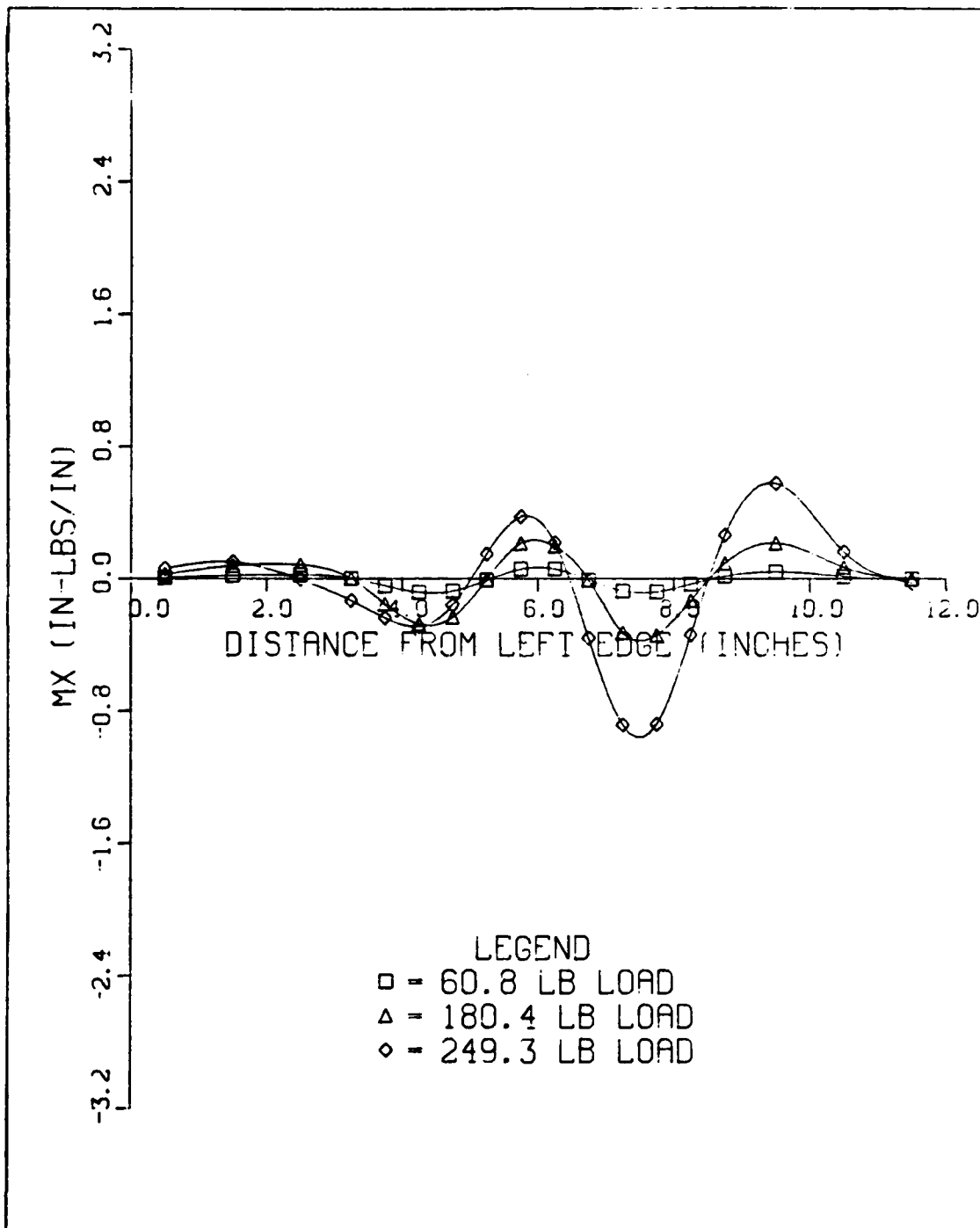
92

Figure 3.45. M_x along a Line 7.75" from Top Edge
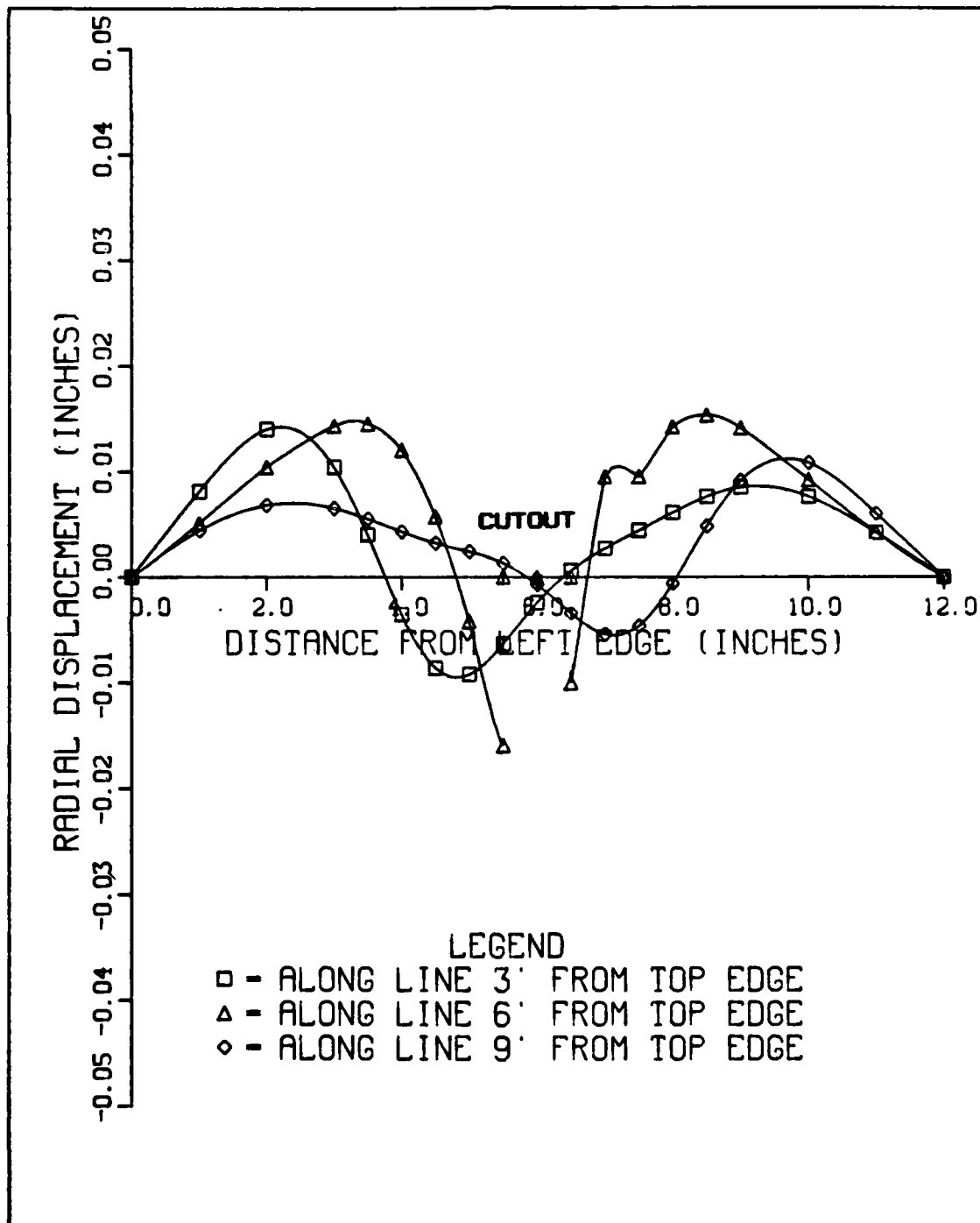of Panel for 1"x2" Notch

93

Figure 3.46. Radial Displacement Profile at Collapse

Load for 2"x1" Notch

cutout). The notch is slightly skewed because the left edge of the notch displaces inward more than the right edge of the notch.   Positive radial displacements correspond to positive moments in Figures 3.47 through 3.49.   Minimum moments correspond to the locations of minimum radial displacement (the trough) in Figure 3.46.   Along the line 4.25" from the top of the panel, the moment is small near the right edge of the panel and the minimum value occurs in the radial displacement trough.   The moments are primarily positive along the line that passes through the notch (Figure 3.48).   On the left edge, the moment goes negative at, collapse load, then makes a large jump to a positive moment on the right edge of the notch.   This is due once again to the cutout being skewed as load is applied.   The values for M_x are very small along the line 7.75" form the top (Figure 3.49) except for a large negative moment in the area of the trough.

The radial displacements and moment resultants for the 2"x2" notch are presented in Figures 3.50 through 3.53.   The positive radial displacements in Figure 3.50 correspond to positive values of M_x. Along the line 4.25" from the top of the panel (Figure 3.51), the moments near the right edge of the panel are less than near the left edge.   This again can be attributed to the buckling shape of the panel with the trough forming from the upper left section of the panel to the lower right section.   The moments directly above the notch are negative. Along the line that passes through the notch Figure 3.52, the moment again jumps in magnitude from

95

Figure 3.47. M_x along a Line 4.25" from Top Edge
of Panel for 2"x1" Notch

Figure 3.48. M_x along a Line 5.75" from Top Edge
of Panel for 2"x1" Notch

97

Figure 3.49. M_x along a Line 7.75" from Top Edge
of Panel for 2"x1" Notch

98

Figure 3.50. Radial Displacement Profile at Collapse Load for 2"x2" Notch
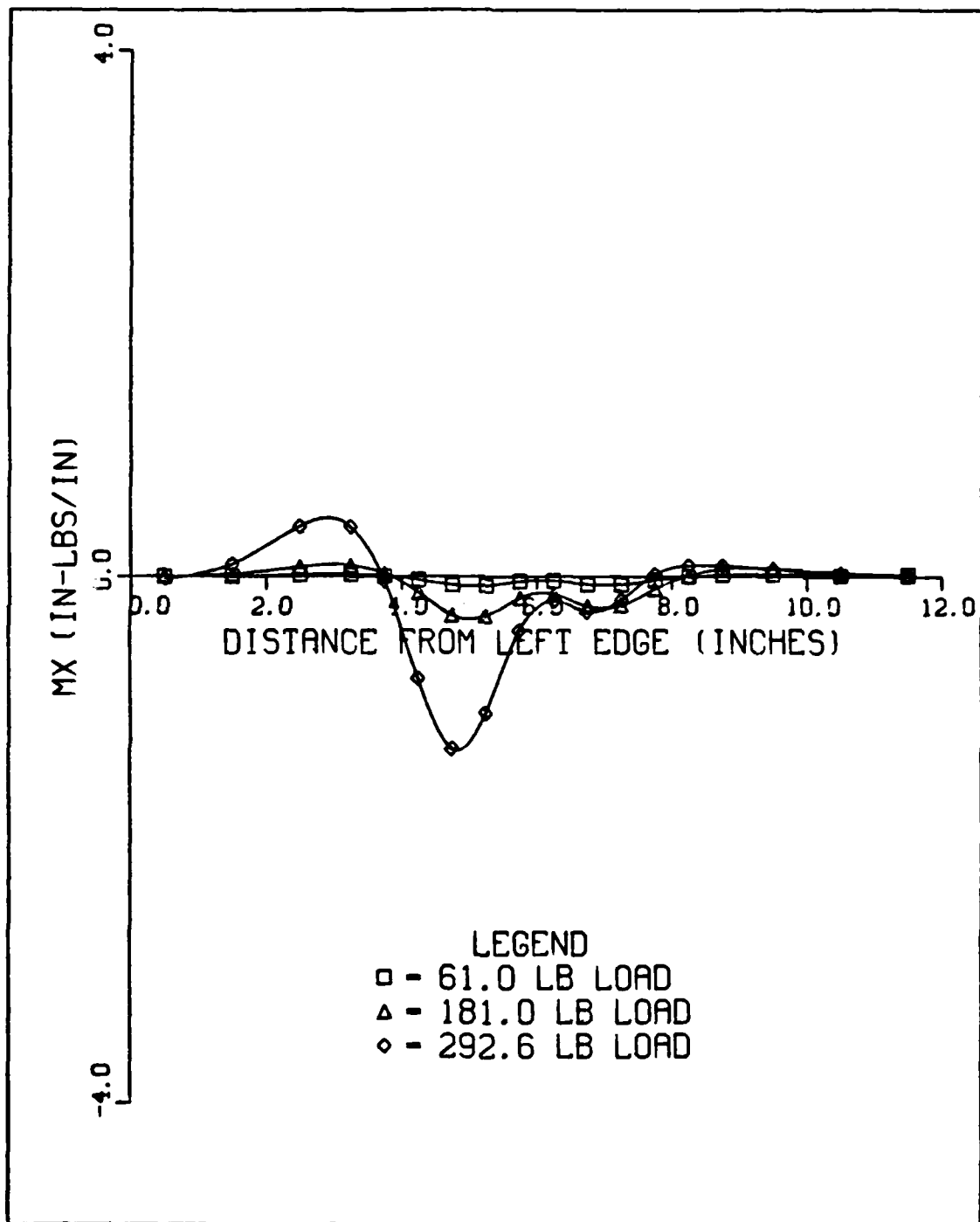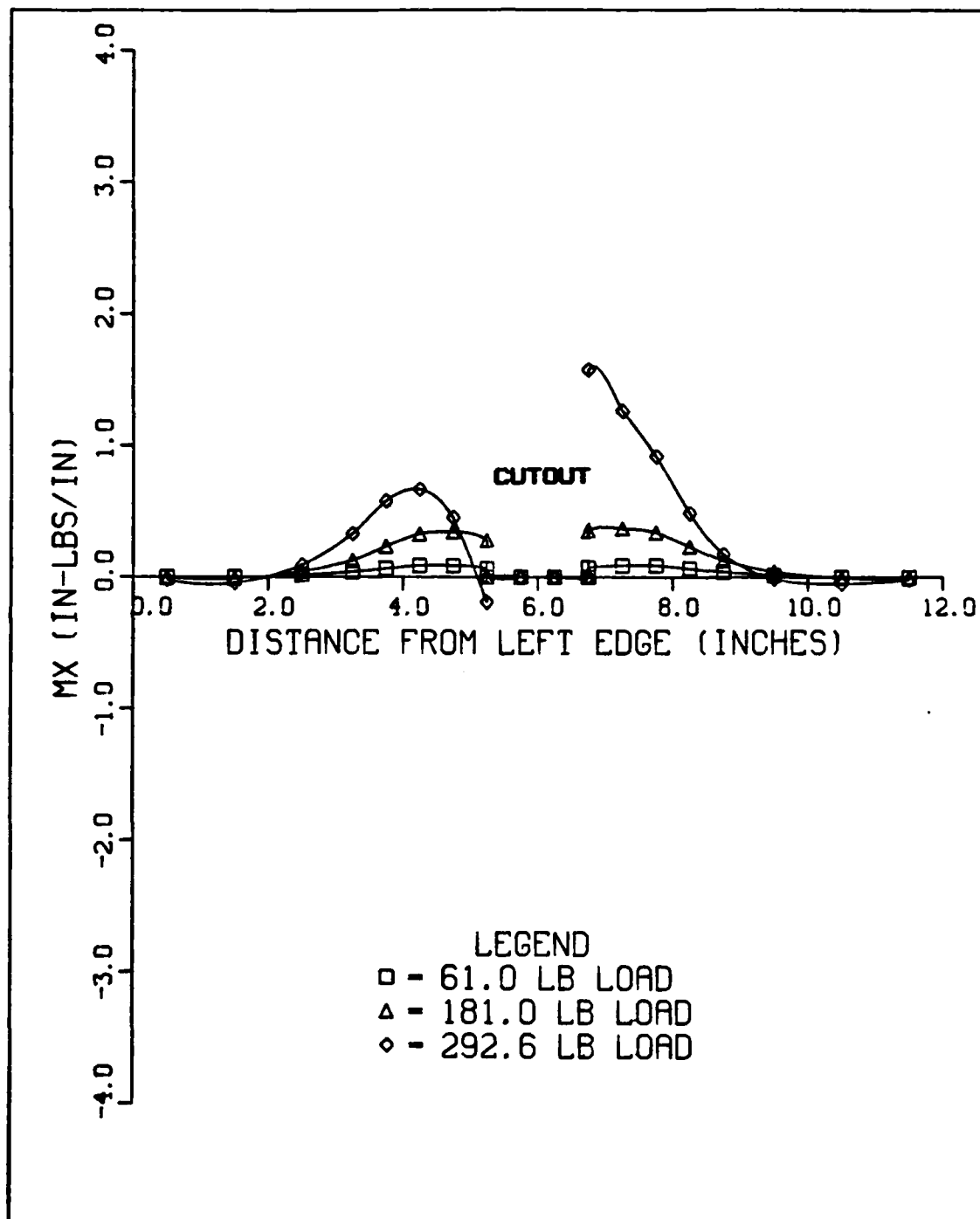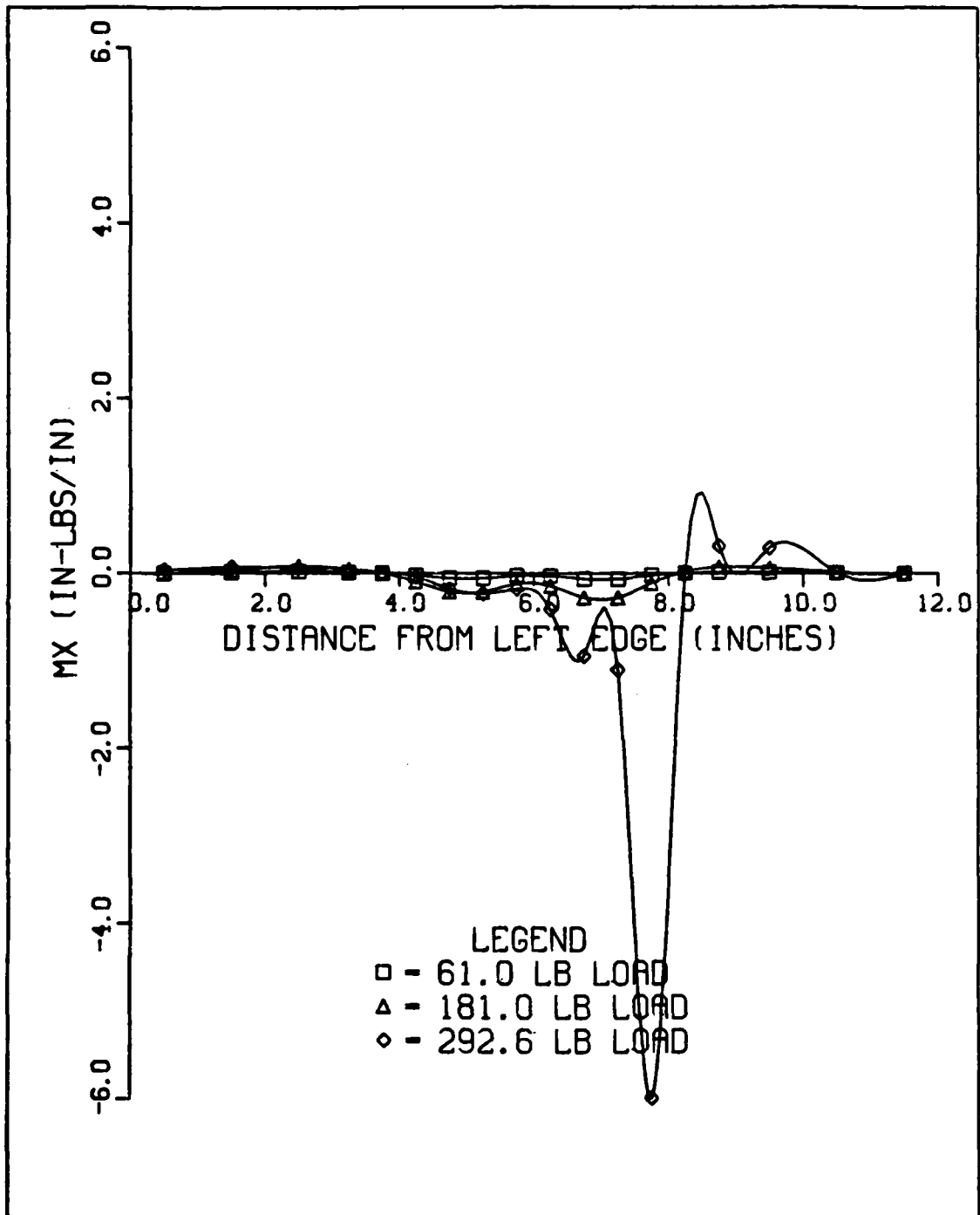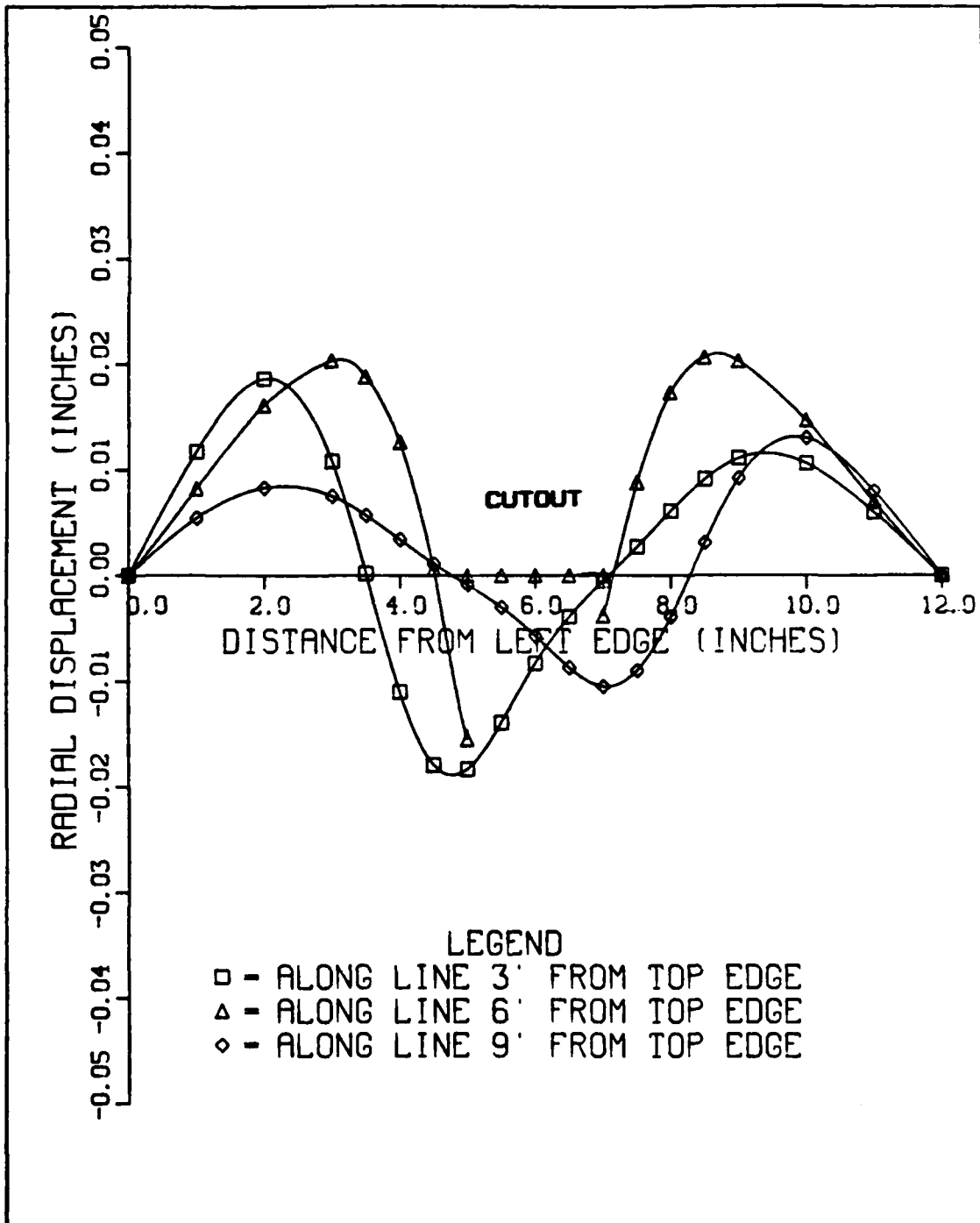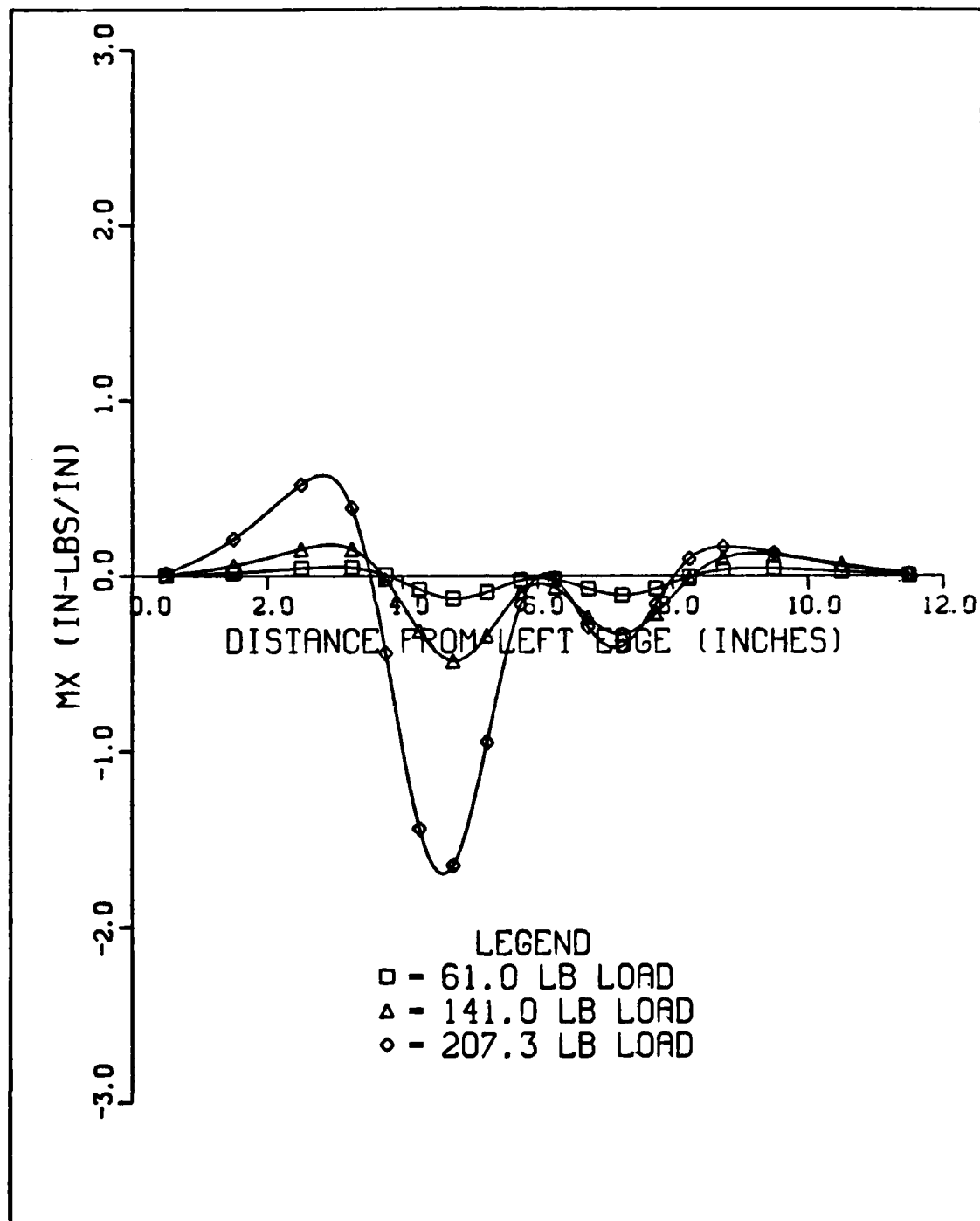
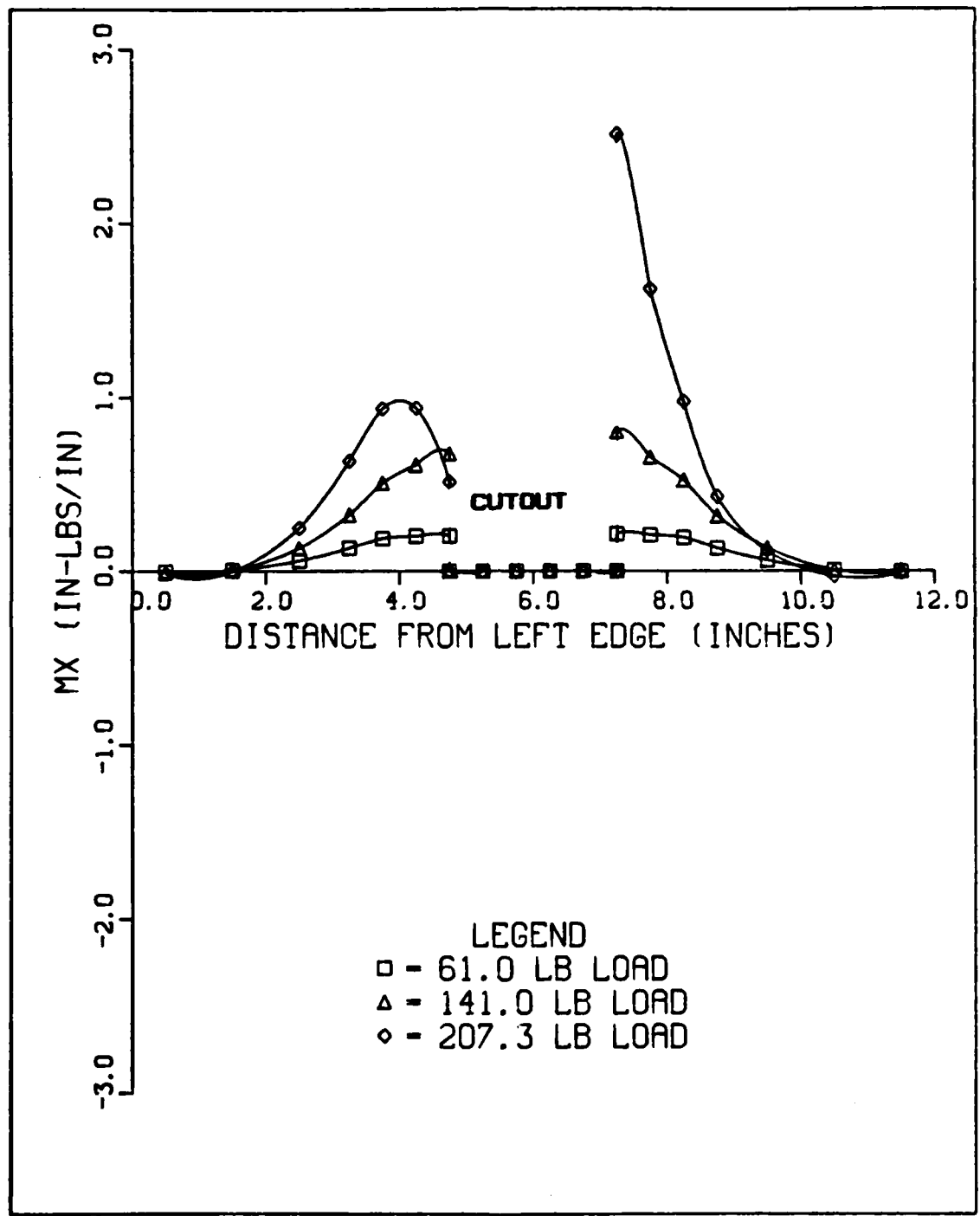Figure 3.51. M_x along a Line 4.25" from Top Edge of Panel for 2"x2" Notch

Figure 3.52. M_x along a Line 5.75" from Top Edge of Panel for 2"x2" Notch

the left edge to the right edge of the notch.   The largest
moments in the panel at collapse load are at the right edge
of the cutout.   There is a large negative moment in the
trough along the 7.75" line (Figure 3.53) which corresponds
to the large negative moment in the trough along the upper
line.

For the 2"x4" cutout, the radial displacement trough is
not diagonal across the panel as with the smaller notches.
The trough is also considerably wider, corresponding to the
width of the cutout.   Figure 3.54 depicts the displacement
pattern for the 2"x4" cutout.   The point of minimum radial
displacement shifts to the right by only one inch from top
to bottom of the panel.   For low load levels, M_x is
symmetric about the center of the panel as can be seen in
Figure 3.55. At collapse load, the moment still retains its
symmetry along the upper line.   The minimum value for the
moment once again occurs in the slight radial displacement
trough. M_x along the line at the center of the panel,
Figure 3.56, is greater at the left side of the cutout.
This is opposite to what happens with the smaller notches.
This effect can be attributed to the fact that there is not
a deep radial displacement trough extending diagonally
across the panel contrary to the smaller notches.   The
moments along the line near the bottom edge (Figure 3.57)
are less than the moments at other locations and retain
their symmetry throughout the load application process.
This is due to the bottom line being a large distance from
the cutout where the effect of the large displacements

102

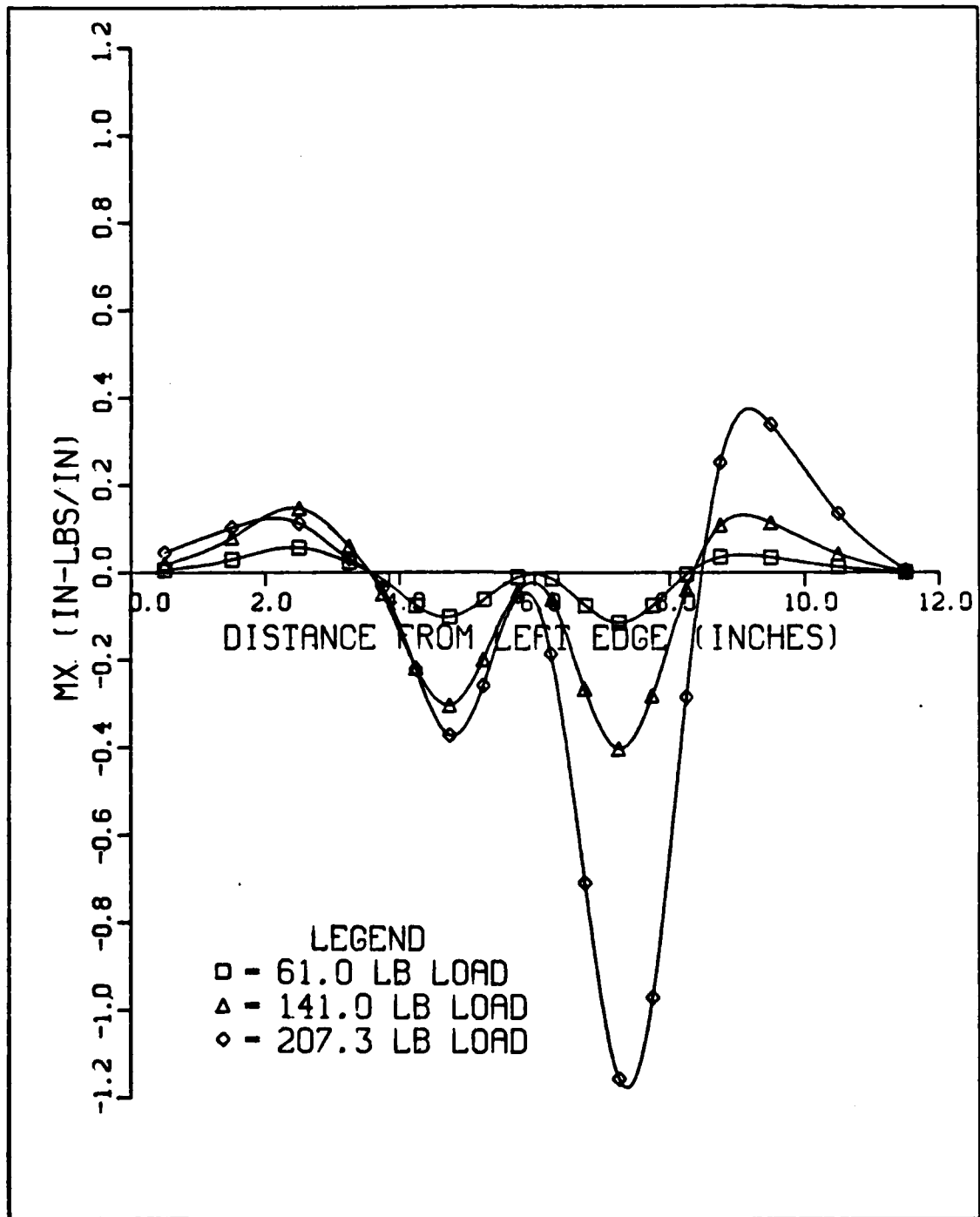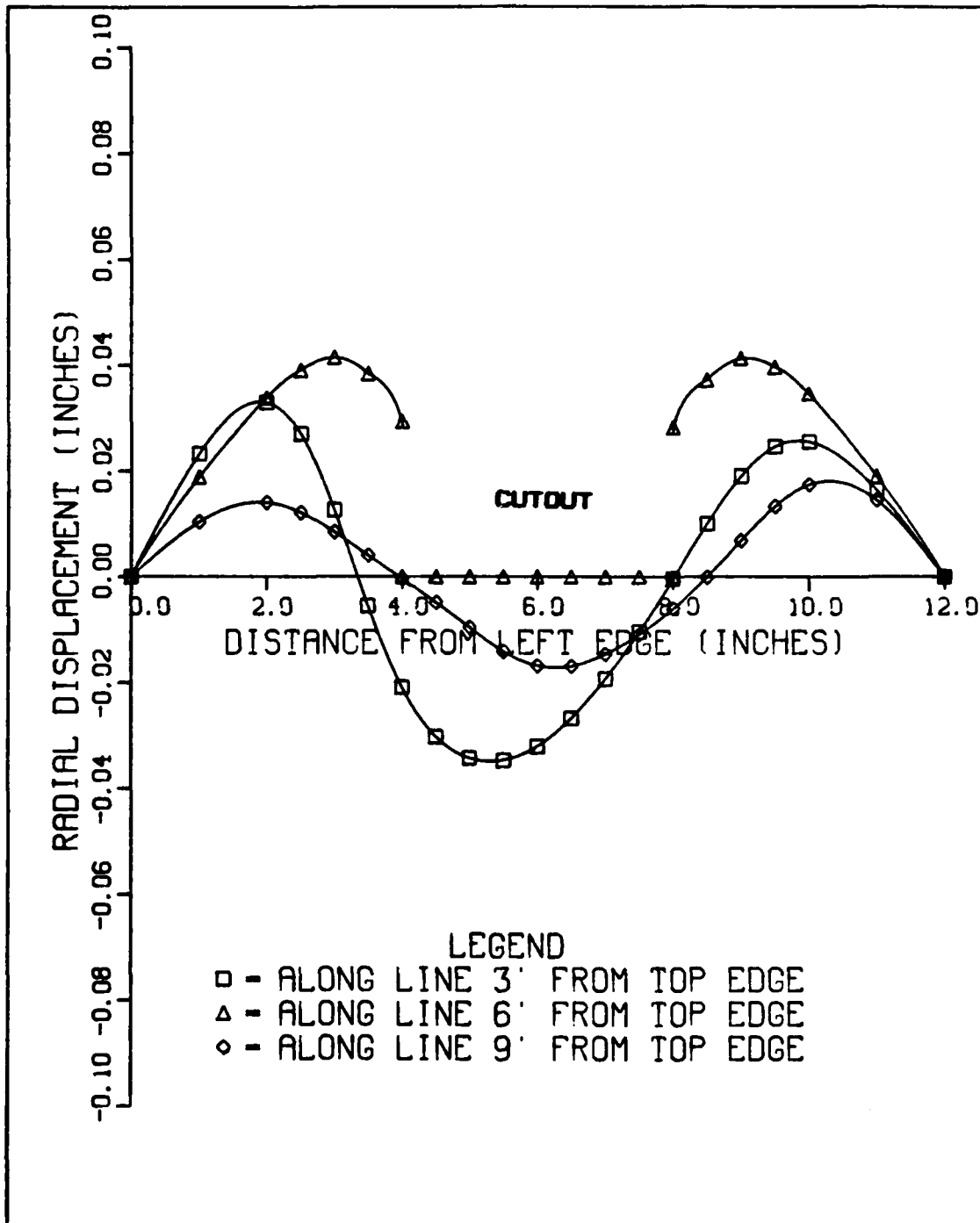Figure 3.53. M_x along a Line 7.75" from Top Edge of Panel for 2"x2" Notch

103

Figure 3.54. Radial Displacement Profile at Collapse
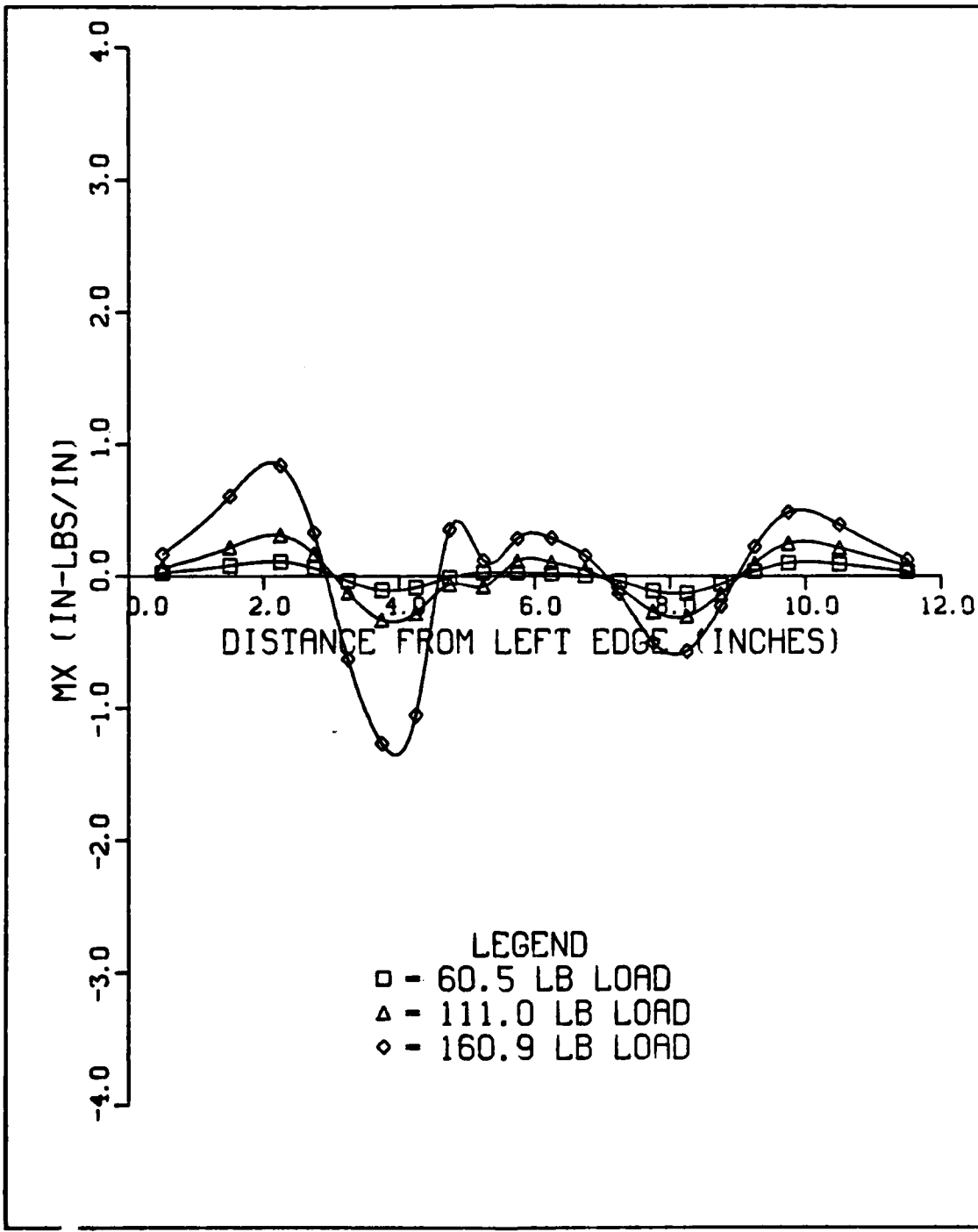Load for 2"x4" Cutout

Figure 3.55. M_x along a Line 3.75" from Top Edge
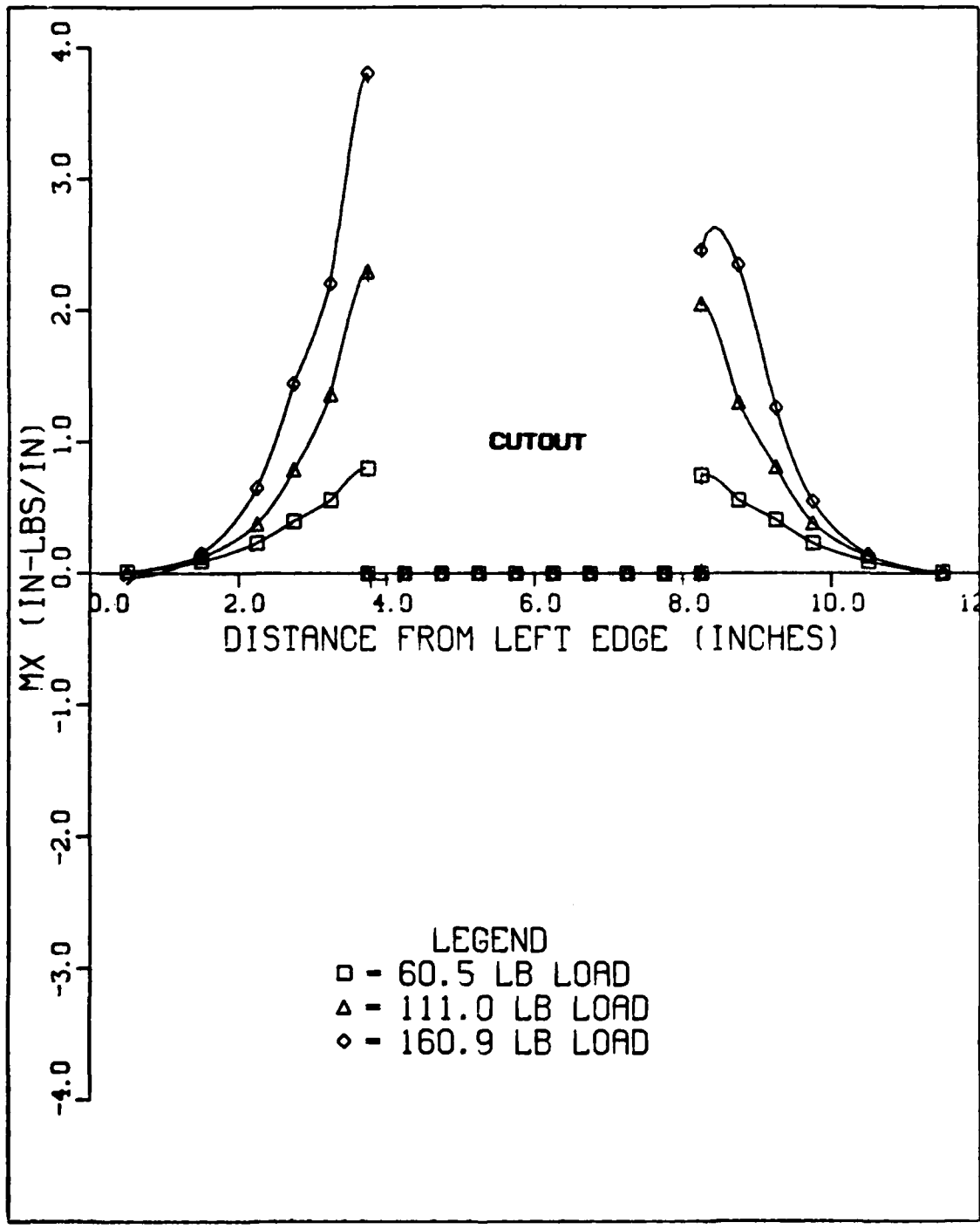of Panel for 2"x4" Cutout

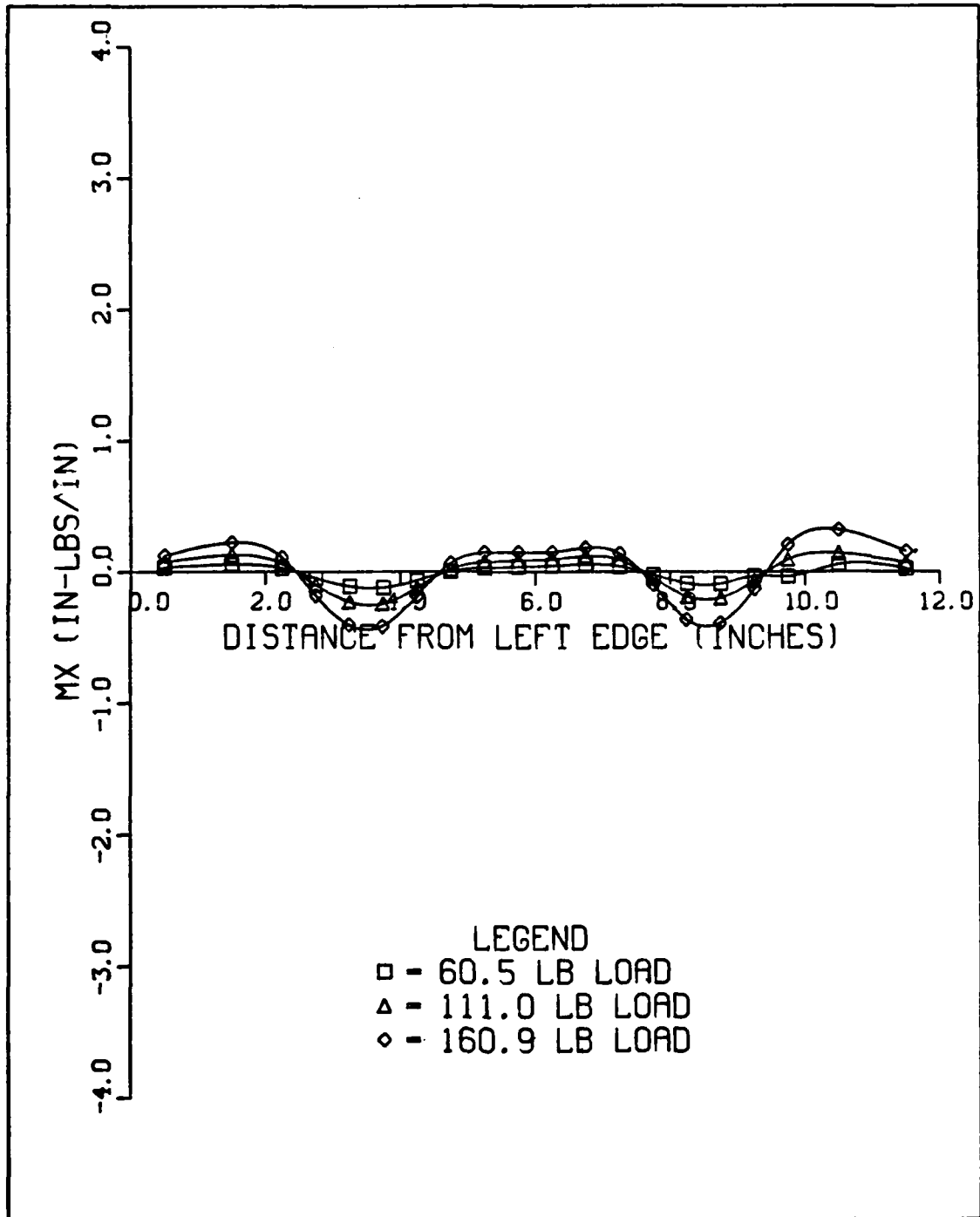Figure 3.56. M_x along a Line 5.75" from Top Edge of Panel for 2"x4" Cutout

Figure 3.57. M_x along a Line 8.25" from Top Edge of Panel for 2"x4" Cutout

around the cutout are not felt. Also, this line is nearer the clamped bottom edge which restrains displacements and therefore results in smaller moments.

Once again the radial displacement profile (Figure 3.58) shows only a slight shift in the location of the displacement trough from top to bottom of the panel for the 4"x2" notch. There are large symmetric peaks in displacement on either edge of the cutout. This is due to the small length of the notch in the circumferential direction which causes the notch not to skew with applied load. The moments along the 3.75" line are much greater than the moments for the smaller notches as can be seen in Figure 3.59. The moments are symmetric about the center of the panel for all load levels. This is because the trough is not diagonal, but rather follows the center line of the panel. M_x along the center of the panel (Figure 3.60) is symmetric about the notch, again indicating that the cutout does not skew. Along the line near the bottom of the panel, Figure 3.61, the moments are greater than for the smaller notches and are symmetric.

The results for the 4"x4" cutout follow the same pattern as for the 4"x2" cutout. Figure 3.62 shows the radial displacement trough does not shift significantly to the right. Maximum radial displacement occurs along a line near the center of the cutout. For the panel with the 4"x4" cutout, the radial displacement plot shows that there are large displacements, and consequently, large rotations near the cutout at collapse load. The maximum displacements are
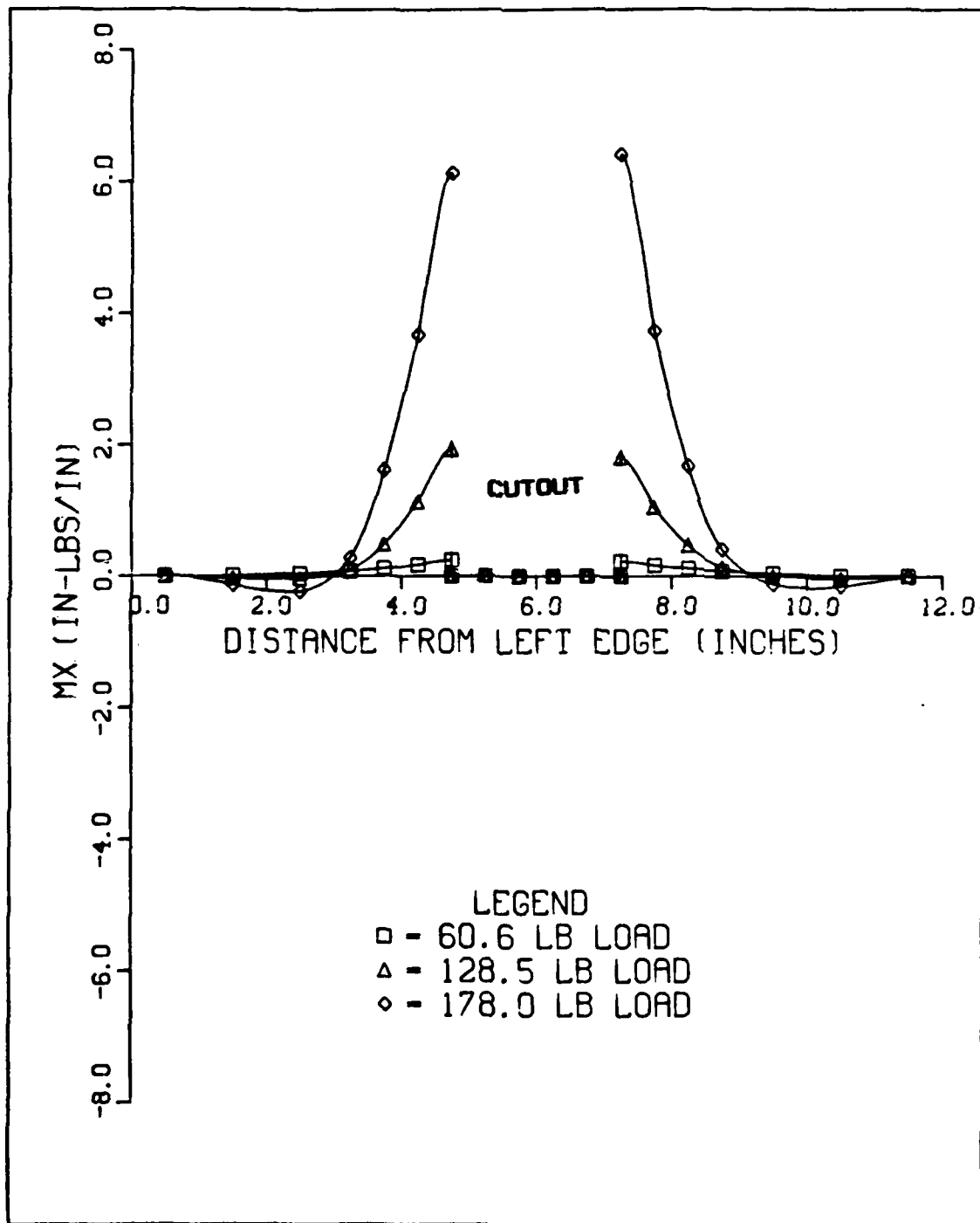
Figure 3.58.   Radial Displacement at Collapse Load

for 4"x2" Cutout

Figure 3.59. M$_x$ along a Line 3.75" from Top Edge of Panel for 4"x2" Cutout

Figure 3.60. M_x along a Line 5.75" from Top Edge of Panel for 4"x2" Cutout

Figure 3.61. M_x along a Line 8.25" from Top Edge
of Panel for 4"x2" Cutout
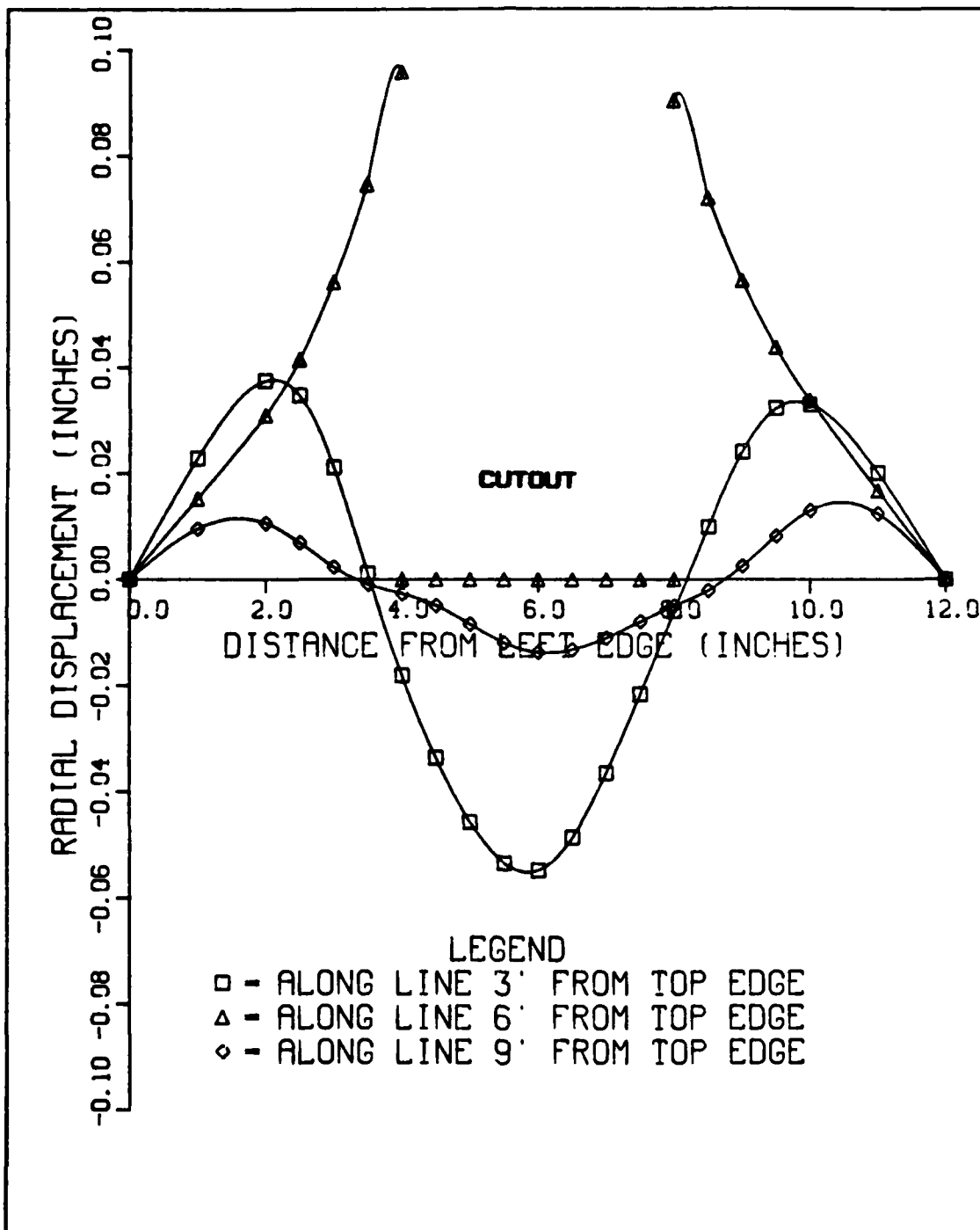
Figure 3.62. Radial Displacement Profile at Collapse Load for 4"x4" Cutout

over twice the thickness of the panel. Since a large amount of the surface area of the panel is removed, the edges of the cutout act like free edges and displace large amounts. This panel and the panel with the 4"x2" cutout are the first cutouts examined in this thesis that truly make use of the large displacement theory portion of STAGSC-1. The rotations are even larger than theory indicates they should be. The large rotation characteristics in the vicinity of the cutout are also due to the free edge effect. The moment along each of the lines (Figures 3.63 through 3.65) are all symmetric about the center of the panel. The characteristics of the moments are different from those for the notches. The moments for these large cutouts are symmetric about the cutout at collapse load. Again, Janisse [23] pointed out that large cutouts (4"x4") displace differently when comparing the nonlinear analysis with the linear results. The eigenvector at buckling contains a trough similar to the small notch cutouts previously considered. The collapse displacement patterns for the large cutouts do not follow this pattern, but are relatively symmetric which is a characteristic of the importance of bending in the resistance for the structure against bending.
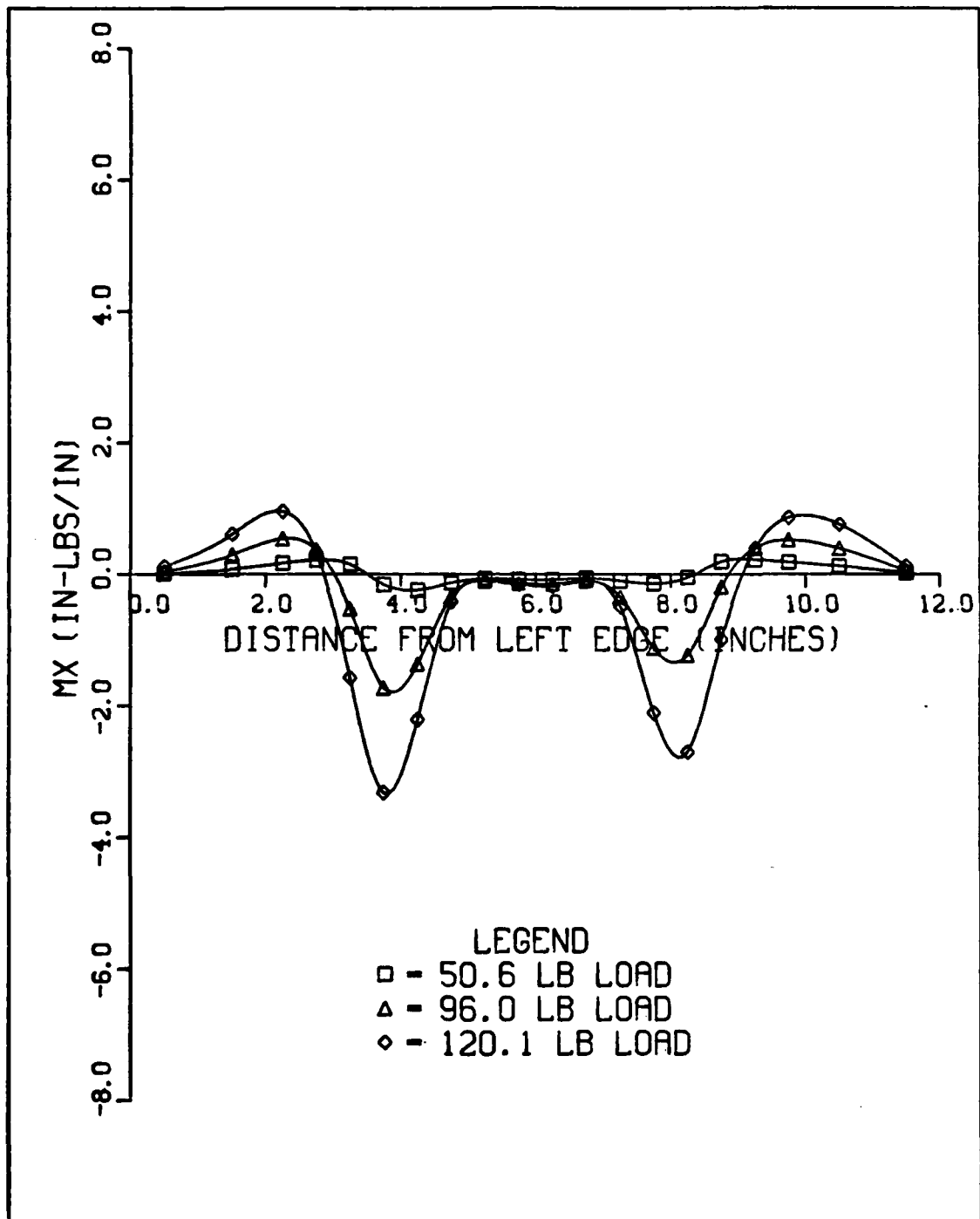
Figure 3.63. M_x along a Line 3.75" from Top Edge of Panel for 4"x4" Cutout
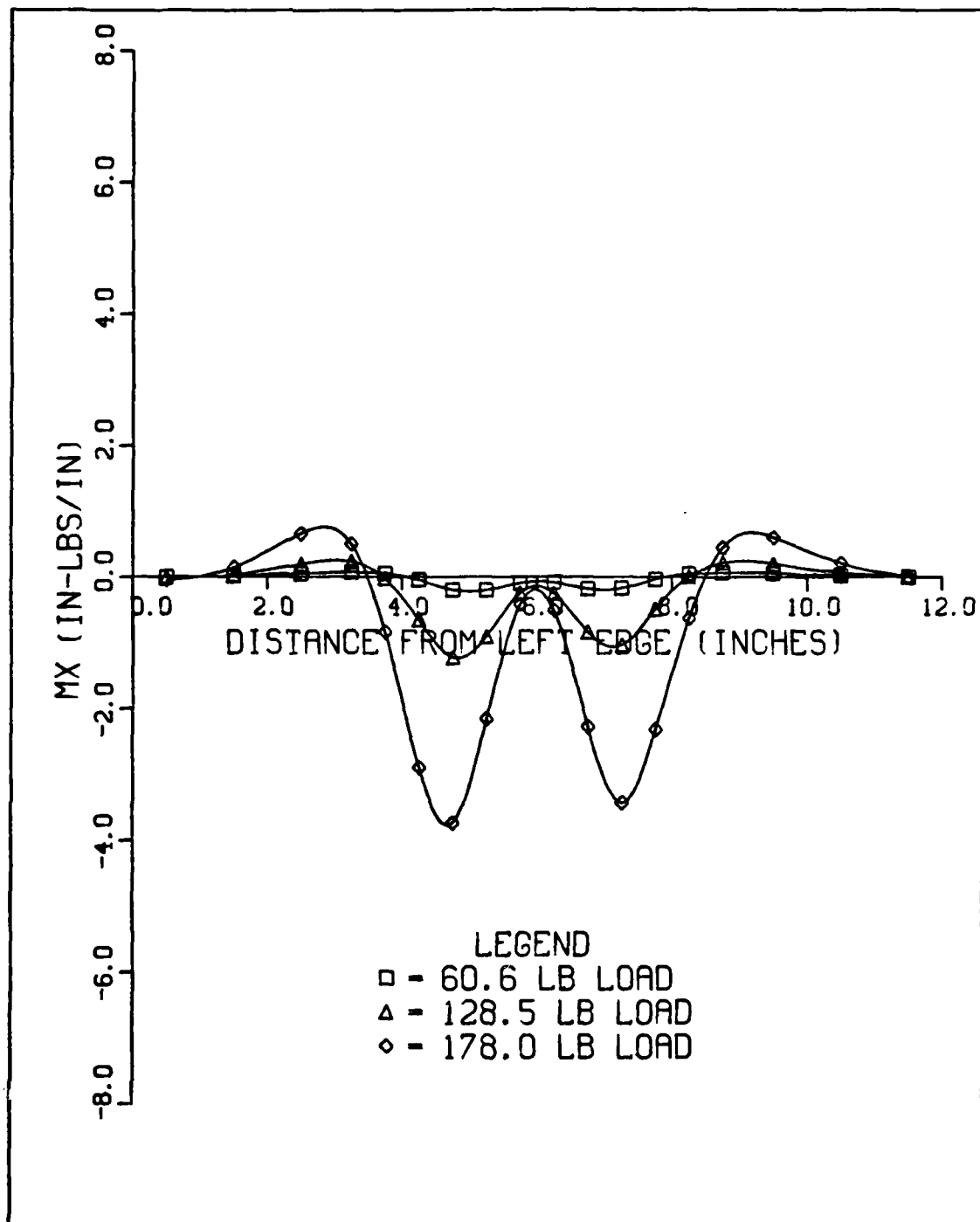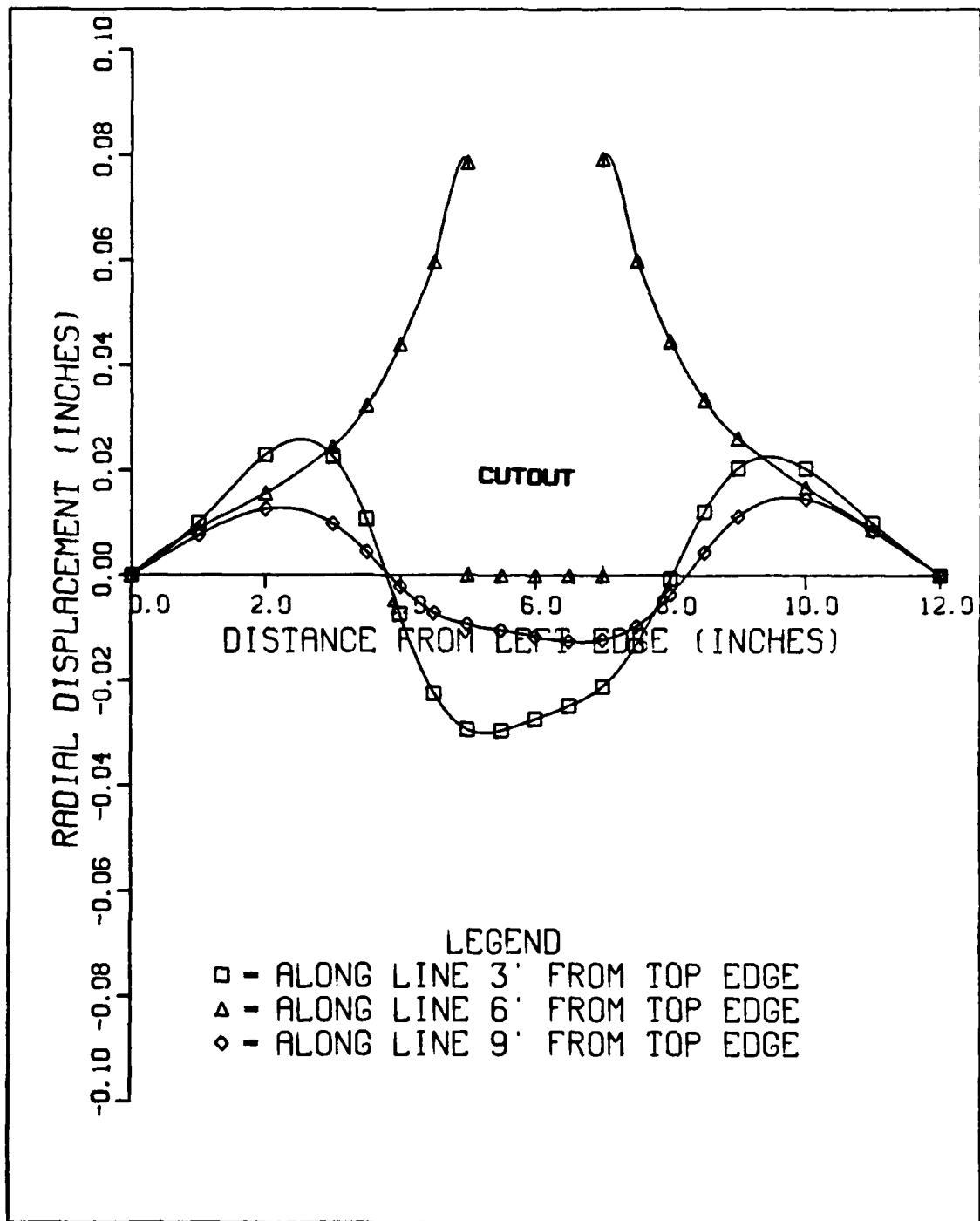
115
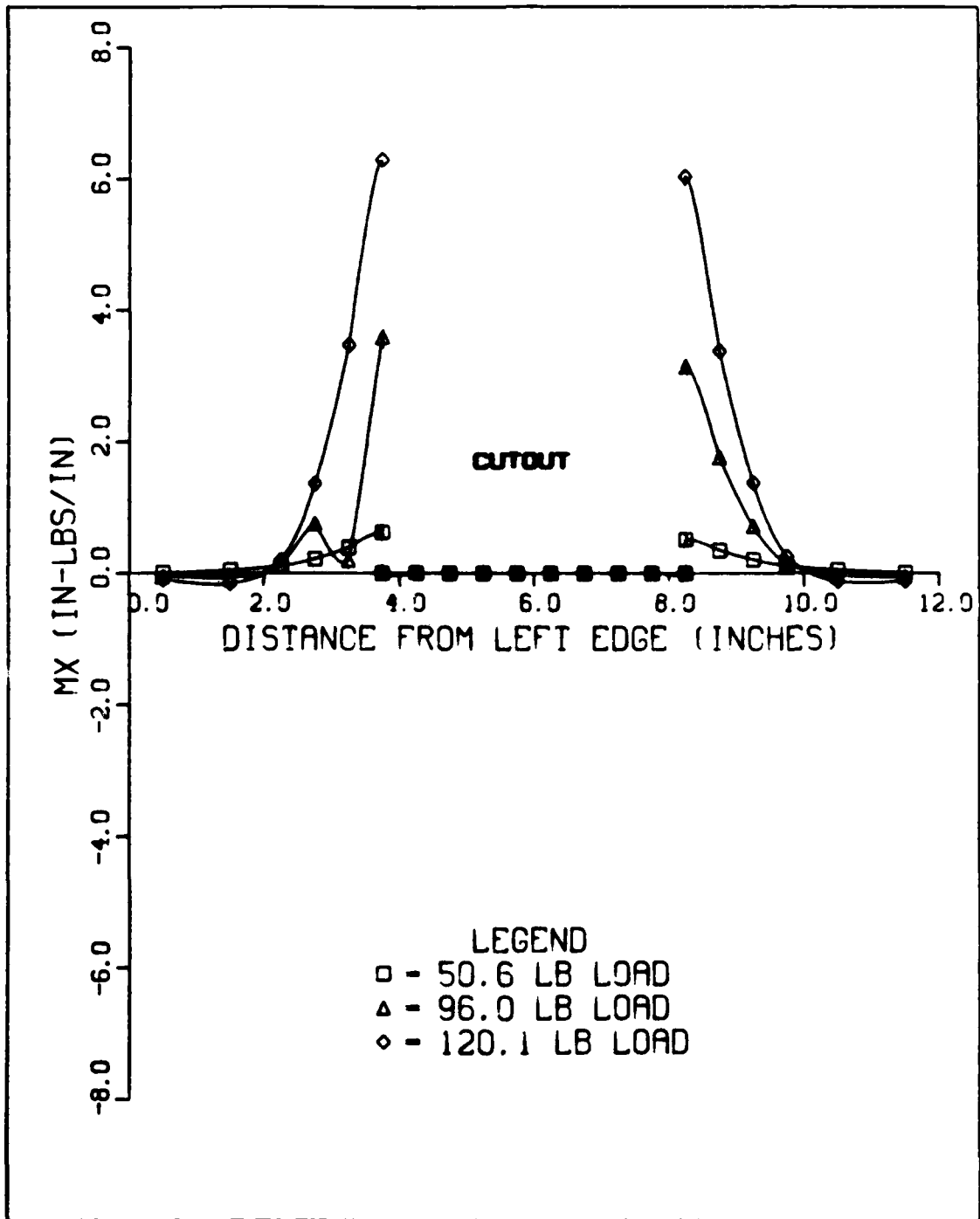
Figure 3.64. M_x along a Line 4.75" from Top Edge of Panel for 4"x4" Cutout
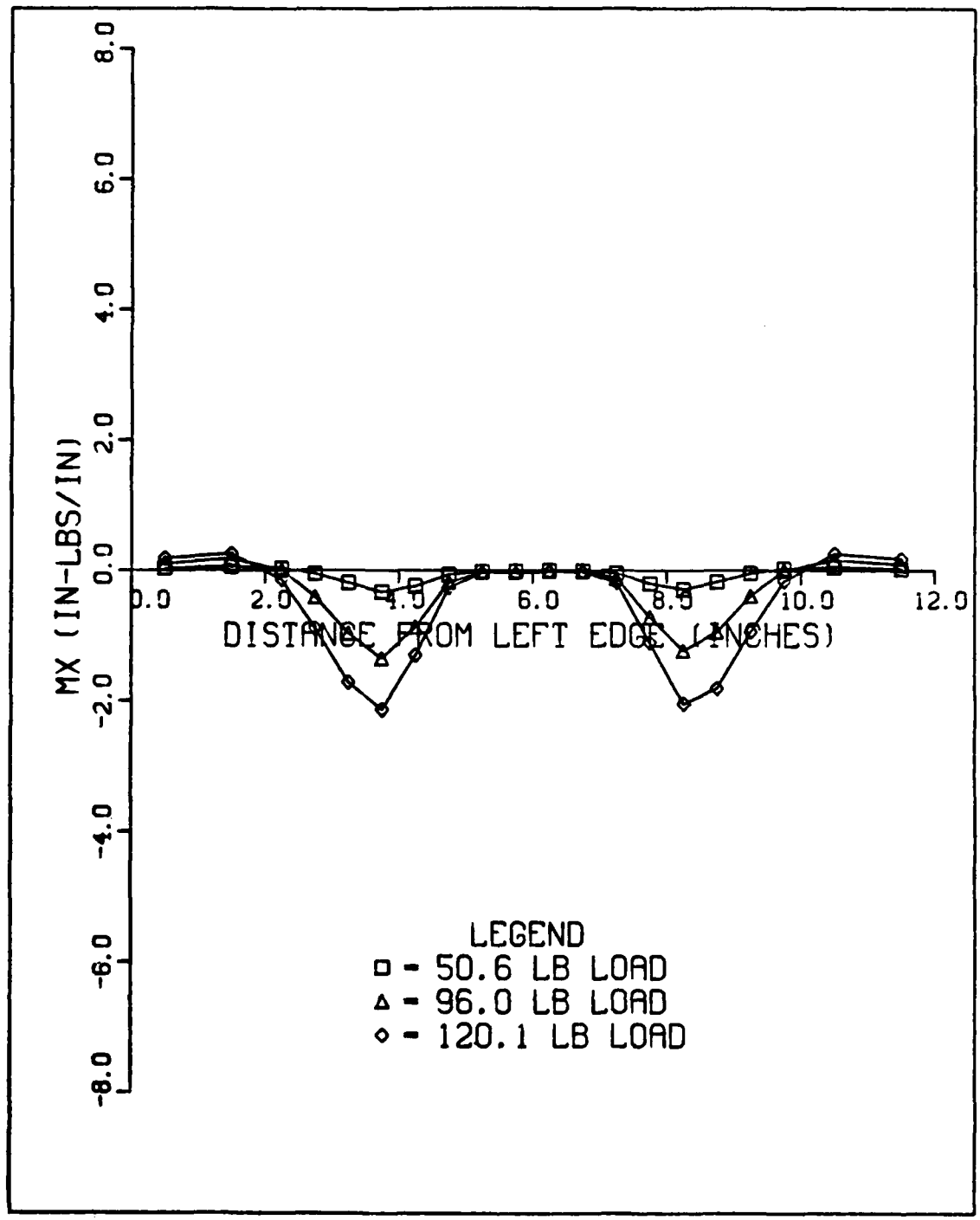
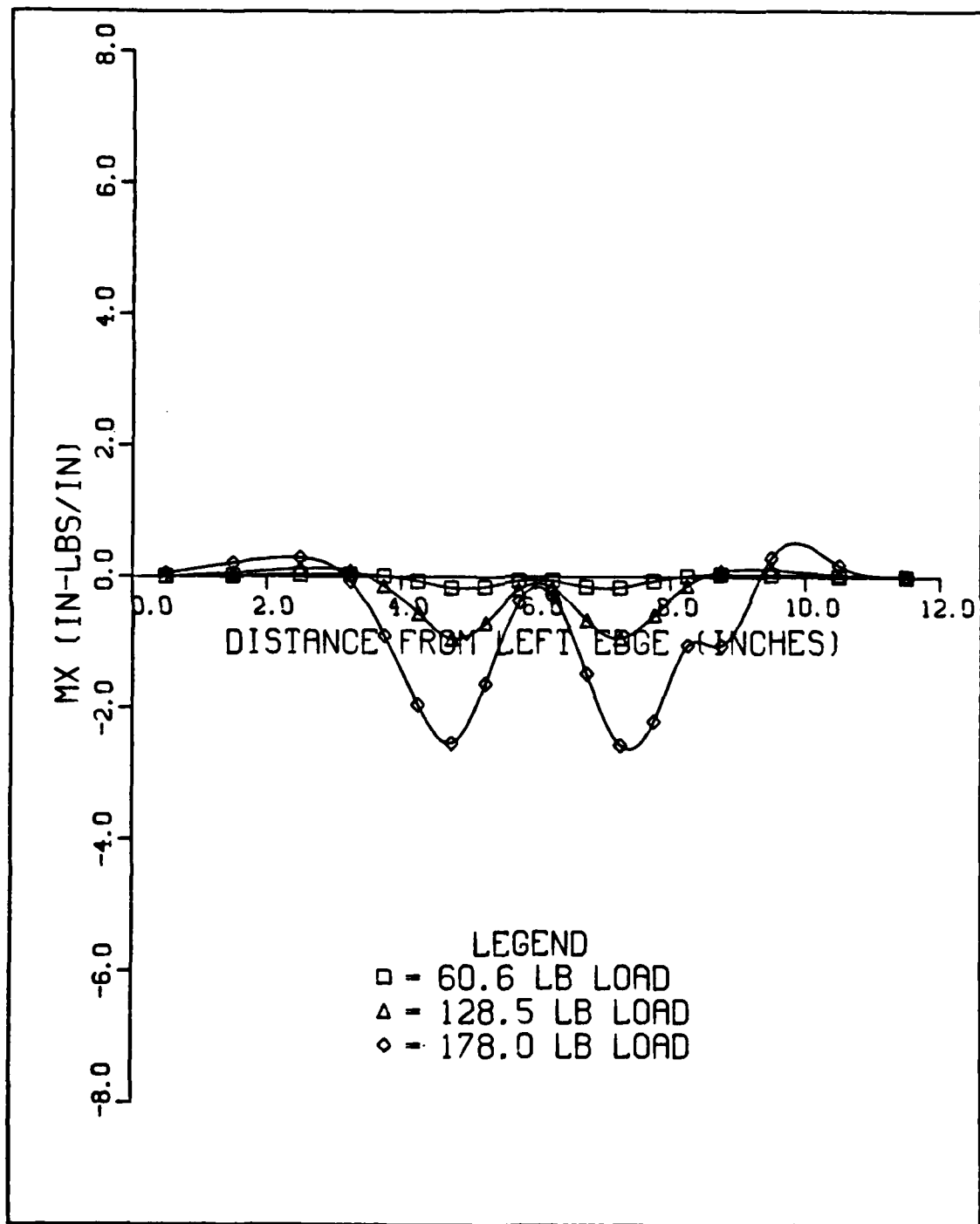Figure 3.65. M_x along a Line 8.25" from Top Edge of Panel for 4"x4" Cutout

117

IV. CONCLUSIONS

Based on the analysis presented in this thesis, the following conclusions can be made:

1. Individual elements in a finite element mesh should preferably have equal dimensions in the x and y directions.

2. In a refined mesh around the area of a cutout, rectangular QUAF 411 elements influence the moments in the direction of their longer dimension to a greater degree than square elements. If elements near the cutout have an aspect ratio of 0.5, the collapse load estimation is not improved as one would expect over the results for a coarse mesh.

3. In a mesh refinement process from one inch square elements to half-inch square elements, the half-inch square elements should be a uniform distance around the cutout for a STAGSC-1 nonlinear collapse analysis. Elements with an aspect ratio of 0.5 should be at least two inches from the cutout and elements with an aspect ratio of 2 should be at least one and a half inches from the cutout.

4. Restraining the v displacement along the upper left or upper right half of the cylindrical panel does not significantly improve the results over the results obtained with symmetric boundary conditions when compared to experimental data.

5. Experimental results considering the given panel and supports, are better approximated by an analytic boundary condition in which the u and v displacements are held fixed along the left edge of the panel between 1 and 6

118

inches from the top edge of the panel. This boundary
condition appears to model the change in boundary conditions
that occurs experimentally with applied load.

6. Surface imperfections in the test panel result in a
lower collapse load and different radial displacement
patterns than those modelled analytically.

7. The restrained boundary condition introduces
greater stiffnesses into the panel which result in a higher
collapse load.

8. It appears to be possible, with the use of the
STAGSC-1 computer program, to actually model an experimental
set of boundary conditions. The ideal boundary condition
was not reached in this thesis, but with additional computer
time, several iterations could be carried out and the ideal
boundary condition attained.

9. For a complete numerical analysis of a panel tested
experimentally, one must take into account surface
eccentricities as well as varying boundary conditions.

10. Panels with notches having an aspect ratio of 2
have higher collapse loads than panels with notches of the
same area but with aspect ratios of 0.5. This is due to the
higher stress concentrations around the corners of the
cutouts with 0.5 aspect ratios. The higher stresses result
in larger displacements and therefore lower collapse loads.
Panels with cutouts with an aspect ratio of 0.5 can carry up
to 17% greater load than panels with the same area cutout
having an aspect ratio of 2.0.

12. The 2"x1" notch is associated with the highest

collapse load but smallest radial displacements. This is because the notch is a small percentage of panel area and therefore, the panel retains much of the structural integrity of a panel without a cutout.

13. The moments in the x direction are symmetric about all cutouts at low load levels. At collapse load, the moments for the 4"x2" and 4"x4" retain their symmetry indicating that these cutouts do not skew with applied load as is the case with the other cutouts.

14. Considering the author's definition of a notch, (a cutout of less than 5% of the panel area) panels with notches behave differently from a collapse displacement function point of view than panels with cutouts. The radial displacement pattern of a panel with a notch forms a diagonal trough whereas panels with cutouts have a vertical displacement trough down the center of the panel. Thus, the notch does not produce the typical nonlinear effect associated with cutouts.

BIBLIOGRAPHY

1. Anderson, Melvin S. "Practical Experience in Analysis of Aerospace Shell Structures," _Theory of Shells_, edited by W. T. Koiter and G. K. Mikhailov. Amsterdam, Netherlands: North-Holland Publishing Co, 1980.

2. Almroth, B. O., and F. A. Brogan. _The STAGS Computer Code_. NASA Contractor Report 2950. NASA. February 1978.

3. Skogh, J. et al. "Instability Analysis of Skylab Structure," _Computers and Structures_, 3: 1219-1240 (1973).

4. Almroth, B. O. "Influence of Edge Conditions on the Stability of Axially Compressed Cylindrical Shells," _AIAA Journal_, 4: 134-140 (1966).

5. Rehfield, L. W. and W. L. Hallauer, Jr. "Edge Restraint Effect on Buckling of Compressed Curved Panels," _AIAA Journal_, 6: 187-189 (January 1968).

6. Sobel, L. H. et al. "Buckling of Cylindrical Panels Under Axial Compression," _Computers and Structures_, 6: 29-35 (February 1976).

7. Andreev, L. V. et al. "Nonlinear Deformation of a Cylindrical Panel Under Axial Compression," _Soviet Applied Mechanics_, 17: 270-274 (September 1981).

8. Almroth, B. O. and A. M. C. Holmes. "Buckling of Shells with Cutouts Experiment and Analysis," _International Journal of Solid Structures_, 8: 1057-1071 (August 1972).

9. Almroth, B. O. et al. "Stability of Cylinders with Circular Cutouts," _AIAA Journal_, 11: 1582-1584 (November 1973).

10. Almroth, B. O. and F. A. Brogan. "Bifurcation Buckling as an Approximation of the Collapse Load for General Shells," _AIAA Journal_, 10: 463-467 (April 1972).

11. Brogan, Frank and B. O. Almroth. "Buckling of Cylinders with Cutouts," _AIAA Journal_, 8: 236-238 (February 1970).

12. Garashchuk, I. N. and I. S. Chernyshenko. "Numerical Investigation of the Stress State of a Cylindrical Shell with a Circular Hole," _Soviet Applied Mechanics_, 15: 484-488 (December 1979).

13. Kosmodamianskii, A. S. and V. I. Chernik. "Stress State of a Plate Weakened by Two Elliptic Holes with Parallel Axes," *Soviet Applied Mechanics*, *17*: 576-581 (December 1981).

14. Khot, N. S. and V. B. Venkayya. *Effect of Fiber Orientation on Initial Post Buckling Behavior and Imperfection Sensitivity of Composite Cylindrical Shells*. AFFDL-TR-70-125. Air Force Flight Dynamics Laboratory, Wright-Patterson AFB OH, December 1970.

15. Bauld, N. R., Jr. and K. Satyamurthy. *Collapse Load Analysis for Plates and Shells*. AFFDL-TR-79-3038. Air Force Flight Dynamics Laboratory, Wright-Patterson AFB OH, December 1970.

16. Khot, N. S. *On the Effects of Fiber Orientation and Nonhomogeneity on Buckling and Post Buckling Equilibrium Behavior of Fiber Reinforced Cylindircal Shells Under Uniform Axial Compression*. AFFDL-TR-68-19. Air Force Flight Dynamics Laboratory. Wright-Patterson AFB OH, May 1968.

17. Harper, Lt James G. *Buckling Analysis of Laminated Composite Circular Cylindrical Shells*. MS Thesis, AFIT/GAE/AA/78D-8. School of Engineering, Air Force Institute of Technology (AU), Wright-Patterson AFB OH, December 1978 (AD-A081904).

18. Becker, M. L. et al. "Experimental Investigation of the Instability of Composite Cylindrical Panels," *Experimental Mechanics*, *22*: 372-376 (October 1982).

19. Bauld, Nelson R., Jr. *Experimental and Numerical Analysis of Axially Compressed Circular Cylindrical Fiber-Reinforced Panels with Various Boundary Conditions*. AFWAL-TR-81-3158. Air Force Wright Aeronautical Laboratory, Wright-Patterson AFB OH, October 1981.

20. Satyamurthy, K. et al. "An Automated, Energy-Based, Finite Difference Procedure for the Elastic Collapse of Rectangular Plates and Panels," *Computer and Structures*, *11*: 239-249 (March 1980).

21. Becker, Capt Marvin L. *Analytical/Experimental Investigation of the Instability of Composite Cylindrical Panels*. MS Thesis, AFIT/GAE/AA/79D-3. School of Engineering, Air Force Institute of Technology (AU). Wright-Patterson AFB OH, December 1979.

22. Hebert, Capt John S. *Analytical/Experimental Linear Bifurcation of Curved Cylindrical Composite Panels*. MS Thesis, AFIT/GAE/AA/82D-14. School of Engineering, Air

Force Institute of Technology (AU). Wright-Patterson AFB OH, December 1982.

23. Janisse, Capt Thomas C. *A Parametric Study of Surface Imperfections and Small Cutouts in a Composite Panel*. MS Thesis, AFIT/GAE/AA/82D-15. School of Engineering, Air Force Institute of Technology (AU), Wright-Patterson AFB OH, December 1982.

24. Singer, Josef. *Buckling Experiments on Shells -- A Review of Recent Developments*. TAE Report Number 403. Technion-Israel Institute of Technology. Haifa, Israel, April 1980.

25. Almroth, B. O. et al. *Structural Analysis of General Shells Volume II User Instructions for STAGSC-1*. LMSC-D633073. Applied Mechanics Laboratory, Lockheed Palo Alto Research Laboratory, Palo Alto CA, July 1979.

26. Jones, Robert M. *Mechanics of Composite Materials*. New York: McGraw-Hill Book Company, 1975.

27. Sobel, L. H. and Kevin Thomas. *Evaluation of the STAGSC-1 Shell Analysis Computer Program*. WARD-10881. Westinghouse Advanced Reactors Division, Madison PA, August 1981.

28. Cook, Robert D. *Concepts and Applications of Finite Element Analysis* (Second Edition). New York: John Wiley and Sons, 1981.

29. Brush, Don O. and B. O. Almroth. *Buckling of Bars, Plates and Shells*. New York: McGraw-Hill Book Company, 1975.

30. Bushnell, David. *Computerized Buckling Analysis of Shells*. AFWAL-TR-81-3049. Air Force Wright Aeronautical Laboratory, Wright-Patterson AFB OH, December 1981.

VITA

Catherine E. Lee was born on 26 February 1957 in Dayton, Ohio. She graduated from high school in Fairborn, Ohio in 1975 and attended Purdue University from which she received a Bachelor of Science degree in Aeronautical/Astronautical Engineering in May 1979. Upon graduation, she received a commission in the USAF through the Air Force ROTC program. She was stationed at Offutt AFB in September 1979 where she was assigned to the 544TH Strategic Intelligence Wing as a Ballistic Missile Trajectory Engineer. In December 1981 she served as a Program Manager for Regular/Special Programs, Air Force Institute of Technology at Wright-Patterson AFB until entering the School of Engineering, Air Force Institute of Technology, in June 1982.

Permanent address: 5932 Bramblewood Court
Dayton, Ohio 45424

REPORT DOCUMENTATION PAGE

1a. REPORT SECURITY CLASSIFICATION UNCLASSIFIED	1b. RESTRICTIVE MARKINGS

2a. SECURITY CLASSIFICATION AUTHORITY	3. DISTRIBUTION/AVAILABILITY OF REPORT Approved for public release; distribution unlimited.
2b. DECLASSIFICATION/DOWNGRADING SCHEDULE	

4. PERFORMING ORGANIZATION REPORT NUMBER(S) AFIT/GA/AA/83D-4	5. MONITORING ORGANIZATION REPORT NUMBER(S)

6a. NAME OF PERFORMING ORGANIZATION School of Engineering Air Force Institute of Technology	6b. OFFICE SYMBOL (If applicable) AFIT/EN	7a. NAME OF MONITORING ORGANIZATION

6c. ADDRESS (City, State and ZIP Code) Wright-Patterson AFB OH 45433	7b. ADDRESS (City, State and ZIP Code)

8a. NAME OF FUNDING/SPONSORING ORGANIZATION Dr N. S. Khot	8b. OFFICE SYMBOL (If applicable) AFFDL/FIBR	9. PROCUREMENT INSTRUMENT IDENTIFICATION NUMBER

8c. ADDRESS (City, State and ZIP Code) Wright-Patterson AFB OH 45433	10. SOURCE OF FUNDING NOS.			
	PROGRAM ELEMENT NO.	PROJECT NO.	TASK NO.	WORK UNIT NO.

11. TITLE (Include Security Classification) See Box 19

12. PERSONAL AUTHOR(S) Catherine E. Lee, Captain, USAF

13a. TYPE OF REPORT MS Thesis	13b. TIME COVERED FROM _____ TO _____	14. DATE OF REPORT (Yr., Mo., Day) 1983 December	15. PAGE COUNT 140

16. SUPPLEMENTARY NOTATION

Approved for public release: IAW AFR 190-17

Lynn E. Wolaver
Dean for Research and Professional Development
Air Force Institute of Technology (ATC)
1 3 JAN 1984

17. COSATI CODES			18. SUBJECT TERMS (Continue on reverse if necessary and identify by block number) Composites, Cylindrical Panels, Cutouts, Plates and Shell Analysis, Nonlinear Analysis, Finite Elements, STAGSC-1, Graphite-Epoxy Composites, Boundary Conditions
FIELD	GROUP	SUB. GR.	
11	04		

19. ABSTRACT (Continue on reverse if necessary and identify by block number)

Title: NUMERICAL DETERMINATION OF THE EFFECTS OF BOUNDARY CONDITIONS ON THE INSTABILITY OF COMPOSITE PANELS WITH CUTOUTS

Thesis Advisor: Anthony N. Palazotto

20. DISTRIBUTION/AVAILABILITY OF ABSTRACT UNCLASSIFIED/UNLIMITED ☒ SAME AS RPT. ☐ DTIC USERS ☐	21. ABSTRACT SECURITY CLASSIFICATION UNCLASSIFIED	
22a. NAME OF RESPONSIBLE INDIVIDUAL Dr Anthony N. Palazotto	22b. TELEPHONE NUMBER (Include Area Code)	22c. OFFICE SYMBOL AFIT/ENG

DD FORM 1473, 83 APR   EDITION OF 1 JAN 73 IS OBSOLETE.

An analytical study using the STAGSC-1 computer code was conducted to determine the effects of notches and unsymmetric boundary conditions on the load bearing capability and radial displacements of axially loaded cylindrical panels. The graphite-epoxy panel consisted of an 8 ply laminate with symmetric ply orientations. A finite element mesh refinement in the vicinity of the cutout was conducted in order to study the non-linear collapse analysis. In additon, the effect of different size cutouts with aspect ratios (axial dimension of cutout divided by circumferential dimension) of 2.0 or 0.5 was studied. Finally, analytic results for a 2"x2" cutout with a varying set of boundary conditions were compared to experimental findings.

It was found that as the surface area of the cutout increased, the buckling load decreased. Cutouts with aspect ratios of 2.0 were found to be capable of carrying higher loads than notches with an aspect ratio of 0.5. By comparing analytic results with experimental data, it was found that unsymmetric boundary conditions for the 2"x2" cutout better approximated experimental data than when symmetric boundary conditions were considered. It was also determined that some of the discrepancy between experimental and analytic results can be attributed to initial eccentricities introduced into the panel by the test apparatus.

END

FILMED

2-84

DTIC